MICELLAR DENDRITIC STRUCTURES AS DRUG DELIVERY AGENTS

by

NAZLI BÖKE

B.S., Chemistry, Bilkent University, 2010

Submitted to the Institute for Graduate Studies in
Science and Engineering in partial fulfillment of
the requirements for the degree of
Master of Science

Graduate Program in Chemistry
Boğaziçi University

MICELLAR DENDRITIC STRUCTURES
AS
DRUG DELIVERY AGENTS

APPROVED BY:

Assoc. Prof. Rana Sanyal ……...….
(Thesis Supervisor)

Assoc. Prof. Amitav Sanyal …..……..

Prof. Dr. M. Fethi Şahin ……

DATE OF APPROVAL: 21.01.2013

To my dear family,

ACKNOWLEDGEMENTS

First of all, I would like to express my deepest thanks to my thesis supervisor, Assoc. Prof. Rana SANYAL for her endless guidance and help throughout my thesis project and for giving a chance to be involved in her successful research group.

I would like to express my special thanks to Assoc. Prof. Amitav Sanyal for his helpful scientific advices and discussions during my thesis project.

I would like to extend my thanks to Prof. Dr. M. Fethi Şahin for his constructive review of the final manuscript of my thesis.

I wish to express my great thanks to Advanced Research and Technologies Center of Boğaziçi University, especially to Bilge Gedik Ulusoy, Ayla Türkekul and Burcu Selen Çağlayan for monitoring DLS, STEM and NMR measurements.

I would like to extend my special thanks to Aslı Erdoğ and Burcu Sümer Bolu for being involved in all the cell culture and internalization experiments.

I also want to thank to all the members of the Chemistry Department of Boğaziçi University and Hülya Metiner.

I wish to express my special thanks to Pelin Ertürk and Özlem İpek Kalaoğlu for sharing all unforgettable moments and their endless friendship, Tuğçe Nihal Gevrek, Özgül Gök, Melike Eceoğlu, my ex-hoodmate Merve Coşar, hoodmate Merve Türksoy and all my labmates Betül, Sedef, Rabia, Mehmet, Yavuz, Nergiz, Sadık, Filiz, Özge, Yasemin, Fatma, Duygu, Merve K. for their friendship, patience and support during my whole research.

Finally, my deepest thanks go to my whole family for their endless love, support and encouragement all my life.

ABSTRACT

MICELLAR DENDRITIC STRUCTURES AS DRUG DELIVERY AGENTS

Among various polymeric systems, amphiphilic block copolymers with stimuli-responsive moities provide significant advantages in drug delivery systems due to their unique self assembly properties which provide interiors that can encapsulate the guest molecules like anti-cancer drugs. The triggered release of these guest molecules can be achieved by external stimuli while minimizing the adverse side effects of the drugs and maximizing the therapeutic effect. In this thesis, various dendron-linear polymer-dendron conjugates are synthesized via Huisgen type “click” reaction using biodegredable polyester dendron and biocompatible PEG. Functionalization of the dendron surface with hydrophobic moiety, which provides pH-sensitivity, increased the tendecy to form micellar structures in water via self-assembly. By changing the length of hydrophilic polymer, type of hydrophobic moiety and generation of the dendron, the optimum micellar structure that can maximize the stability can be achieved. The stability of these micelles at neutral pH is demonstrated by the release rate of a hydrophobic dye. A variety of micelles are phsically encapsulated with an anti-cancer therapeutic agent by co-solvent evaporation method and the drug release is monitored by UV-VIS spectroscopy and LC/MS.

ÖZET

İLAÇ SALIM SİSTEMLERİ OLARAK DENDRİTİK YAPIDAKİ MİSELLER

Çeşitli polimerik sistemlerin yanı sıra, dış etkenler ile bozunabilen amfifilik kopolimerler, biyo-uyumluluk ve yeterli yükleme kapasitesi nedeni ile son yıllarda ilaç salım sistemleri arasında çeşitli avantajlar sağlamaktadır. Amfifilik kopolimerler hidrofilik/ hidrofobik bloklardaki çözünürlük farkı sebebi ile su içerisinde herhangi bir dış etken olmaksızın hidrofobik bloğun iç çekirdeği, hidrofilik bloğun ise dış katmanı oluşturduğu misel adı verilen eşsiz bir yapı oluşturmaktadır. Bu tez çalışmasında, biyo-uyumlu hidrofilik özellikteki PEG ve biyobozunur hidrofobik özellikteki poliester dendronlar kullanılarak Huisgen tipi "klik" reaksiyonu ile dendron-polimer-dendron konjugeler sentezlenmiştir. Dendron yüzeyine bağlanan hidrofobik gruplar sayesinde, asidik ortamda bozunur konjugeler elde edilmiş ve pyrene (hidrofobik ilaca eşdeğer molekül) kullanılarak micel yapısında yeni nano taşıyıcılar oluşturulmuştur. Etkili bir ilaç salım sistemi yaratmak için nötral ortamda bozunmayan yani bütün ilaç yükünü sadece asidik ortamda bırakabilen bir micel yapısı yaratmak önemlidir. Bu sebeple, en dayanıklı misel yapısını oluşturmak için hidrofilik polimer uzunluğu, hidrofobik grubu ve dendron jenerasyonu değiştirilmiş ve en dayanıklı dendritik yapıdaki miceller ilaç yüklemek için uygun görülmüştür. Dendritik yapıdaki bu micellerin taşıyıcı özelliğe sahip hidrofobik kabuğu fiziksel olarak kanser karşıtı ilaç molekülleri ile yüklenmiş ve ilaç salım profili incelenmiştir.

TABLE OF CONTENTS

LIST OF FIGURES

LIST OF TABLES

LIST OF SYMBOLS

J	Coupling constant
μ	Wavelength

LIST OF ACRONYMS/ABBREVIATIONS

Bis-MPA	2,2-bis(hydroxymethyl)propionic acid
CA-4	Combrestatin A-4
$CDCl_3$	Deuterated Chloroform
CH_2Cl_2	Dichloromethane
CMC	Critical Micelle Concentration
CuAAC	Copper catalyzed azide alkyne cycloaddition
DCC	Dicyclohexylcarbodiimide
DDS	Drug Delivery System
DLS	Dynamic Light Scattering
DMAP	N,N Dimethylaminopyridine
EPR	Enhanced Permeability and Retention
Et_2O	Diethyl ether
FT-IR	Fourier Transform Infrared
G_1	Generation 1 dendron
G_2	Generation 2 dendron
G_3	Generation 3 dendron
NMR	Nuclear Magnetic Resonance
PAMAM	Poly(amido amine)
PEA	Poly Ethyl Acrylate
PEG	Poly(ethylene glycol)
PEO	Poly(ethylene oxide)
PCL	poly-ε-caprolactone
PMDETA	N,N,N',N',N''-Pentamethyldiethylenetriamine
STEM	Scanning Transmission Electron Microscope
TEA	Triethylamine
THF	Tetrahydrofuran

1. INTRODUCTION

Cancer is the second leading cause of death all around the world. According to the World Health Organization, 84 million of people will die because of cancer between 2005 and 2015. In 2007 alone, 7.9 million of people died all around the world, which indicates 13% of all deaths. In 2008, more than 1.4 million of new cancer cases were estimated in US [1].

Over the past 30 years, survival rates for most forms of cancer have increased significantly according to a statistical database provided by the American National Cancer Institute. Overall, 5 year cancer survival rates show an increment from 48.9% in 1975 to 66.7% in 2003 [2]. The following figure shows the survival rates for some of the most common types of cancer. According to this figure, the survival rates of some types of cancer like prostate, melanoma, and breast have been significantly increased; however, there are still some kinds of cancer like pancreas, liver and lung which have survival rates below 30%. Therefore, there is need to develop novel 'innovative' drug delivery systems. This section mentions the advancements in the targeted drug delivery systems and the types of nanocarriers that maximize the efficacy of the therapeutic agents while minimizing the side effects.

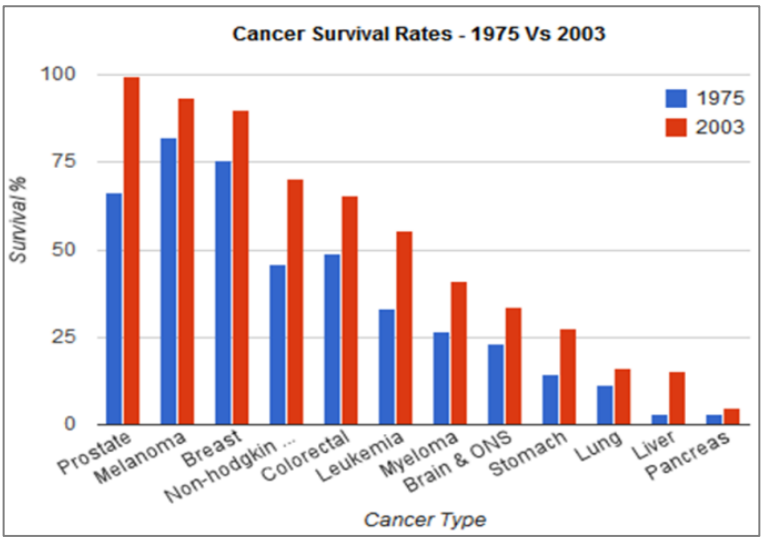

Figure 1.1. 5-year survival rates for some of the most common types of cancer [2].

1.1. Targeted Drug Delivery Systems

Targeted drug delivery systems have been developed in order to increase the survival rates and the life quality of the patient. The aim of a targeted drug delivery system is to prolong, localize, target and have a protected drug interaction with the diseased tissues while affecting as few healthy cells as possible, in other words, it maximizes the efficacy of the drug while minimizing the adverse side effects of the therapeutic agents. These new drug delivery systems have several advantages over the conventional drug delivery systems such as increasing drug concentration in the tumor while decreasing the drug concentration in normal tissues, increasing drug stability to reduce drug degradation, releasing maximum of drug at the targeted sites while releasing minimum of drug during transit, also, improving the solubility of drug and pharmacokinetics profile of the therapeutic agent.

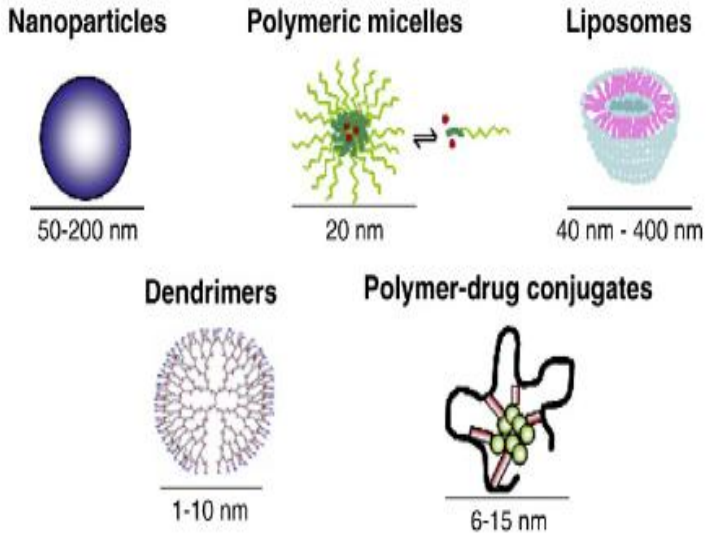

Figure 1.2. Types of nanocarriers currently described in preclinical and clinical studies [3].

Conventional drug delivery systems such as chemotherapy, radiotherapy or immunotherapy have dramatically increased the survival rates of cancer patients in the last few decades; however, there are some challenges associated with anti-cancer medications such as poor water solubility, low stability, low bioavailability, high toxicity, rapid clearance and metabolism, inability to penetrate and accumulate in cancer cells, and uncontrollable uptake by healthy cells. Therefore, in order to get rid of adverse effects of

anti-cancer drug molecules, the nano sized drug carriers are widely used such as polymeric micelles, polymer-drug conjugates, nanoparticles, dendrimers and liposomes [3]. Types of nanocarriers in preclinical and clinical studies are shown by Figure 1.2 and the commercial availability of these drug carriers in the market and their clinical status is shown by Table 1.1. These nanocarriers can be functionalized with hydrophilic polymers such as poly (ethylene glycol) in order to improve the water solubility or help the particle evade uptake by the immune system, functionalize with targeting molecules such as antibodies or aptamers in order to control the cellular uptake, or, functionalize with imaging contrast agents such as SPIO for diagnostics [4].

Targeted drug delivery systems are divided into two types of drug delivery. One of them is active targeting like some antibody medications; and the other one is passive targeting, such as the enhanced permeability and retention effect (EPR-effect). This passive targeting approach discovered by Matsumura and Maeda in 1986 [5]. This is a unique feature of solid tumors related to their anatomical and pathophysiological differences from healthy tissues. The order of endothelial cells of tumor cells are differ from the normal cells which means normal vessels have tight endothelium; therefore, only small drug molecules can pass through these vessels; on the other hand, tumor vessels are leaky and permeable, so that either small drug molecules or macromolecules (drug carriers) can extravasate these tumor vessels. Figure 1.3 shows the differences between normal and tumor vessels that explain the passive targeting of drug carriers by the Enhanced Permeability and Retention effect.

Table 1.1. Clinical status of nanocarriers and commercially available drug carriers in the market.

Nanocarriers	Drug	Name	Indications	Status
Polymeric micelles	Paclitaxel	Genexol-PM	Breast, lung, pancreas	II-III
	Doxorubicin	NK911	Various	IV
Nanoparticles	Albumin-paclitaxel	Abraxane	Metastaic breast cancer	Approved
	Doxorubicin	Transdrug	Hepatocarcinoma	Approved
	Paclitaxel	Nanoxel	Advanced Breast Cancer	I
Polymer-drug conjugates	Paclitaxel	Xyotax (CT-2103)	Breast, ovarian cancer	II
	Doxorubicin	PK1	Breast, lung, colon	II
Liposomes	Doxorubicin	Doxil	Ovarian, Kaposi carcinoma	Approved
	Daunorubicin	DaunoXome	Kaposi carcinoma	Approved
	Vincristine	Onco-TCS	Non-Hodgkin	Approved

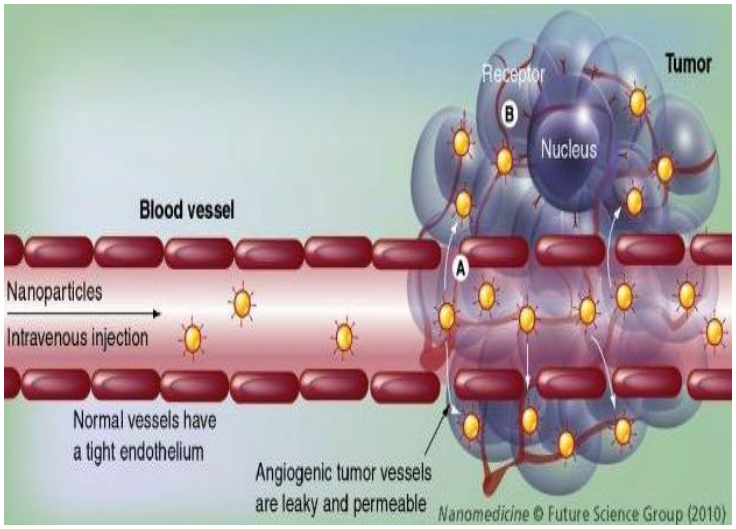

Figure 1.3. Differences between normal and tumor vessels that explain the passive targeting of nanocarriers by the Enhanced Permeability and Retention effect [5].

1.2. Polymeric Micelles as Drug Carriers

The success in rapid development of the use of amphiphilic block copolymers improves the performance of the existing therapeutic agents. Polymeric micelles (PMs) are nanoscopic delivery systems that are formed through the self-assembly of amphiphilic copolymers in aqueous solutions. These micelles are characterized with core-shell architecture in aqueous environment, in which the hydrophobic core acts as a reservoir for the encapsulation of hydrophobic therapeutic agents, proteins or DNA through physical or chemical conjugations which demonstrate prolonged circulation; on the other hand, hydrophilic shell provides water solubility, steric stability and minimizes protein adsorption on micelles. In addition, the sizes of polymeric micelles are between 20 and 100 nm, which indicates not only the effectiveness in avoiding rapid renal filtration; but also they are small enough to avoid undesirable cell uptake. They can passively accumulate in solid tumors with leaky vasculature due to the enhanced permeability and retention (EPR) effect. The formation of a polymeric micelle from an amphiphilic AB block copolymer in aqueous solution is shown by Figure 1.4 [6].

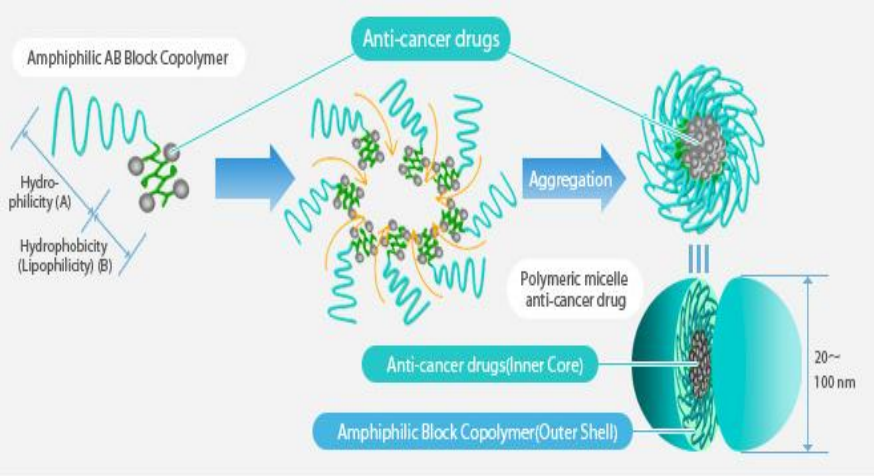

Figure 1.4. Formation of a polymeric micelle from an amphiphilic AB block copolymer in aqueous solution [6].

The first polymeric micelle was reported by Ringsdorf *et al.* in the early 1980s [7]. They formed micelle from block co-polymer–drug conjugates of cyclophosphamide (CP) sulfide and PEO-poly (L-lysine). In 1987, Kataoka *et al*. made the most significant contribution to the field of polymeric micellar delivery systems by conjugating doxorubicin (DOX) to PEO–poly(aspartic acid) (PEO–P(Asp)–DOX) [8]. Since then they developed several polymeric micellar delivery systems as drug carriers for different hydrophobic drugs, including several anticancer agents, as well as nucleic acid-based therapeutics [9-11]. Their progress in polymeric micellar drug delivery systems contributed four formulations in clinical trials. Burt and co-workers have reported a polymeric micellar formulation for paclitaxel which is based on PEO-PDLLA that could increase the water solubility of this hydrophobic drug up to 50,000-fold by avoiding the use of toxic solubilizing agent, Cremophor EL [12]. This new micellar formulation of paclitaxel came to the pharmaceutical market in the 21st century.

1.2.1. Polymeric Micelles: Advantages & Challenges

Self-assembly of amphiphilic block co-polymers composed of hydrophilic and hydrophobic blocks leads to the formation of nanometer sized drug carriers of different morphologies. Their unique core/shell architectures provide widespread applications in drug delivery systems. The hydrophobic core of these micelles creates a space for

encapsulation of hydrophobic drugs, proteins or DNA, on the other hand, hydrophilic shell of these micelles increases the water solubility of water insoluble drugs, minimizes the protein adsorption on micelles and their cellular adhesion [13] (Figure 1.5). Another advantage of these micelles is the ability to avoid non-specific uptake by reticuloendothelial system (RES). The sizes of these micelles are also higher for filtration by kidneys; therefore, this advantage of polymeric micelles prolongs the blood circulation time of the therapeutic agents. They can also passively accumulate in solid tumors with leaky vasculature due to the EPR effect [14]. The critical micelle concentration (CMC) is also very effective in the stability of block co-polymers. More hydrophobic block co-polymers have lower CMCs, indicating a higher thermodynamic stability of the micellar structure. Improvement in the stability also prolongs the blood circulation time of the therapeutic agent after administration.

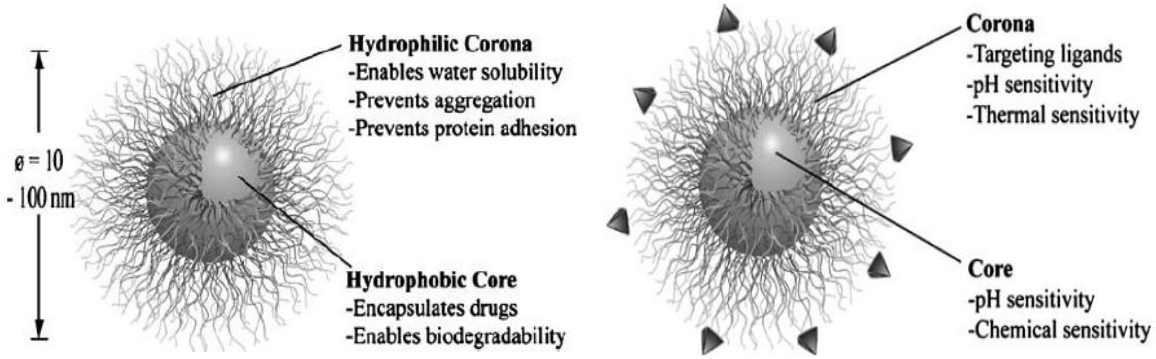

Figure 1.5. Schematic representation of the self-assembly of amphiphilic block copolymers to polymeric micelles [13].

Despite several potential advantages, the improvements of new drug formulations from polymeric micelles have been still challenging. The low drug loading efficiency, poor blood stability, difficulty in delivery through the cell membrane and selective drug release are some of the drawbacks of these nanocarriers [15]. In order to solve these problems, both the core and shell of the polymeric micelles can be functionalized to achieve optimum delivery with maximum therapeutic effect and minimum side effects. In this regard, the micellar core and shell can be engineered to increase drug loading capacity, improve micellar stability, achieve active drug targeting, enhanced cellular uptake and stimuli-responsive drug release. For instance, Kataoka *et al*. have generated multifunctional polymeric micelle [folate–PEO–p(Asp–Hyd–DOX] bearing cancer-specific targeting

ligands (folate) on the surface and an anti-cancer drug (DOX) conjugated via an acid-labile hydrazone bond in the core. (Figure 1.6) The folate conjugated micelles can avoid the non-specific cell uptake by internalizing through receptor-mediated endocytosis and due to the acidic cleavable bonds the therapeutic agent can be released from these micelles under intra-endosomal acidic environment [16].

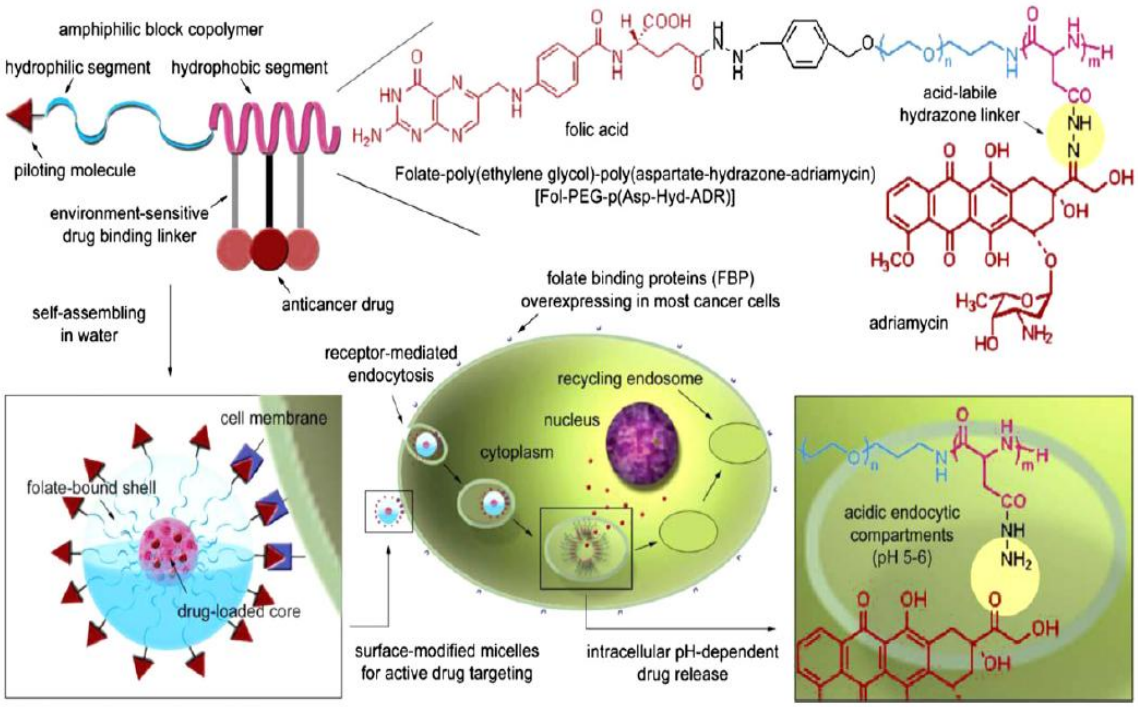

Figure 1.6. Preparation of multifunctional folate–PEO–P(Asp–Hyd–DOX) block co-polymers and micelles with tumor selectivity for active drug targeting and pH-sensitivity for intracellular site-specific drug release [16].

Engineering of the micellar core and shell has still some challenges due to limitations during functionalization. According to a report on comparison of linear polymers and dendrimers by Gingras *et al*., the controlled multivalency of dendrimers provides more advantages over linear polymers. They have reported that dendrimers can be used to physically encapsulate or chemically conjugate similar or different drug molecules inside the core while attaching targeting and/or solubilizing moieties on the same architecture, and their low polydispersity provides more reproducible pharmacokinetic behavior [17].

1.3. Dendrimers in Drug Delivery Systems

Dendrimers are unique class of monodisperse macromolecules, having perfectly branched, well defined three-dimensional architectures with very low polydispersity and high functionality. All these promising properties make them attractive candidates for targeted drug delivery systems as drug carriers.

In 1978, the first dendrimer have been reported by Vögtle *et al*. through divergent synthesis. In the early 1980's, Tomalia *et al*. synthesized PAMAM dendrimers [18] (Figure 1.7a) and Newkome *et al*. [19] also followed the divergent route, which extends the multifunctional core outward by a series of reactions, commonly a Michael reaction. In 1990, Fréchet *et al*. synthesized polyaryl ether dendrimers (Figure 1.7b) by introducing a convergent method which is based on a building from small molecules that end up at the surface of the sphere. Reactions proceed inward building and are eventually attached to a core. This method makes it much easier to remove impurities; therefore, the final dendrimer is more monodisperse. However, due to the steric effects along the core, dendrimers made with a convergent method are not as large as those made by divergent methods [20]. All these macromolecules have uniform size and water solubility. They have also modifiable surface functionality as well as internal cavities which make them attractive for biological applications, targeted drug-delivery systems, macromolecular carriers, enzyme-like catalysis, sensors, light harvesting systems and surface engineering [21].

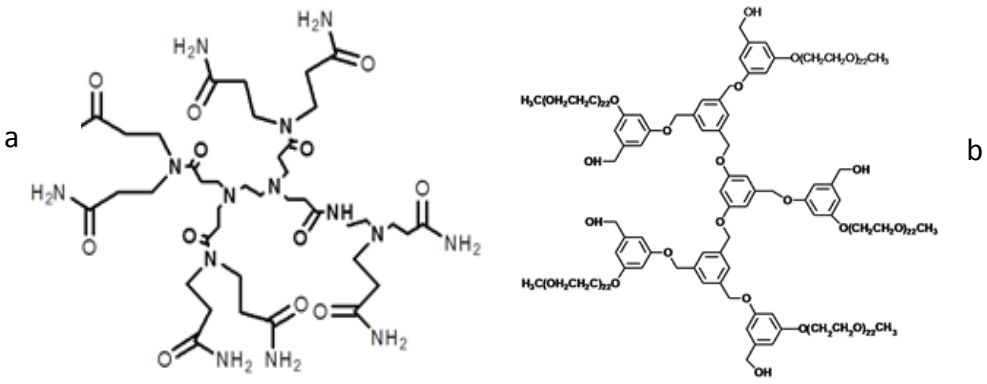

Figure 1.7. Examples of dendritic scaffolds commonly used in drug delivery applications. (a) PAMAM (b) polyaryl ether.

In recent years, several research groups use an attractive approach to increase drug loading capacity while increasing cell specificity. Tomalia *et al*. have been reported folate conjugated PAMAM dendrimers labeled with fluorescein isothiocyanate (FITC) for targeting tumor cells (Figure 1.8a). After conjugation of Methotrexate and Taxol drugs to these folate/FITC-conjugated PAMAM dendrimers, their *in vitro* and *in vivo* cytotoxicity and drug targeting specificity studies were investigated [22]. Modifications of dendrimers with antibodies or aptamers are also useful in targeted drug delivery systems due to their inherent specificity of the antibody–antigen interactions. Roberts *et al.* have been reported an effective targeted drug delivery system which is based on an antibody-PAMAM dendrimer (Figure 1.8b). They investigated that these antibody conjugated dendrimers retained %90 of the immunoreactivity of the unmodified antibody [23].

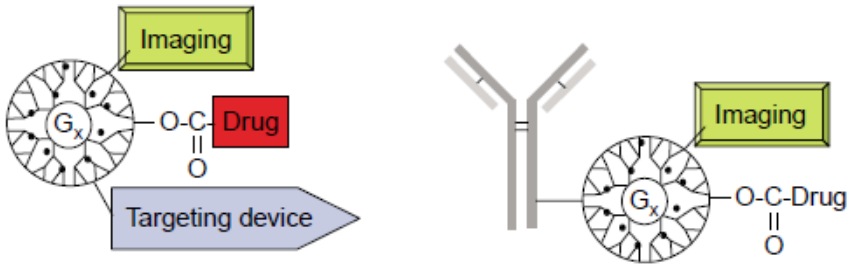

Figure 1.8. Dendritic nanocarriers for therapeutic applications (a) Surface-modified PAMAM dendrimer for targeting, imaging and drug delivery (b) Antibody–dendrimer conjugate [22,23].

1.4. Huisgen Type of Click Reaction

In recent years, most of the polymers can be conjugated with dendrons by click chemistry. The metal catalyzed azide/alkyne click reaction is a variation of the Huisgen 1,3-dipolar cycloaddition reaction between terminal acetylenes and azides. In 2001, click reaction were first described by K. Barry Sharpless using Cu[I] catalyst. In the reaction below (Figure 1.9), azide unit reacts with alkyne unit to afford the triazole as a mixture of 1,4-adduct and 1,5-adduct [24].

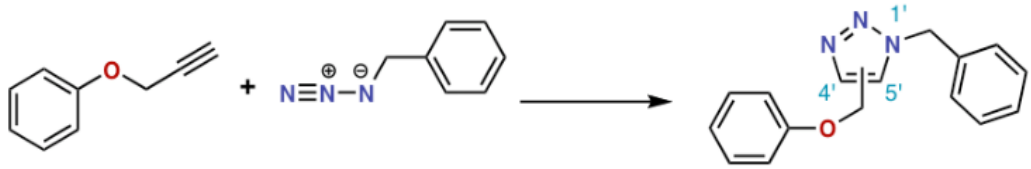

Figure 1.9. Huisgen type of click reaction[24].

Since 2001, the click reaction is widely used in various applications for the synthesis and modifications of dendritic polymers, hyperbranched polymers and linear-dendritic polymers due to its reliability, specificity and biocompatibility. Dong *et al*. have been reported a versatile approach to synthesize dendron-polymer-dendron conjugates, poly(*ε*-caprolactone)-*b*-poly(ethylene glycol)-*b*-poly(*ε*-caprolactone) tri-block copolymers by using click chemistry [25]. These tri-block copolymers self-assembled into flower like micelles with biodegradable dendron-like PCL core and biocompatible PEG shell which will provide higher drug loading efficiency and longer drug-release time than the linear polymers (Figure 1.10).

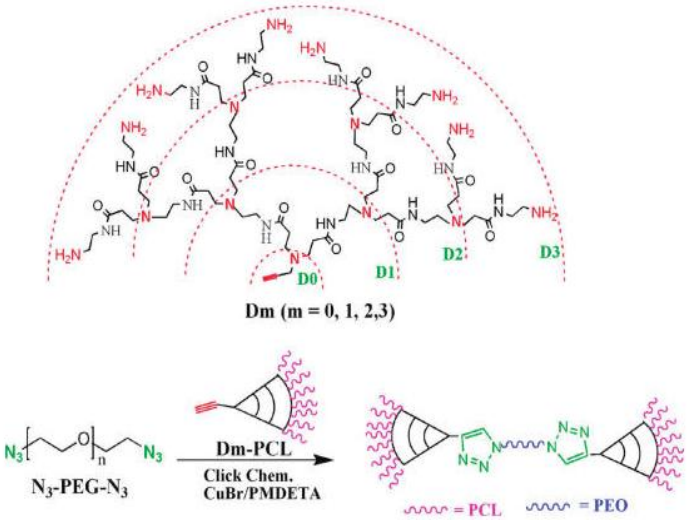

Figure 1.10. Synthesis of dendron-like/linear/dendron-like D*m*-PCL-*b*-PEG-D*m*-PCL triblock copolymers by using click chemistry [25].

1.5. Dendron-Polymer Conjugates

Linear-dendritic architectures like dendron-polymer or dendron-polymer-dendron conjugates received much attention in the past decades. These linear–dendritic copolymers can self-assemble into several supramolecular architectures, which will provide

compartments for encapsulating therapeutic agents. Fréchet and Gitsov are the pioneers of combining chain-entangled linear polymers with densely chain-packed dendritic molecules (Figure 1.11) [26]. Due to their unique self-assemble properties, linear-dendritic architectures are widely used in many applications like diagnosis, drug or gene delivery systems and tissue engineering.

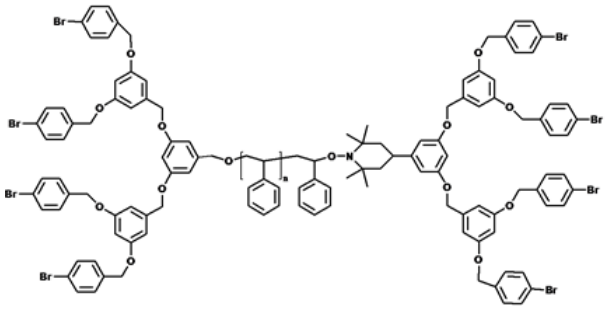

Figure 1.11. The first dendritic-linear ABA type of copolymer synthesized by Fréchet and Gitsov.

In recent years, dendron-polymer-dendron or dendron-polymer conjugates have been obtained a variety of methods such as click chemistry, thiolene chemistry etc for biological applications. The stability of these conjugates at blood pH is very hot topic for targeted drug delivery systems. For instance, Fréchet *et al*. synthesized PEG-dendrimer hybrids used as backbones for acid sensitive micelles [27]. They have been investigated the effect of the length of the polymer, the type and generation of the dendrimer and type of the acetal linker on the micellar stability and the hydrolysis rates (Figure 1.12). They demonstrated that structural properties of polymer-dendron conjugates affect the pH sensitivity of the systems and also the release rate of encapsulated payload.

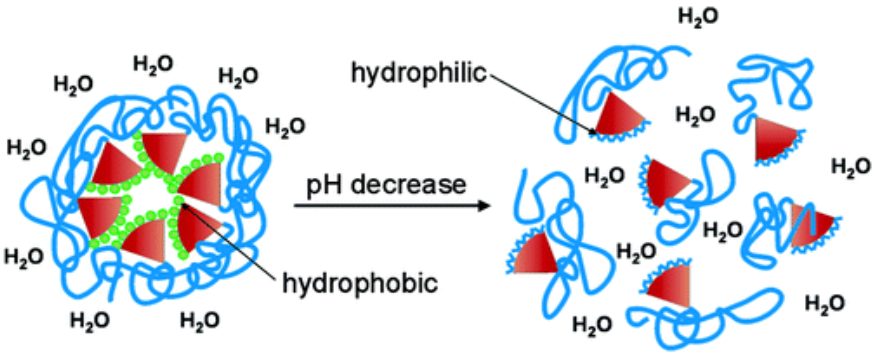

Figure 1.12. Schematic representation of pH-sensitive micelles [27].

Cheng *et al*. reported a novel amphiphilic dumbbell-shaped tri-block copolymer with PLLA end groups and linear PEG block connected by using fourth generation polyester dendrons [28]. They synthesized these high molecular weight macromolecules with narrow molecular weight distribution and improved hydrophilicity with a high multiplicity of functional groups for tissue engineering applications (Figure 1.13).

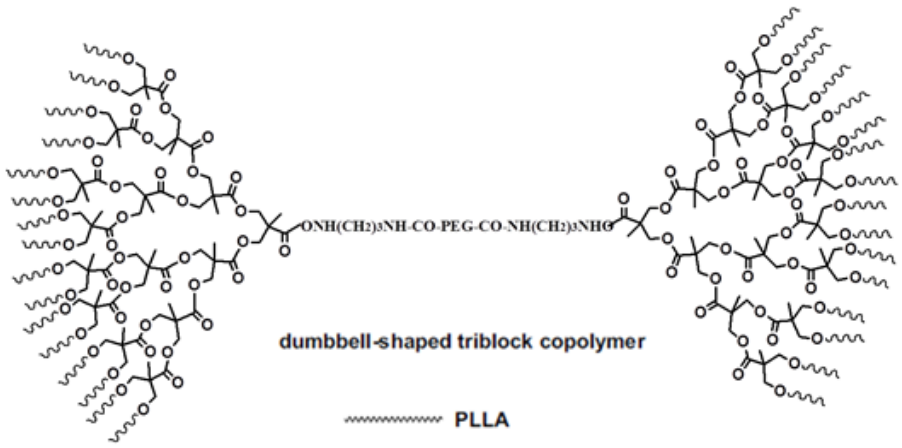

Figure 1.13. Dumbbell-shaped tri-block copolymers.

Linear-dendritic architectures can also be functionalized with targeting moieties in order to decrease the non-specific cell uptake. Zhu and coworkers designed a potential bone-targeting drug delivery systems [29]. Alendronate conjugated H40-star-PEG was synthesized for encapsulation of DOX into the micellar core and the highest binding efficiency of bone-targeted micelles were successfully investigated (Figure 1.14).

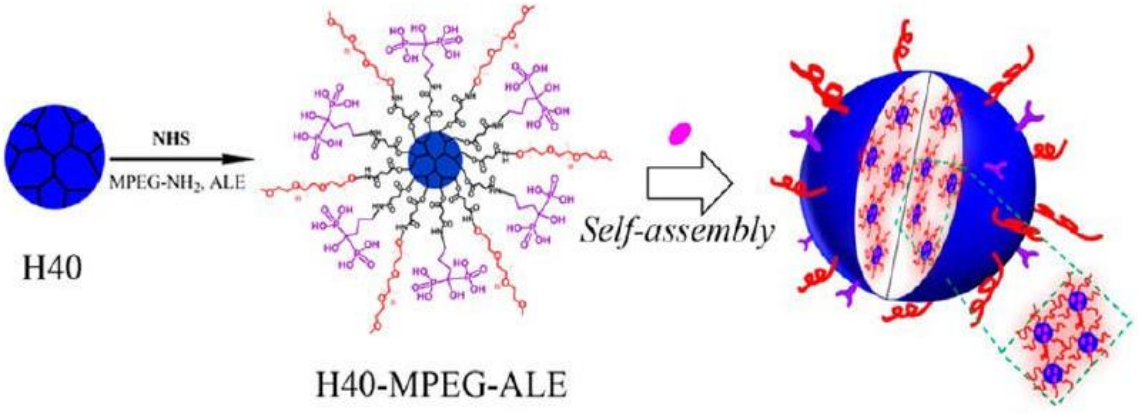

Figure 1.14. Alendronate conjugated H40-star-PEG linear-dendritic architecture [29].

1.6. Drug Encapsulation and Macromolecular Prodrugs

In micellar drug delivery systems, a drug molecule is either covalently conjugated or non-covalently encapsulated in the interior of a dendrimer to form a prodrug. For instance, in early studies, Szoka *et al.* complexed DNA molecules with PAMAM dendrimers for gene delivery applications [30], on the other hand, hydrophobic drugs and dye molecules were incorporated into various dendritic cores by Newkome *et al.* and Meijer *et al* [31]. However, most of these systems release their drug payload over several hours; therefore, the main drawback of these prodrugs is the lack of controlled drug release kinetics. In some cases, harsh conditions are required, whereas in others the encapsulated drug is released faster [32]. In order to provide better control over drug release rate and improve biocompatibility, poly(ethylene glycol) PEG chains conjugated on the dendrimer periphery.

An alternative approach in the development of dendrimers as drug delivery carriers is to exploit their well-defined multivalency for the covalent attachment of drug molecules. Dendrimer/drug conjugates generally consist of a therapeutic agent covalently linked to the peripheral groups of the dendrimer. This method offers distinct advantages over physically encapsulated systems. Multiple drug molecules can be attached to each dendrimer and the release of these therapeutic agents is partially controlled by the nature of the linkages. The drug loading can be tuned by varying the generation number of the dendrimer, and release kinetics can be controlled by incorporating degradable linkages between the drug and the dendrimer. As example, Duncan and co-workers have prepared conjugates of PAMAM dendrimers with cisplatin, a potent anticancer drug with non-specific toxicity and poor water solubility [33, 34]. The conjugates show increased solubility, decreased systemic toxicity, and selective accumulation in solid tumors.

1.7. Stimuli-Responsive Nanocarriers

The drug encapsulation, delivery and selective drug release into the tumor tissues are very significant topics for targeted drug delivery systems. Stimuli-responsive materials can undergo relatively large and abrupt physical or chemical changes in response to external

stimuli in the environmental conditions [35]. Some of the external stimuli are physical like temperature, ionic strength, light, solvents, and strength of magnetic or electrical field while others are chemical such as pH-shift, redox microenvironment, enzyme over-expression, host-guest recognitions etc.

The general concept of triggered drug release from nanocarriers can be divided into two types according to the nature of the interaction between the drug molecule and the nanocarrier. In the encapsulation approach, the release can be triggered by structural change within the nanocarrier like backbone degradation or cleavage of shell while in chemical conjugation approach, the mechanism of drug release involves the separation of the linker between the nanocarrier and the drug molecule. Figure 1.15 shows the mechanisms of stimuli-responsive drug release from non-covalently and covalently conjugated nanocarriers.

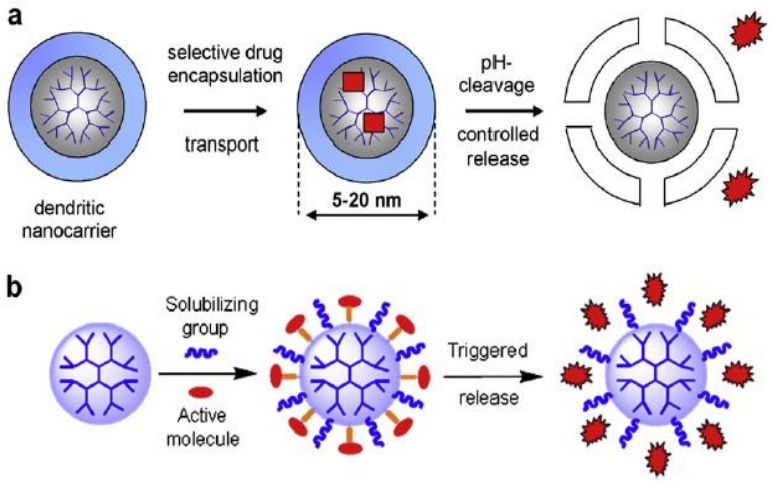

Figure 1.15. Different mechanisms for stimuli-responsive release of drug molecules: (a) from non-covalent complexes (b) from covalently conjugated architectures [35].

Gingras *et al*. have been reported some of the chemical linkers that respond to various stimuli such as photo-sensitive systems, thermo-responsive systems, pH-responsive systems, enzymatic stimuli and redox microenvironment for applications in biology, drug delivery, recyclable catalysis. Figure 1.16 shows these chemical entities which involve in stimuli-responsive cleavage [36].

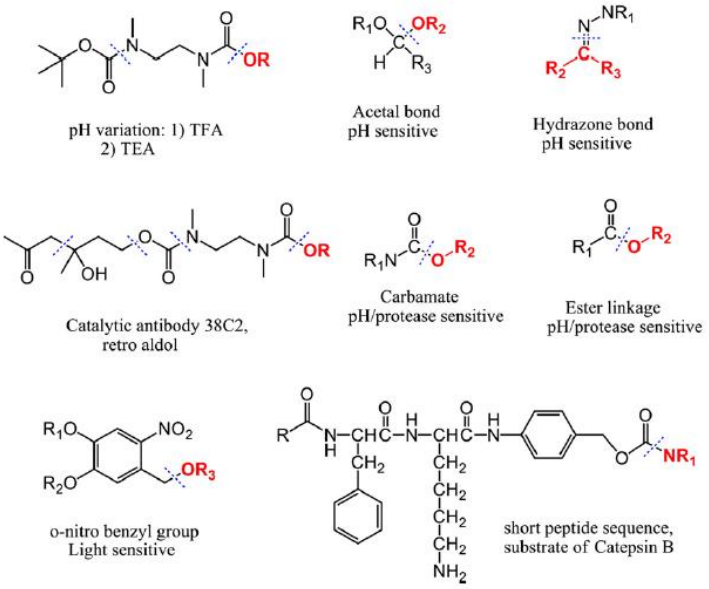

Figure 1.16. Chemical linkers involved in stimuli-responsive cleavage [36].

1.7.1. pH-Responsive Systems

The pH values of tumor tissues are significantly different from healthy tissues. The extracellular pH in solid tumors is more acidic (5.5) than the pH of the blood (7.4) at body temperature which means the extracellular and intracellular pH of tumor tissues are dramatically affected by diseases [37]. Therefore, the differences in pH could help the release profile of drug payload by a simple protonation of the nanocarrier structure or by the cleavage of acid-labile moieties.

Jin *et al*. have been reported a novel long circulating and pH-responsive PAMAM derivative, poly(2-(N,N-diethylamino)ethyl methacrylate) (PDEA) with methoxy-poly(ethylene glycol)-poly(amido amine) (PPD) as a nanocarrier for delivering an anticancer drug, 5-FU (5-fluorouracil), with very high encapsulation efficiency, tumor targeting and rapid release in more acidic tumor tissues (Figure 1.17). These dendrimer nanocarriers rapidly enter into the tumor tissues with the help of the EPR effect and due to the protonation of PDEA under acidic conditions, the hydrophobic block became hydrophilic which causes the release of drug payload from dendritic nanocarrier [38].

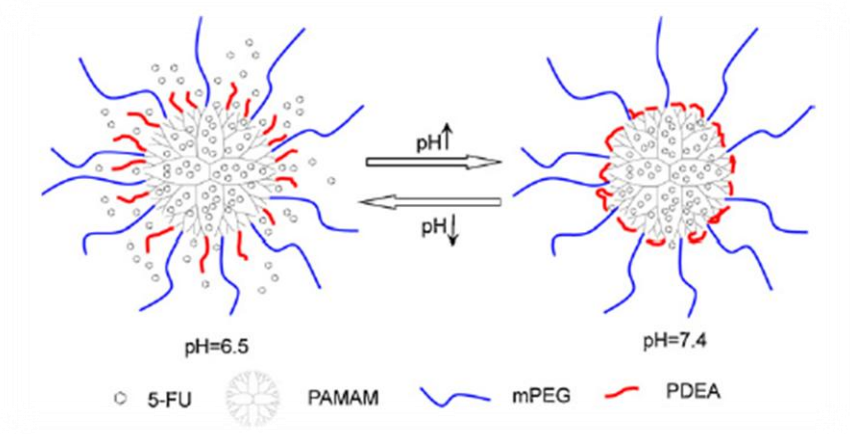

Figure 1.17. pH responsive PAMAM nanocarrier [38].

An alternative approach for triggering the drug release under acidic environment is the usage of pH-sensitive linkages such as hydrazones or acetals that degrade under acidic environment which will cause conformational changes of supramolecular aggregates. Fréchet *et al*. have been reported a new approach to the design of acid-sensitive micelles using PEO-polyester dendrimer. They synthesized linear-dendritic copolymers with hydrophobic acetal groups on the core-forming dendrimer block. Under acidic conditions like in solid tumors, hydrolysis of acid-sensitive acetal groups were observed; therefore, the core forming block became hydrophilic and destabilized the DOX loaded micelles. Due to the hydrolysis of acetal groups, DOX release rate from its encapsulating micellar compartment was also monitored [39].

1.7.2. Photo-Sensitive Systems

In recent years, an alternative approach for triggering the drug release is the utilization of light as an external stimulus. This way of drug release provides some advantages, including the ease of application, relative biocompatibility and controllability. The principle relies on the controllable release of encapsulated drug payload from the nanocarriers under the influence of light of specific frequency. For instance, Kim *et al*. reported a novel dendritic building block with photo cleavable units, nitro benzyl or azobenzene, that can self-assemble into a drug nanocarrier and undergo structural conformation under an external stimuli [40] (Figure 1.18).

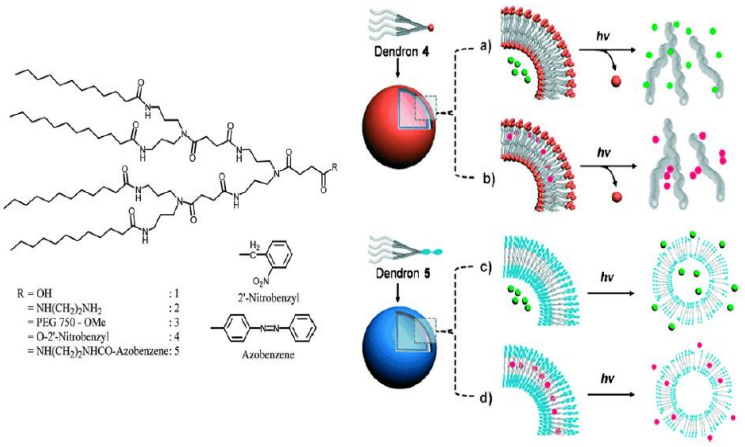

Figure 1.18. Dendritic block with photo cleavable units [40].

The controllable drug release can also be achieved by changing the time required for the irradiation. Dong *et al*. designed a novel class of Janus-type dendritic PAMAM amphiphiles with the help of click chemistry and they combined NIR-sensitivity and lectin binding properties on these macromolecules [41]. They controlled the rate of drug release by changing the time required for the irradiation (Figure 1.19).

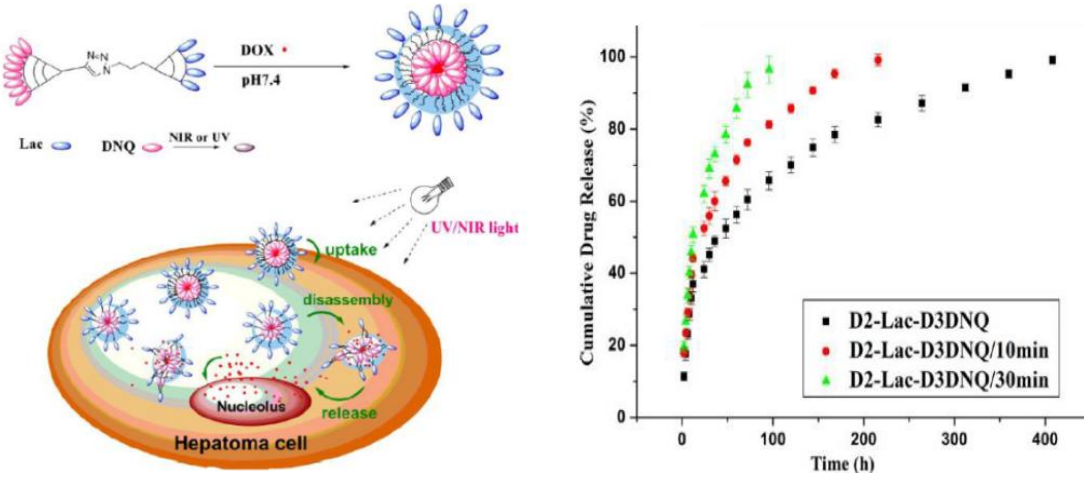

Figure 1.19. NIR-sensitive Janus type dendritic PAMAM and drug release [41].

1.7.3. Thermo-Sensitive Systems

Utilization of stimuli responsive drug delivery systems is a novel strategy for achieving controllable drug release. Among the stimuli responsive materials, temperature sensitive moieties have been widely used to trigger the drug release. Drug nanocarriers containing thermo-sensitive moieties provide various advantages. After the first synthesis

of thermo-sensitive dendrimer by McElhanon *et al.* [42], a significant amount of research was done in this field. For instance, Zhang *et al*. designed a novel thermo-sensitive star-shaped copolymers from poly(N-isopropylacrylamide) (PNIPAAm) segment and three hydrophobic poly(3-caprolactone) (PCL) arms [43]. These copolymers were able to self-assemble into nano-sized spherical micelles in water at temperature below LCST and hydrophobic MTX were loaded into the micellar core (Figure 1.20). The controlled drug release was achieved by the temperature-responsive phase transition of micelles which enables them good candidates for intelligent drug delivery systems.

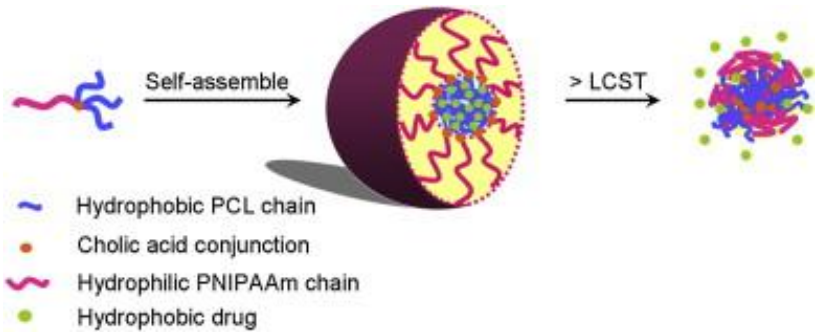

Figure 1.20. Thermo-sensitive star-shaped copolymers from PNIPAAm segment and three hydrophobic PCL arms [43].

1.7.4. Enzymatic Stimuli

Another attractive stimulus for targeted drug delivery systems is the enzymatic-stimuli. There are some common functional moieties that can be used as enzymatic responsive materials such as ester derived units or short peptide sequences which are substrates for various enzymes over-expressed in tumors. For instance, Calderon *et al*. designed a maleimide bearing prodrug of DOX from thiolated hyperbranched polyglycerol (PG) conjugated with either self-immolative para-aminobenzyloxycarbonyl (PABC) linker coupled to dipeptide Phe-Lys or the tripeptide D-Ala-Phe-Lys as the protease substrate [44]. Both of these prodrugs were cleaved by Cathepsin B which is an enzyme over-expressed by various types of malignant tumors. (Figure 1.21)

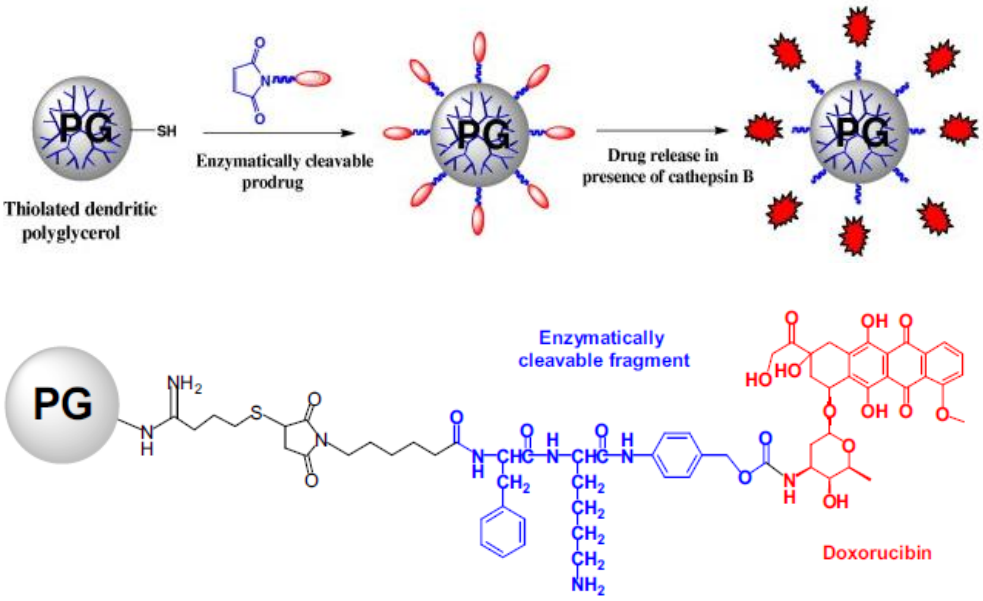

Figure 1.21. Enzymatic cleavable prodrugs derived from dendritic Polyglycerol [44].

2. AIM OF THE STUDY

Among various polymeric systems, amphihilic block copolymers with stimuli-responsive moities provides significant advantages in drug delivery systems due to their unique self-assemble properties which provide interiors that can encapsulate the guest molecules like anti-cancer drugs. The triggered release of these guest molecules can also be obtained by external stimuli while minimizing the adverse side effects of the therapeutic agent. In this thesis, dendron-linear polymer-dendron conjugates are synthesized via Huisgen type “click” reaction using biodegredable polyester dendron and biocompatible PEG. Functionalization of the dendron surface with hydrophobic moiety, which provides pH-sensitivity, increased the tendecy to form micellar structures in water via self-assembly.

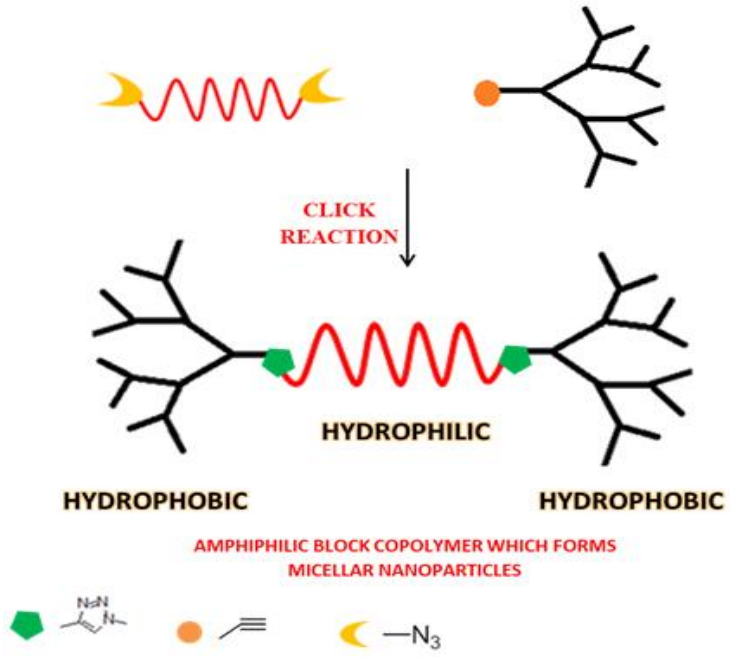

Figure 2.1. General representation of amphiphilic block copolymers.

To achieve more stable micelles for drug delivery applications, the length of hydrophilic polymer, the type of acetal moiety and the generation of the dendron were changed to find the optimum micellar nanoparticle. The stability of these micellar structures at neutral pH was shown by the release rate of the hydrophobic dye and the most stable copolymer system choose for further drug loading studies. [G4]-[PEG6K]-[G4]

micelles were phsically encapsulated with anti-cancer therapeutic agent (CA-4) by co-solvent evaporation method and the drug release period was monitored. As expected, the drug nanocarrier carried all its payload at neutral pH, while destabilizing the micellar structure and releasing its drug payload under acidic conditions like in the solid tumor tissues.

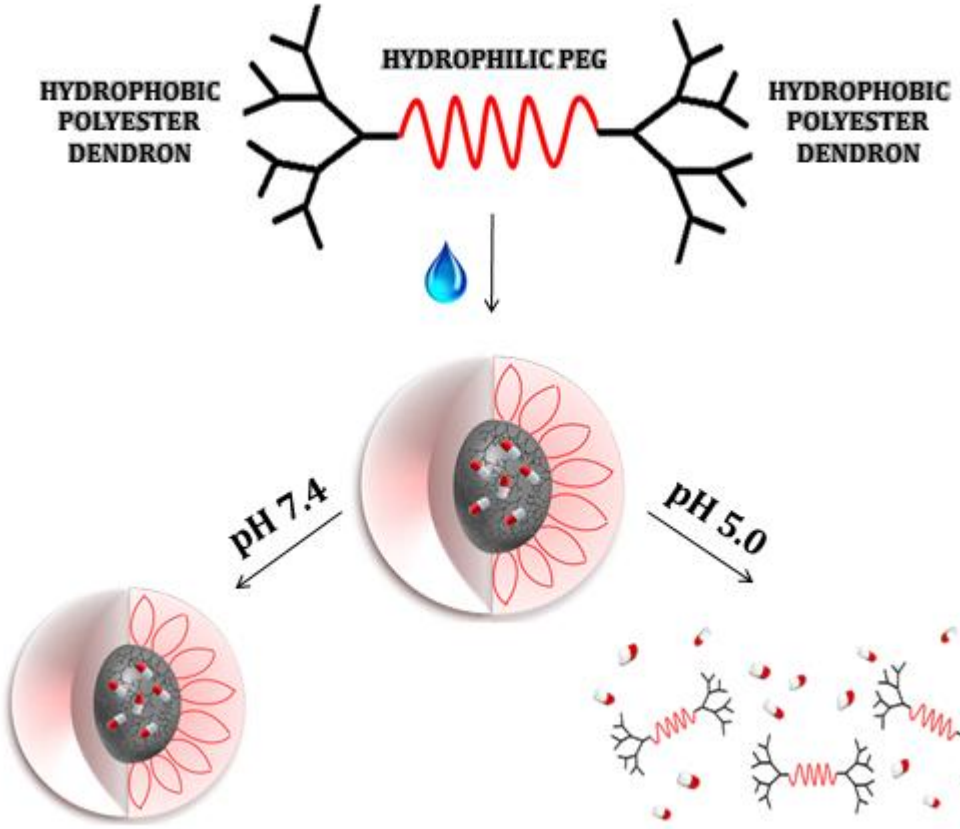

Figure 2.2. Schematic representation of self-assembly of dendron-linear polymer-dendron conjugate, drug loading and release profile.

3. RESULTS AND DISCUSSION

3.1. Synthesis of Dendron-Linear Polymer-Dendron Conjugates via Click Chemistry

In this project, dendron-linear polymer-dendron tri-block copolymers with dumbbell topology were successfully synthesized by using click chemistry. As illustrated in Figure 3.1, first the hydrophobic dendritic blocks with alkyne focal unit synthesized, then hydrophilic polymer block functionalized with azide units followed by the conjugation of the hydrophobic and hydrophilic block to form dendron-linear polymer-dendron conjugates.

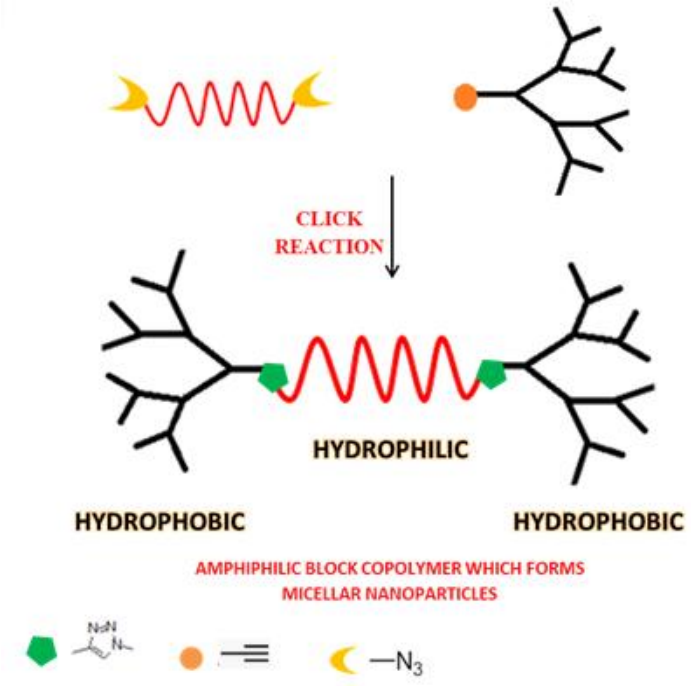

Figure 3.1. Schematic representation of formation of amphiphilic dendron-linear polymer-dendron conjugates.

Different generations of polyester dendrons (G3, G4) with several pH-sensitive acetal groups were conjugated with various lengths of biocompatible PEG via Huisgen type [3+2] cycloaddition reaction in the presence of Cu(I)Br. To achieve the most stable micellar structure that can encapsulate the effective dose of therapeutic agent at neutral pH,

four different amphiphilic copolymers were synthesized by varying the length of hydrophilic polymer, generation of the polyester dendron and type of the acetal moiety. The conjugates are named according to the generation of the dendron used, type of acetal unit and the length of polymer chain, for instance, [G4]-[PEG6K]-[G4] micelles indicate the fourth generation polyester dendron clicked with 6K PEG diazide (Figure 3.2a) or [G3]-[Bn]-[PEG6K]-[G3]-[Bn] micelles indicate the third generation dendron with acetal groups clicked with 6K PEG diazide (Figure 3.2b).

a

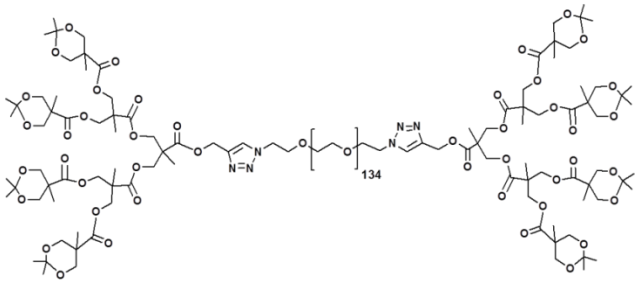

b

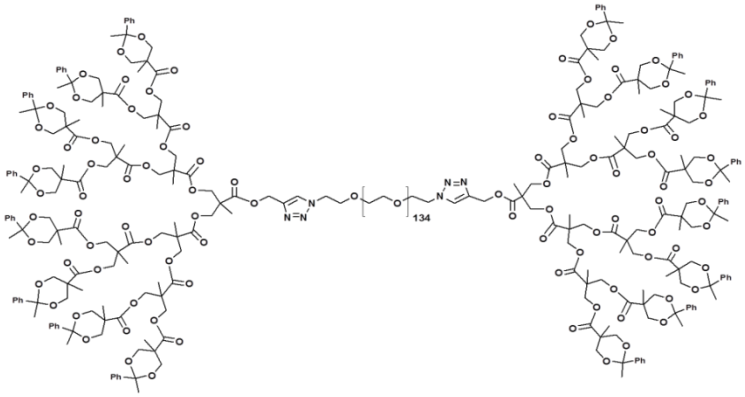

c

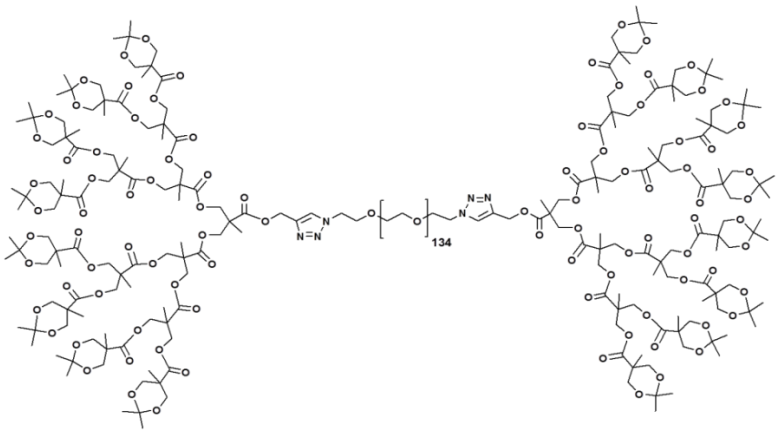

Figure 3.2. Representations of (a) [G3]-[PEG6K]-[G3], (b) [G3]-[Bn]-[PEG6K]-[G3]-[Bn], (c) [G4]-[PEG6K]-[G4].

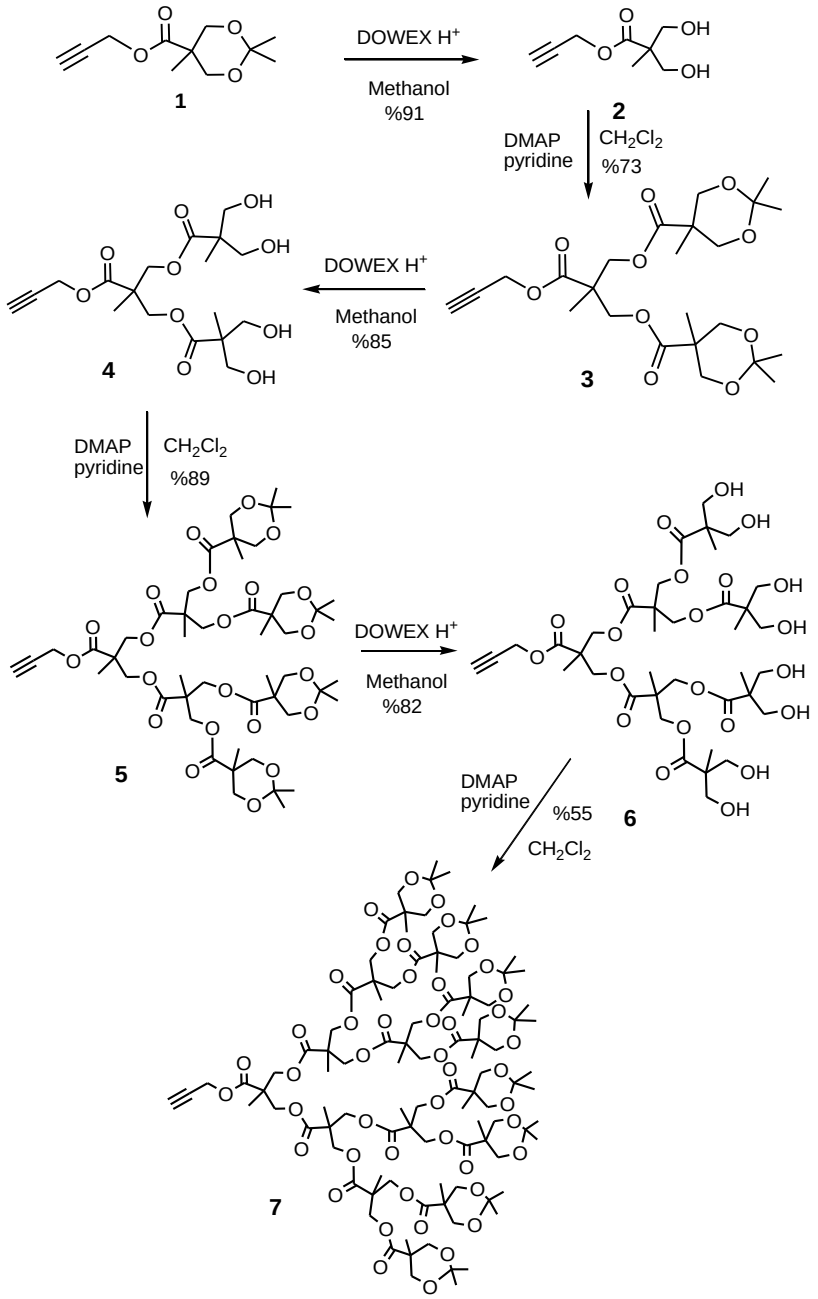

Figure 3.3. Synthesis of polyester dendrons.

Various generations of polyester dendrons **1**, **3**, **5** and **7** with propargyl focal units were synthesized according to the literature [45]. The synthesis approach of dendritic block is based on a biocompatible building block, Bis-MPA. After the successful access of first generation polyester dendron with alkyne focal unit, removal of the acetonide protecting groups and acylation with the resulting anhydride provide the growth of the dendritic block (Figure 3.3). Functionalization of the resulting third generation dendron surface with

hydrophobic moieties increases the tendecy to form micellar structures. Hence, after the deprotection of the acetonide units by DOWEX, dendrons with alcohol units at the periphery (**6)** can be functionalized with additional generation of polyester dendron (**7**) or acetal moieties (**12**).

All the synthesized products were characterized by FT-IR and ^{1}H NMR, where the functional group changes can be tracked easily. As illustrated in Figure 3.4, after the deprotection of the acetonide groups of **5** by the treatment with DOWEX, H^{+}, the characteristic broad peak of the hydroxyl groups on the dendron appears at 3319 cm^{-1}.

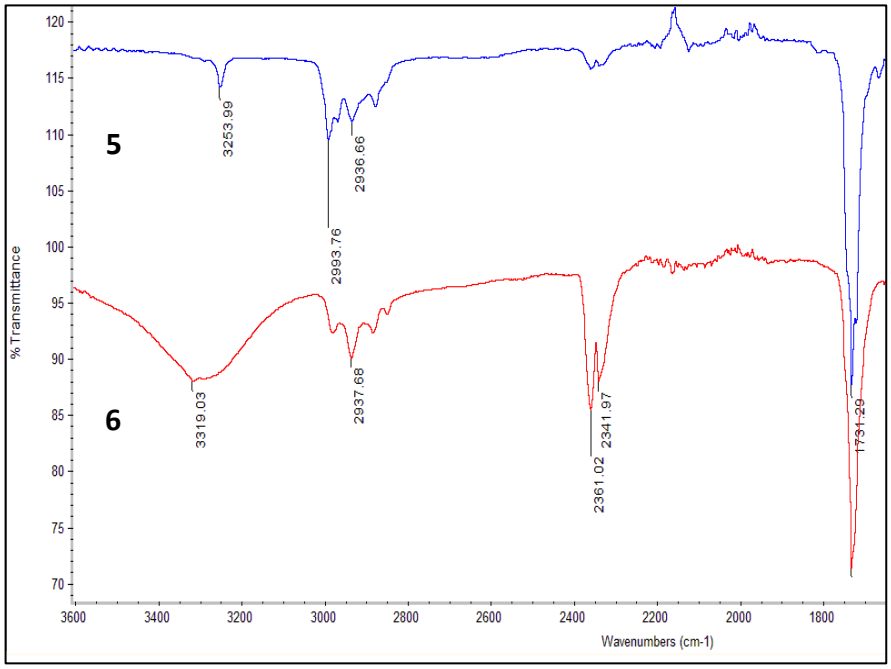

Figure 3.4. FT-IR spectrum of 5 and 6.

The proton assignments of dendron **5** and **6** from ^{1}H NMR is shown by Figure 3.5. For both dendrons (**5**, **6**) the alkyne unit H_a shows a triplet at 2.51 and 2.99 ppm, respectively. A doublet near 4.72 ppm belongs to the H_b and the $–CH_3$'s namely H_c, H_e and H_g shows 3 singlets at 1.27, 1.26, 1.12 ppm, respectively. The protons namely H_{f1} and H_{f2} show different chemical shift behaviors since one of them is in axial position and the other one is in equatorial position. Therefore, these protons appear at different ppm values and split each other. After the deprotection, the $–CH_3$'s namely H_h of dendron **5** at 1.38 and 1.33 completely disappears due to the removal of the acetonide.

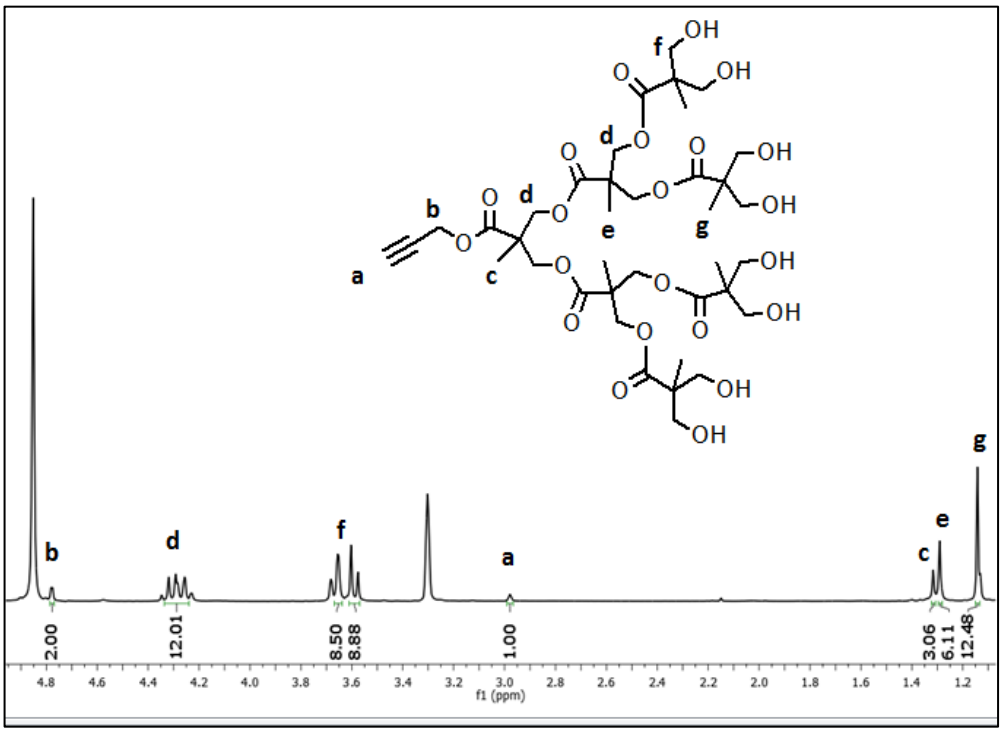

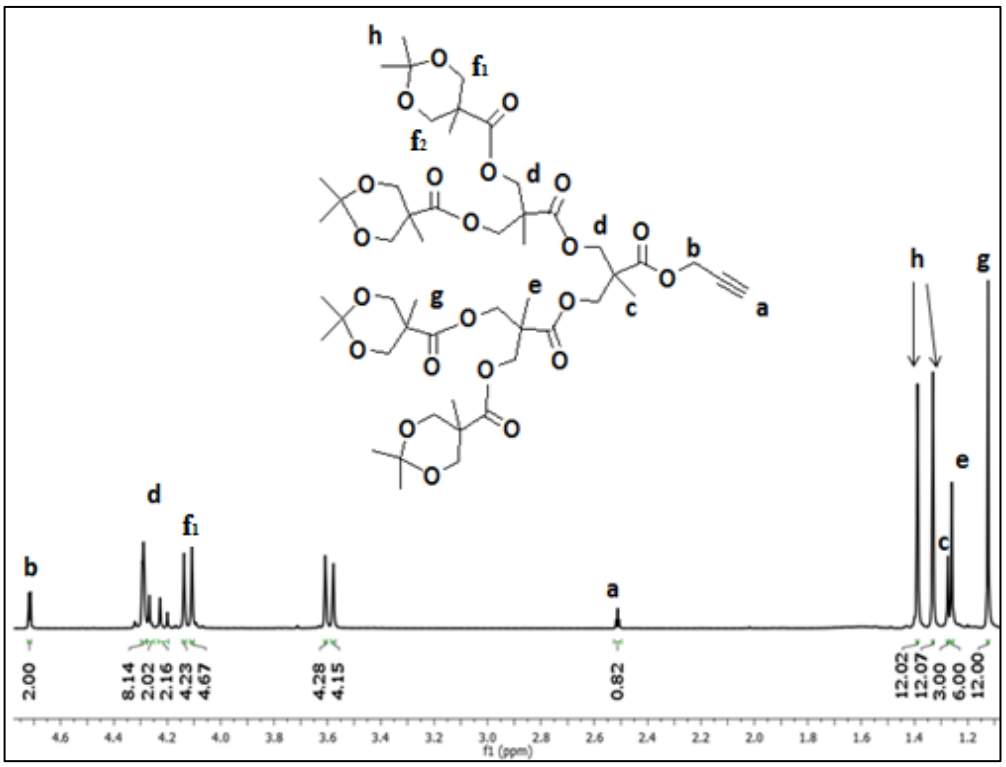

Figure 3.5. ^{1}H NMR spectrum of 5 and 6.

In order to functionalize the periphery of the dendron **6** with additional hydrophobic moieties, fourth generation of same polyester dendron was synthesized by the reaction of **6** with corresponding anhydride, DMAP and pyridine in CH_2Cl_2. As illustrated in Figure 3.6, after acylation of all hydroxyl groups, the characteristic broad peak of the hydroxyl units at 3319 cm^{-1} completely disappear. The proton assignment from ^1H NMR also demonstrates the formation of the new generation dendron (Figure 3.7). The alkyne unit H_a shows a triplet at 2.99, a doublet near 4.72 ppm belongs to the H_b and the $–CH_3$'s namely H_c and H_d shows 2 singlets at 1.27 and 1.14 ppm, respectively. The $–CH_2$'s namely H_d is present at 4.27 ppm as a multiplet. After the acetylation reaction, the new$–CH_3$'s belongs to the fourth generation of dendron namely H_e appears as 2 singlets at 1.40 and 1.34 ppm and the new $–CH_2$'s namely H_g appears as 2 doublets at 4.14 and 3.61 ppm. The MALDI-TOF spectrum of **7** also demonstrates the formation of the next generation of the dendron, successfully. As illustrated in Figure 3.8, the MALDI-TOF spectrum gives the exact molecular weight of **7** as calculated.

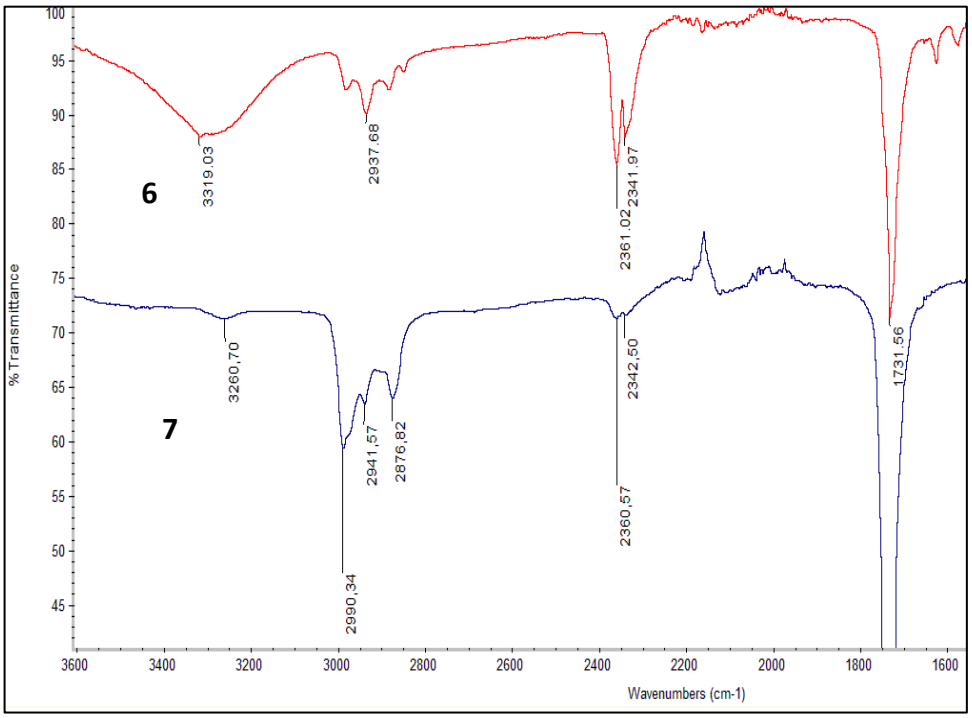

Figure 3.6. FT-IR spectra of 6 and 7.

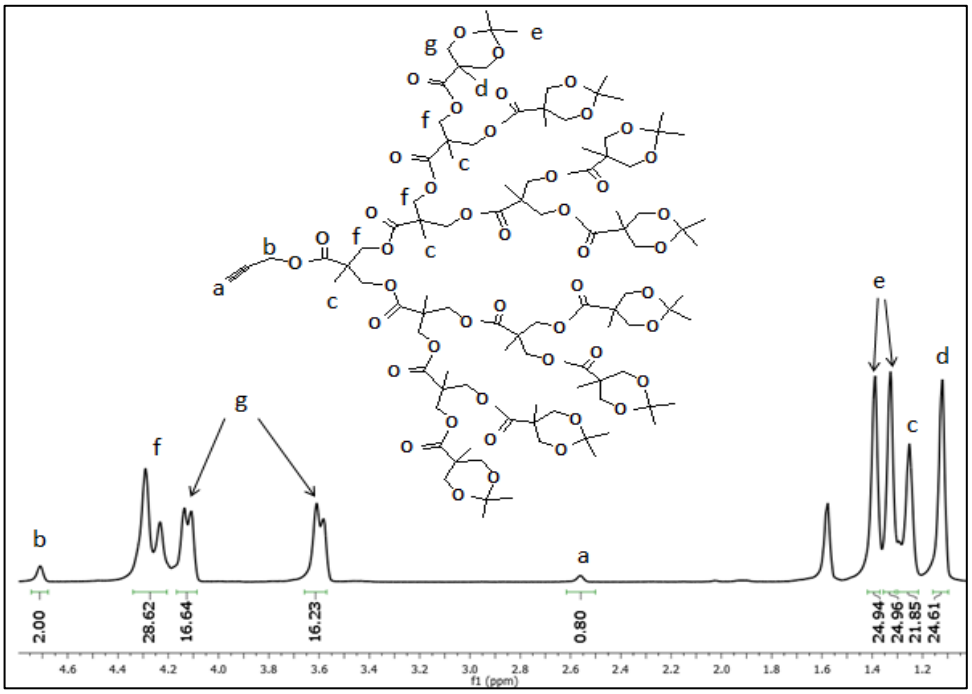

Figure 3.7. ^{1}H NMR spectrum of 7.

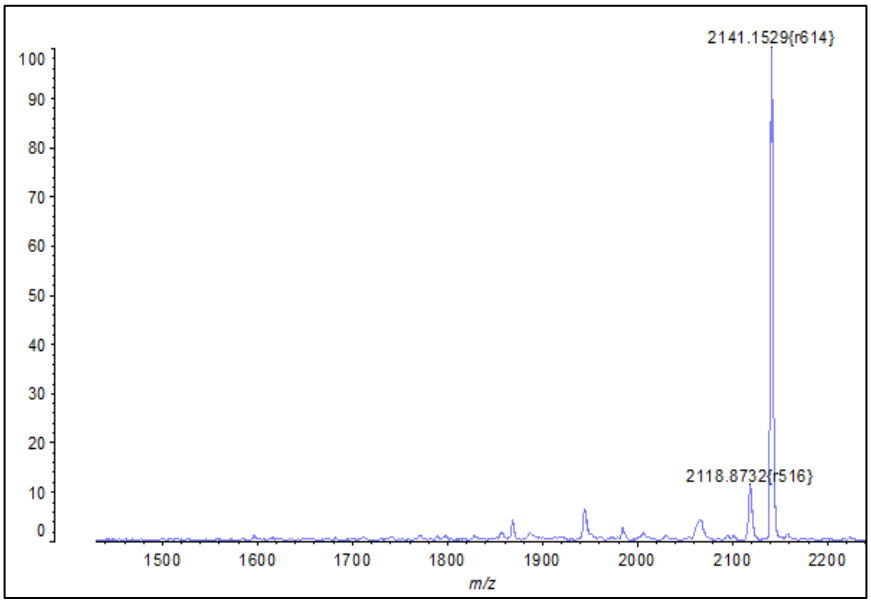

Figure 3.8. MALDI-TOF spectrum of 7.

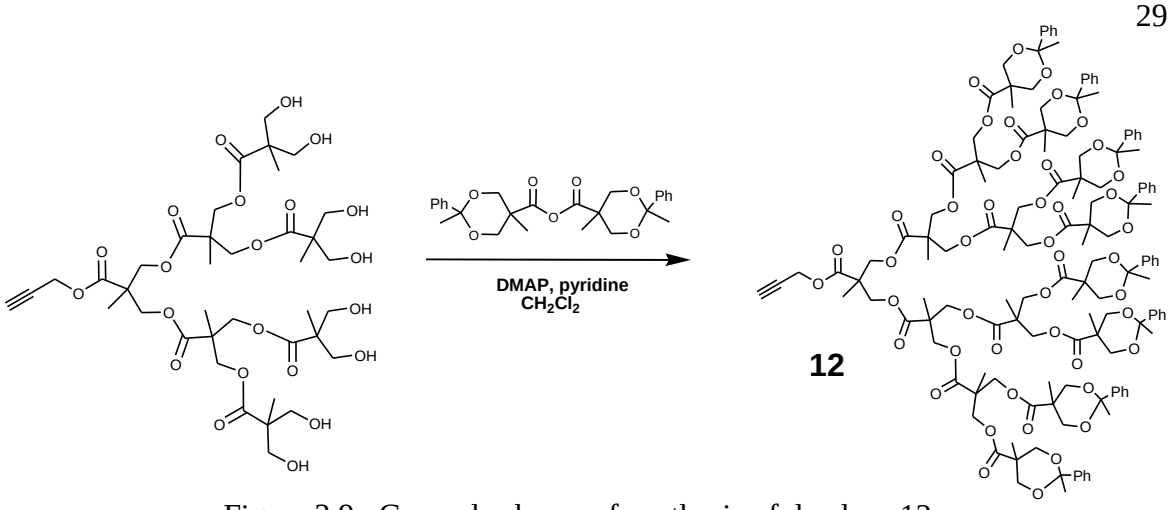

Figure 3.9. General scheme of synthesis of dendron 12.

In order to change the acetal units at the periphery of dendron **5** to more hydrophobic acetal moieties, simple benzylidene acetal groups were used (Figure 3.9). After the acetylation reaction of **6** with corresponding anhydride, DMAP and pyridine in CH_2Cl_2, the characteristic broad peak of the hydroxyl units at 3319 cm^{-1} completely disappear (Figure 3.10).

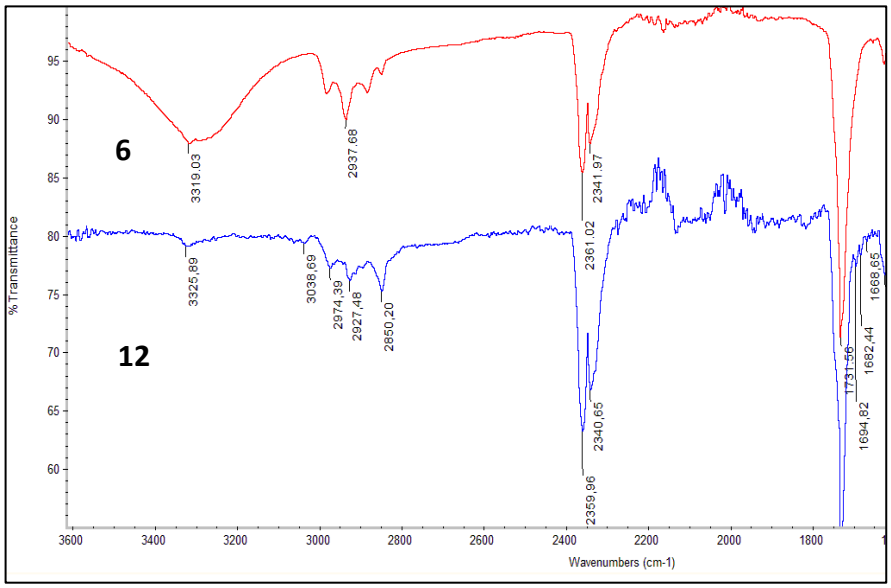

Figure 3.10. FT-IR spectra of 6 and 12.

The proton assignment from ^{1}H NMR also demonstrates the formation of the new generation dendron with benzylidene acetal units at the periphery (Figure 3.11). The proton assignment from ^{1}H NMR also demonstrates the formation of the new generation of dendron with benzylidene acetal units at the periphery (Figure 3.7). The alkyne unit H_a

shows a triplet at 2.45 ppm and a doublet near 4.73 ppm belongs to the H_b. After the acetylation reaction, the new protons belong to the aromatic rings at 7.40-7.25 ppm demonstrates the formation of dendron 12.

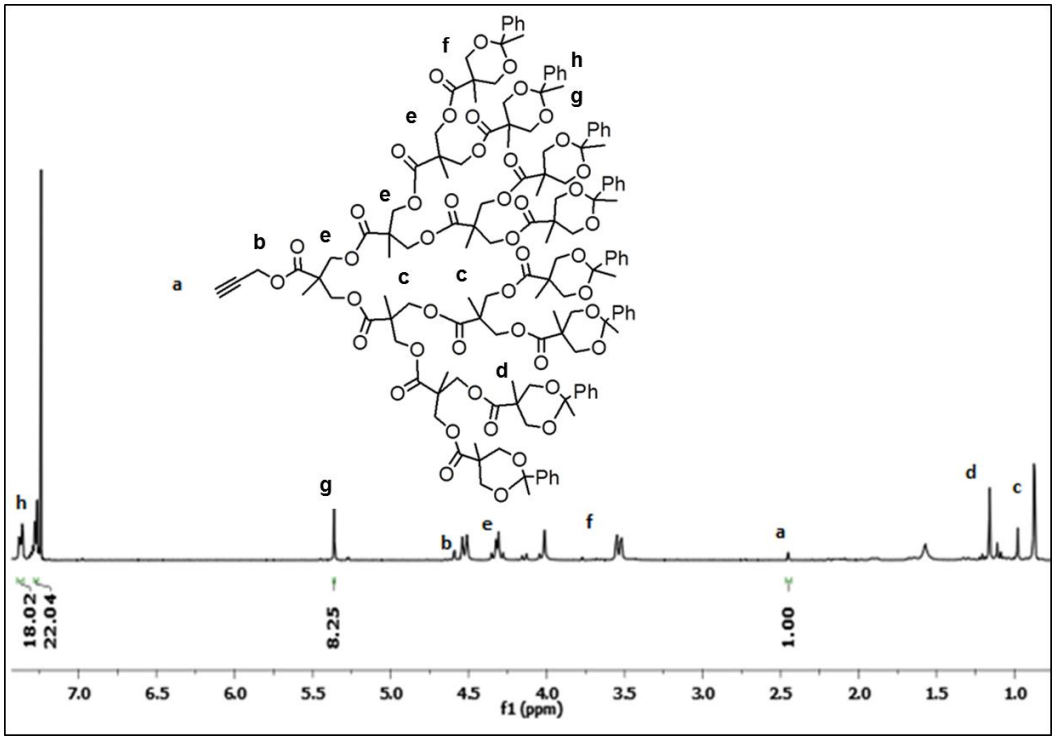

Figure 3.11. ^{1}H NMR spectrum of 12.

In order to obtain the hydrophilic segment of dendron-linear polymer-dendron conjugates, PEG was used as a biocompatible water soluble polymer. Different lengths of bifunctional azide terminated PEG (N_3-PEG-N_3) was synthesized by the reaction of PEG diols with MsCl followed by the reaction with NaN_3 (Figure 3.12). After the functionalization of polymer block with azide units, characterization was done by FT-IR and ^{1}H NMR. As illustrated in Figure 3.13, both N_3-PEG 6K-N_3 (**10**) and N_3-PEG 10K-N_3 (**11**) show a sharp peak at 2093 cm^{-1} and 2101 cm^{-1} due to the C-N bond stretching which indicates the successful azide functionalization of PEG diols. From the ^{1}H NMR of bisazido-PEG 6000 Da, just $–CH_2$ near nitrogen at 3.37 ppm and the –CH2's of PEG at between 3.4-3.8 ppm are present (Figure 3.14).

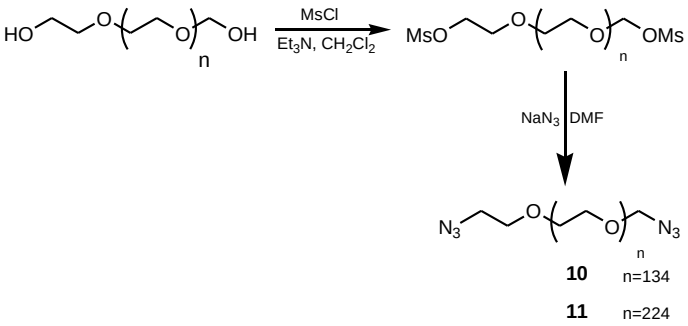

Figure 3.12. General scheme of the synthesis of PEG diazide.

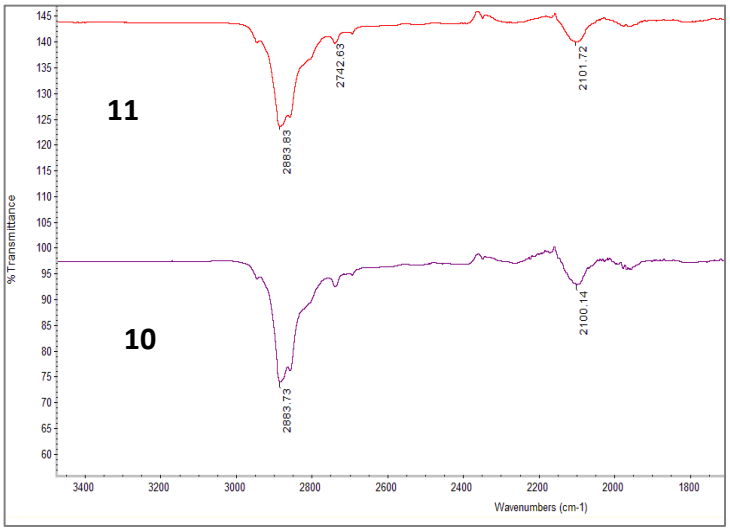

Figure 3.13. FT-IR spectra of 10 and 11.

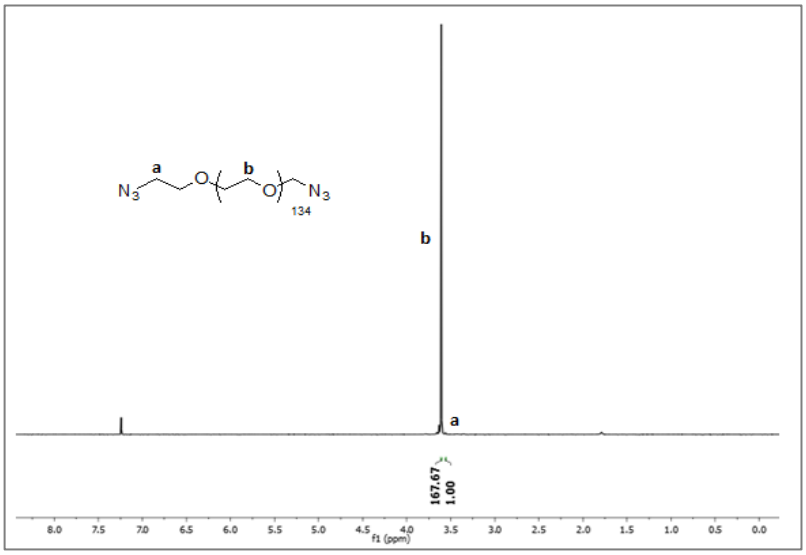

Figure 3.14. ^{1}H NMR spectrum of 10.

In order to obtain amphiphilic dendron-linear polymer-dendron conjugates, Huisgen type of [3+2] cycloaddition reaction was used. Via the reaction of the alkyne unit at the focal point of the dendron and the azide units of the polymer, in the presence of Cu(I)Br and PMDETA at 37^{o}C in THF, ABA block copolymers with various polymer lengths, acetal groups and generations were synthesized.

The first amphiphilic block copolymer composed of a 10000 MW bifunctional azide-terminated PEG (**11**) as a hydrophilic block and third generation polyester dendritic block (**5**) with acetal units as a hydrophobic block (Figure 3.15). On the basis of FT-IR analysis, it is demonstrated that the dendron-linear polymer-dendron conjugates were successfully synthesized via click reaction. The comparison of FT-IR spectra of dendron **(5)**, polymer **(11)** and dendron- linear polymer-dendron conjugate **(13)** shows that the azide functional groups of polymer and alkyne focal unit of dendron completely disappear which indicates the formation of triazole ring during the click reaction. According to the Figure 3.13, the FT-IR spectrum of third generation polyester dendron (**5**) shows the alkyne functionality through the peak at 3263 cm^{-1} and the N_3-PEG 10K-N_3 (**11**) shows a sharp peak at 2100 cm^{-1} due to the C-N bond stretching (Figure 3.16). After the click reaction, conjugation of the azide unit of polymer block and the alkyne unit of the dendritic block forms a triazole ring to obtain ABA type of triblock copolymer [G3]-PEG10K-[G3] (**13**). As expected, after the conjugation the characteristic peaks of azide and alkyne units completely disappeared which indicates the successful conjugation.

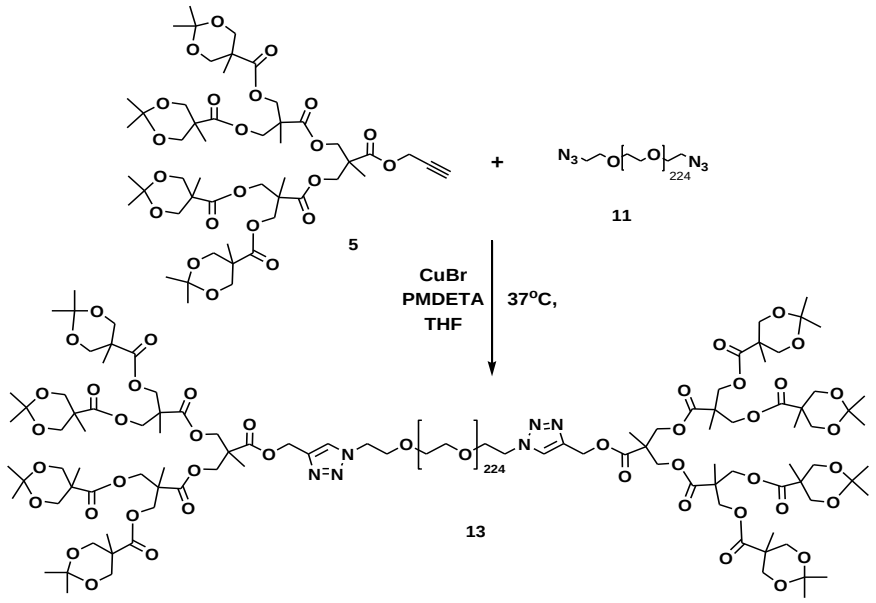

Figure 3.15. General scheme for the synthesis of the [G3]-PEG10K-[G3] conjugates.

After the Huisgen type of click reaction between dendron **5** and polymer **11**, 1,4-triazole formation occurs between the alkyne core of dendron and N_3 ends of PEG. This triazole proton can be observed from the ^1H NMR of dendron-linear polymer-dendron conjugates as a singlet at 7.84 ppm (Figure 3.17). Dendron **5** and polymer **11** preserve the characteristic proton shifts on NMR spectrum, except the triplet at 2.51 ppm which belongs to the alkyne focal unit of the dendron **5**. Also the terminal 2Hs near –O-OC of dendron shift to 5.23 (peak d) ppm from 4.75 ppm after the conjugation because its position changed to a deshielded field.

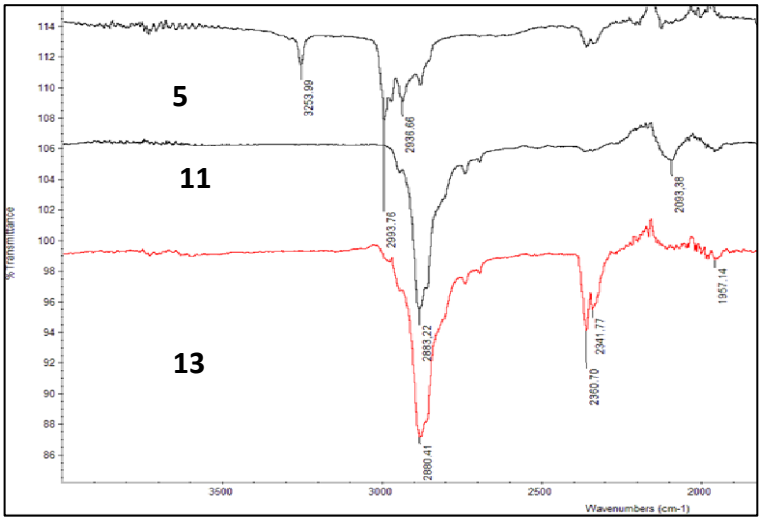

Figure 3.16. FT-IR spectra of 5, 11 and 13.

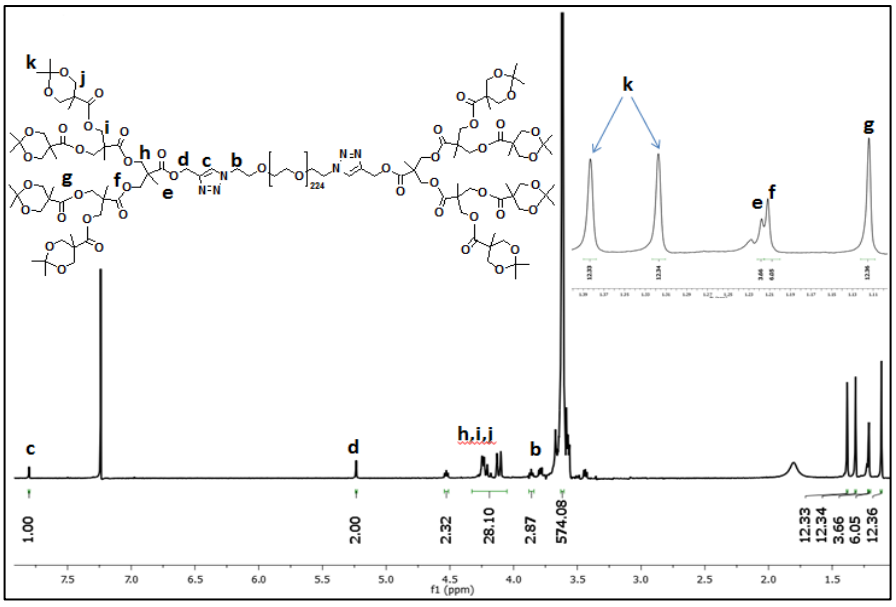

Figure 3.17. ^1H NMR spectrum of 13.

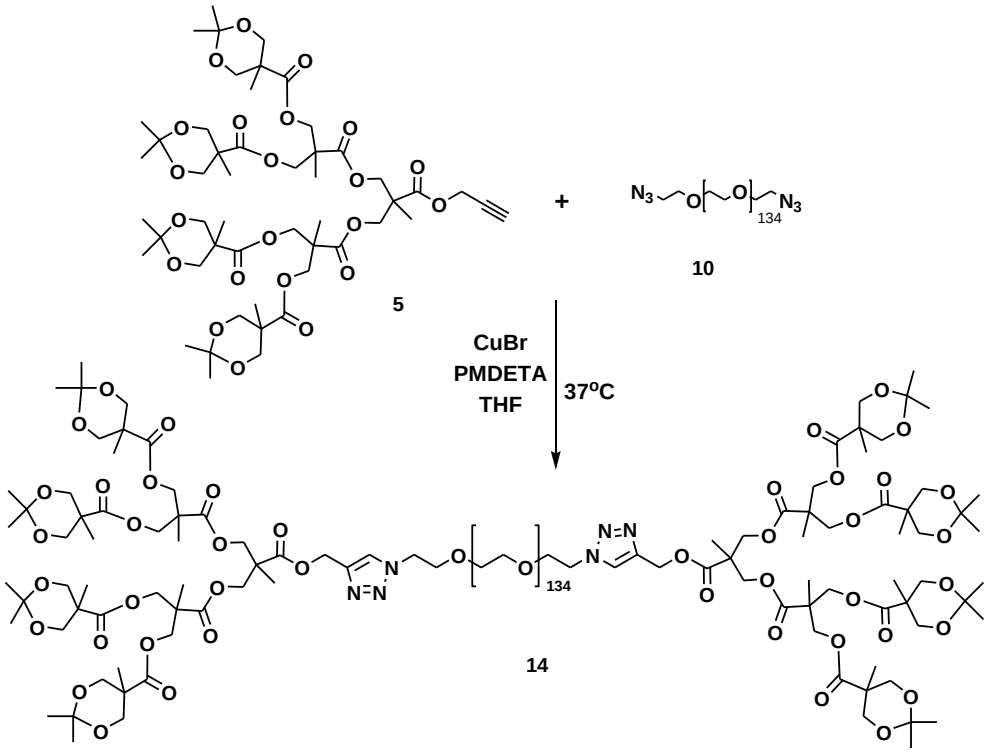

Figure 3.18. General scheme for the [G3]-PEG6K-[G3] conjugates.

The same changes on FT-IR measurement were observed for the conjugates composed of 6000 MW bifunctional azide-terminated PEG (N_3-PEG6K-N_3) (**10**) as a hydrophilic block and third generation polyester dendritic block (**5**) with acetal units as a hydrophobic block (Figure 3.18). The characteristic peak of azide unit due to the C-N stretching at 2093 cm^{-1} and the alkyne functionality through the peak at 3253 cm^{-1} completely disappear after the click reaction of **5** and **10** which demonstrates the success of conjugation (Figure 3.19). The same changes on ^1H NMR measurement were also observed for the dendron **5** and polymer **10.** These molecules preserve the characteristic proton shifts on NMR spectrum, except the triplet at 2.51 ppm which belongs to the alkyne focal unit of the dendron **5**. Also the terminal 2Hs near –O-OC of dendron shift to 5.23 (peak d) ppm from 4.73 ppm after the conjugation because its position changed to a benzylic position that result in a deshielded field.

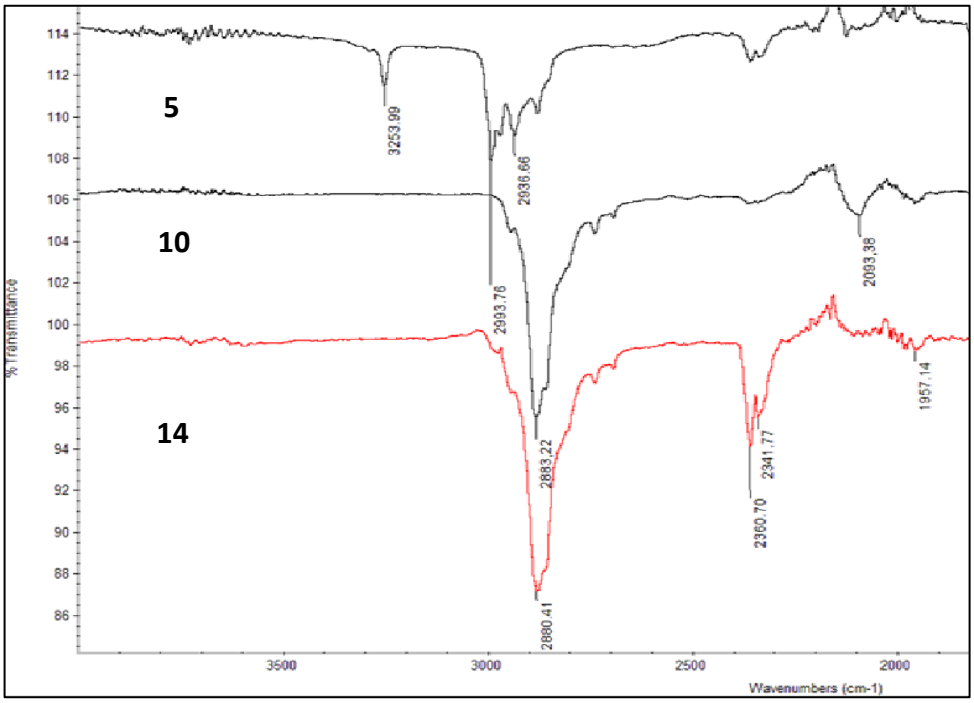

Figure 3.19. FT-IR spectra of 5, 10 and 14.

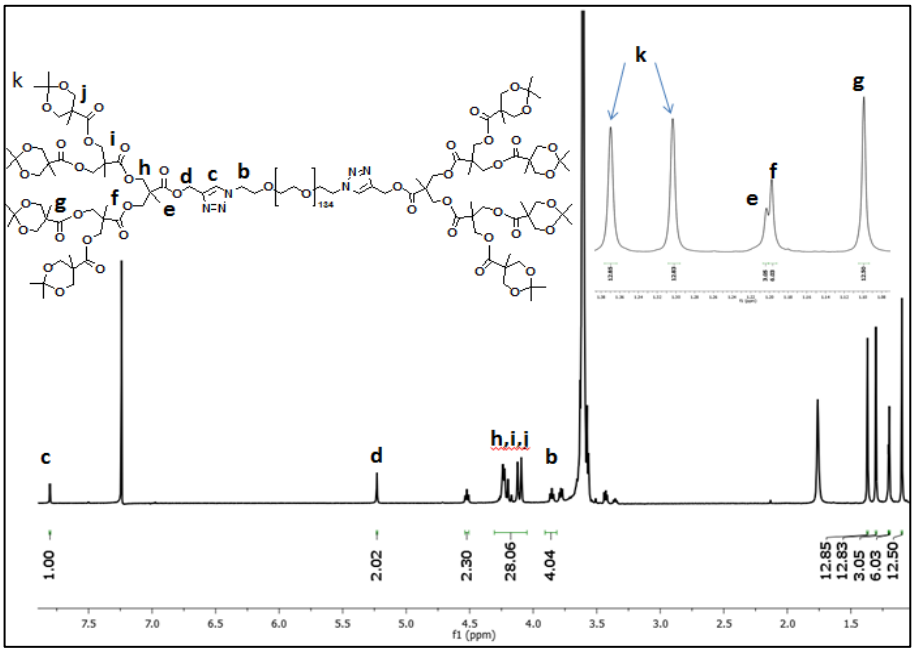

Figure 3.20. ^{1}H NMR spectrum of 14.

The third amphiphilic block copolymer composed of a 6000 MW bifunctional azide-terminated PEG (N_3-PEG6K-N_3) (**11**) as a hydrophilic segment and third generation polyester dendritic block (**12**) with acetal units as a hydrophobic block (Figure 3.21). On the basis of FT-IR analysis, it is demonstrated that the dendron-linear polymer-dendron conjugates were successfully synthesized via click reaction. The comparison of FT-IR spectra of dendron, polymer and dendron-linear polymer-dendron conjugate shows that the azide functional groups of polymer and alkyne focal unit of dendron completely disappeared and a new stretching formed which indicates the formation of triazole ring during the click reaction. According to the Figure 3.22, the FT-IR spectrum of dendron (**12**) shows the alkyne functionality through the peak at 3325 cm^{-1} and the N_3-PEG 6K-N_3 (**11**) shows a sharp peak at 2101 cm^{-1} which indicates the characteristic peak of azide functional group due to the C-N bond stretching. As expected, after the click reaction both the peaks belonging to alkyne and azide units completely disappeared which indicates the formation of [G3]-[Bn]-[PEG6K]-[G3]-[Bn] conjugates (**15**).

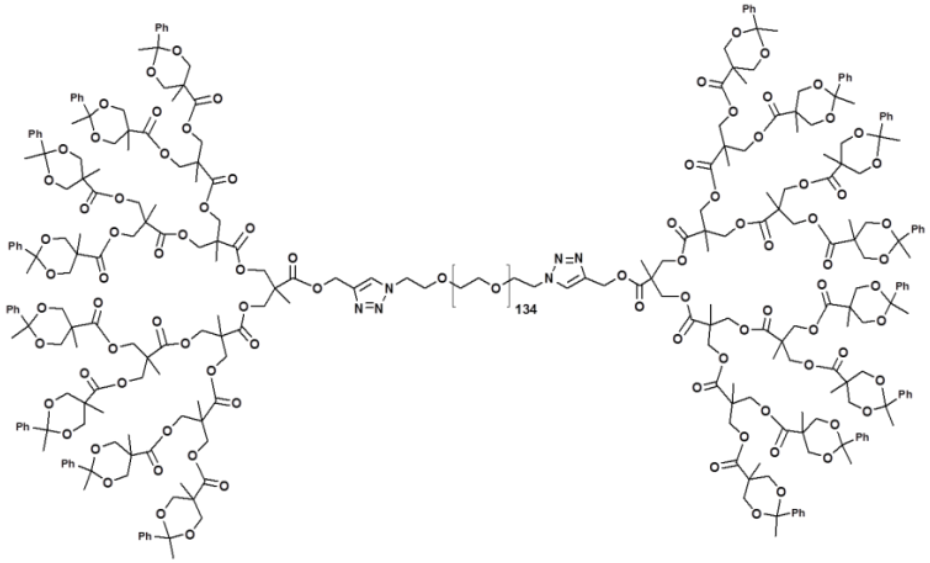

Figure 3.21. Representation of [G3]-[Bn]-[PEG6K]-[G3]-[Bn] conjugate.

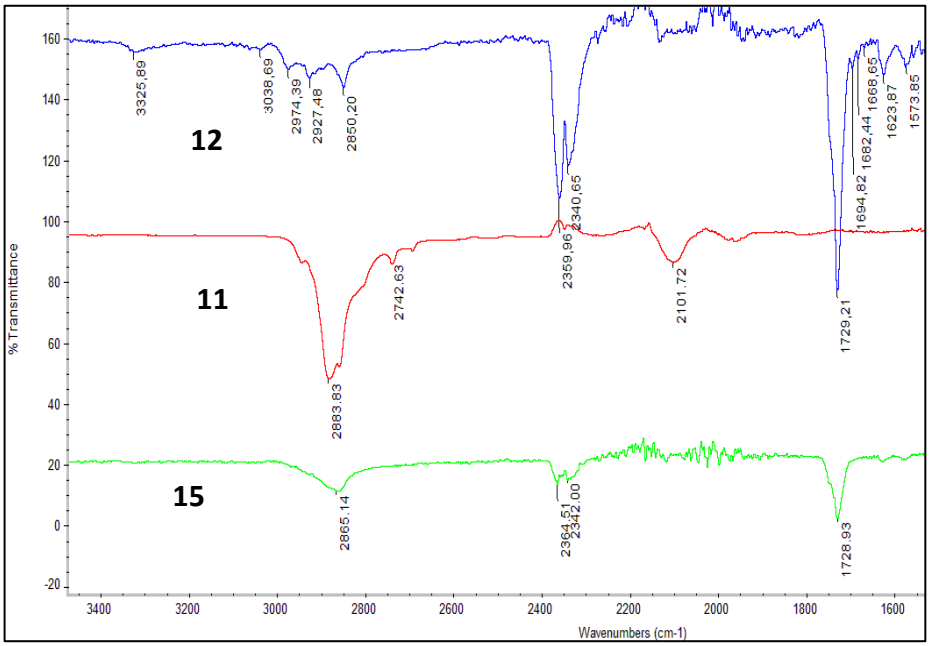

Figure 3.22. FT-IR spectra of 11, 12 and 15.

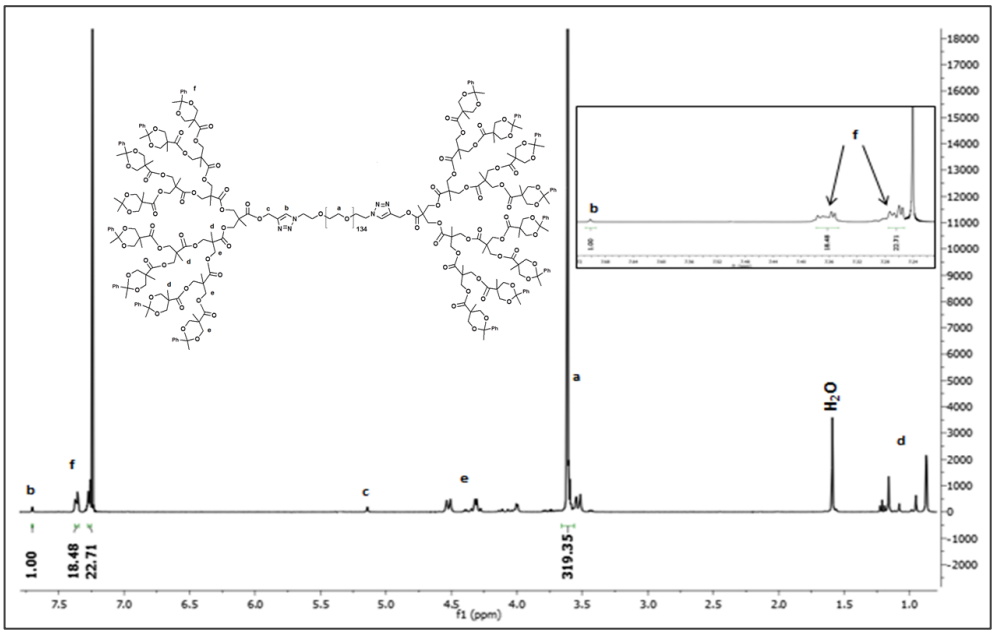

Figure 3.23. ^{1}H NMR spectrum of 15.

The last amphiphilic block copolymer composed of a 6000 MW bifunctional azide-terminated PEG (**11**) as a hydrophilic block and fourth generation polyester dendritic block (**7**) with acetal units as a hydrophobic block (Figure 3.24). The same changes on FT-IR measurement were observed for the [G4]-PEG6K-[G4] conjugates. According to the Figure 3.25, the FT-IR spectrum of fourth generation polyester dendron (**7**) shows the alkyne functionality through the peak at 3263 cm^{-1} and the polymer (**10**) shows a sharp peak at 2095 cm^{-1} which shows the characteristic peak of azide functional group due to the C-N bond stretching. As expected, after the click reaction, conjugation of the azide unit of the polymer block and the alkyne unit of the dendritic block form a triazole ring to obtain [G4]-PEG6K-[G4] (**16**) conjugate which causes the disappearance of the alkyne and azide peaks.

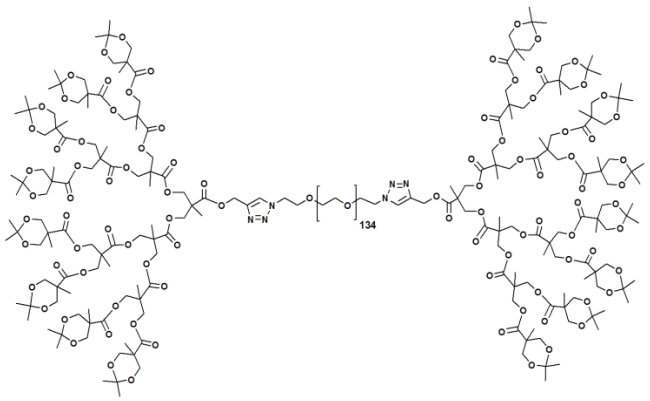

Figure 3.24. Representation of [G4]-PEG6K-[G4] conjugate.

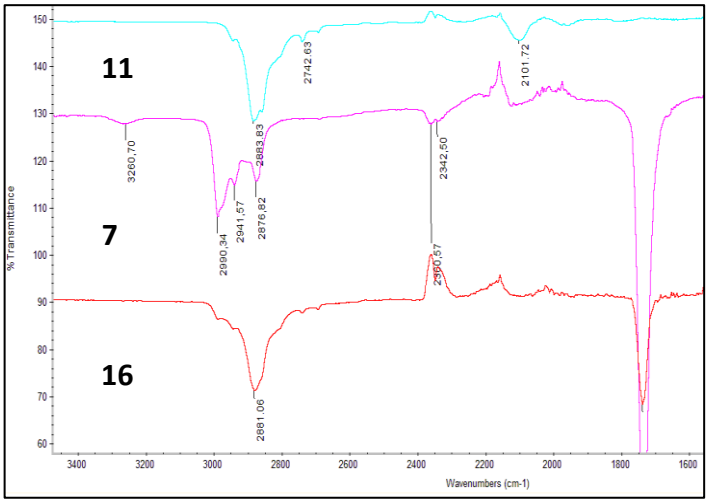

Figure 3.25. FT-IR spectra of 7, 11 and 16.

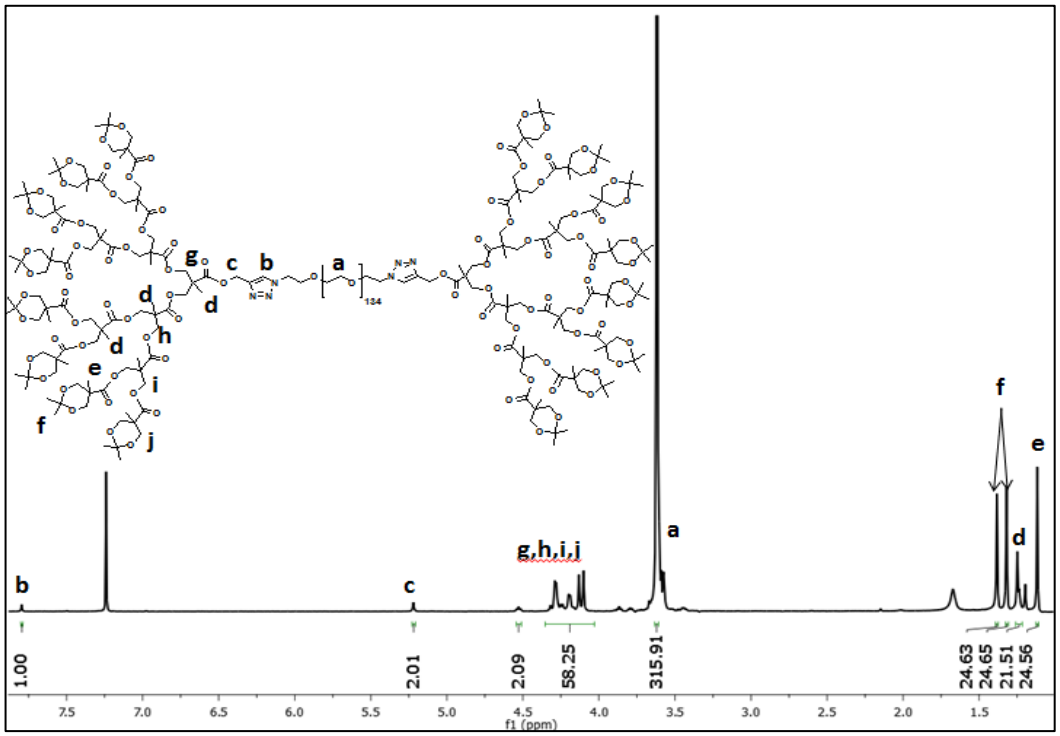

Figure 3.26. ^{1}H NMR spectrum of 16.

As illustrated in Figure 3.26, the success of click reaction between dendron **7** and polymer **10** can also be charactezied by ^{1}H NMR. After the conjugation, dendron **5** and polymer **10** preserve the characteristic proton shifts on NMR spectrum, except the triplet at 2.51 ppm which belongs to the alkyne focal unit of the dendron **5**. Also the terminal 2Hs near -O-OC of dendron shift to 5.20 (peak c) ppm from 4.72 ppm after the conjugation because its position changed a benzylic position that result in a deshielded field.

3.2. Micelle Formation of Dendron-Linear Polymer-Dendron Conjugates

The amphiphilic nature of the dendron-linear polymer-dendron conjugates are composed of hydrophilic linear PEG and hydrophobic dendritic blocks which provides an opportunity to form flower-like micellar aggregates in aqueous phase (Figure3.27). The formation of these flower-like micelles from amphiphilic dendron-linear polymer-dendron conjugates was monitored by using fluorescence technique, dynamic light scattering (DLS) and scanning transmission electron microscopy (STEM).

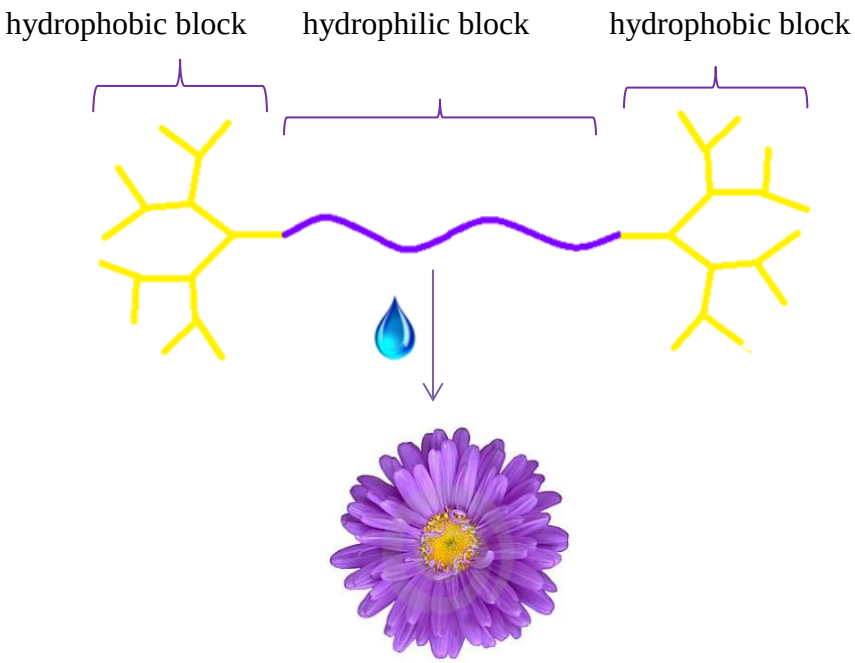

Figure 3.27. Schematic representation of ABA triblock copolymer and self-assembled micellar structure.

3.2.1. Fluorescence Measurements

As a Fluorescent probe, a hydrophobic dye, pyrene, was used. The excitation spectra of pyrene have a characteristic feature that is the shift of band (0,0) from 334 to 338 nm due to the pyrene partition in the micellar hydrophobic core. Therefore, when the pyrene is in the hydrophobic core, it gives an excitation peak at 338 nm, which indicates the critical aggregation behavior of the conjugates in water; on the other hand, when it is in the hydrophilic environment, the excitation peak of pyrene shifts to 334 nm.

In order to prepare various concentrations of micellar solutions, 1.8 x 10^{-4} M (0.6 mg in 25 mL acetone) pyrene stock solution was prepared and 10 µL of pyrene-acetone solution was added into each sample. Acetone was removed under high *vacuo* in desicator for 2 hours. After sonication for 1 hour at room temperature and keeping for 24 hours, different concentrations of micellar aggregates (10^{-4} to 10^{-9} M) in 3 mL distilled water were ready to be monitored. The final pyrene concentration was 6x10^{-7} M and micelles were monitored by Fluorescence Spectroscopy. Excitation measurements were performed at 300-360 nm range using 5 nm width. Table 3.1. shows the molecular weight and

hydrophobic/hydrophilic ratios of each dendron-linear polymer–dendron conjugates and Figure 3.27 shows the excitation spectra of pyrene loaded (a) [G3]-PEG6K-[G3], (b) [G3]-[Bn]-[PEG6K]-[G3]-[Bn] and (c)[G4]-PEG6K-[G4] micelles.

Table 3.1. M_w and hydrophobic/hydrophilic ratio of each copolymer conjugate

PRODUCT	**M_w (g/mol)**	**Hydrophobic/hydrophilic ratio**
G3-PEG 10K-G3	12428	1:5
G3-PEG 6K-G3	8467	1:3
[G3]-[Bn]-[PEG6K]-[G3]-[Bn]	11188	1:1
G4-PEG 6K-G4	10311	1:1.5

According to the Table 3.1, the hydrophobic/hydrophilic ratio of [G3]-PEG 10K-[G3] micelles is 1 to 5 which indicates that the molecular weight of hydrophilic polymer block is 5 times larger than the hydrophobic dendritic block. As expected, the hydrophobic part was not enough to form micellar structures, thus pyrene could not be encapsulated into the micellar core, thus fluorescence spectra could not be monitored by using 10 K hydrophilic PEG.

To obtain flower-like micellar structures in aqueous phase, the length of the hydrophilic polymer, PEG, was decreased 10000 MW to 6000 MW; therefore, the hydrophobic/hydrophilic ratio is increased. In this case, the molecular weight of hydrophilic polymer block is 3 times larger than the hydrophobic dendritic block, thus, these dendron-linear polymer-dendron conjugates were able to form micelles in water. Excitation spectra of G3-PEG6K-G3 which is given in Figure 3.28a shows the Fluorescence Intensity of each copolymer concentration from $5x10^{-4}$ to 10^{-9}. As the copolymer concentrations increase, the ability to form micellar aggregates also increases. Obviously, as the concentration decreases, the shift of the characteristic peaks of pyrene from 338 nm to 334 nm can be easily observed, which indicates the formation of micelles after a certain concentration.

a

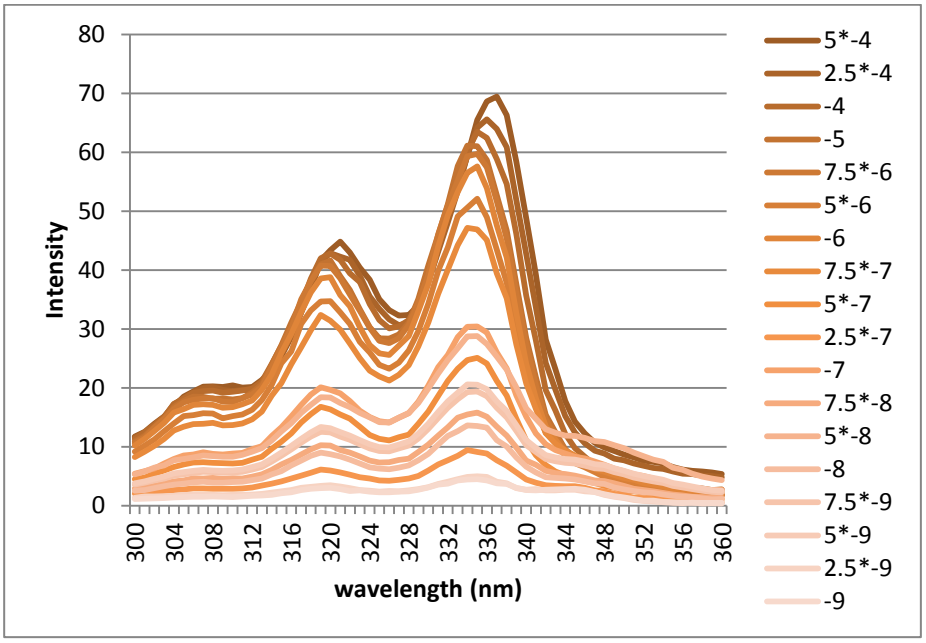
Intensity
wavelength (nm)
5*-4
2.5*-4
-4
-5
7.5*-6
5*-6
-6
7.5*-7
5*-7
2.5*-7
-7
7.5*-8
5*-8
-8
7.5*-9
5*-9
2.5*-9
-9

b

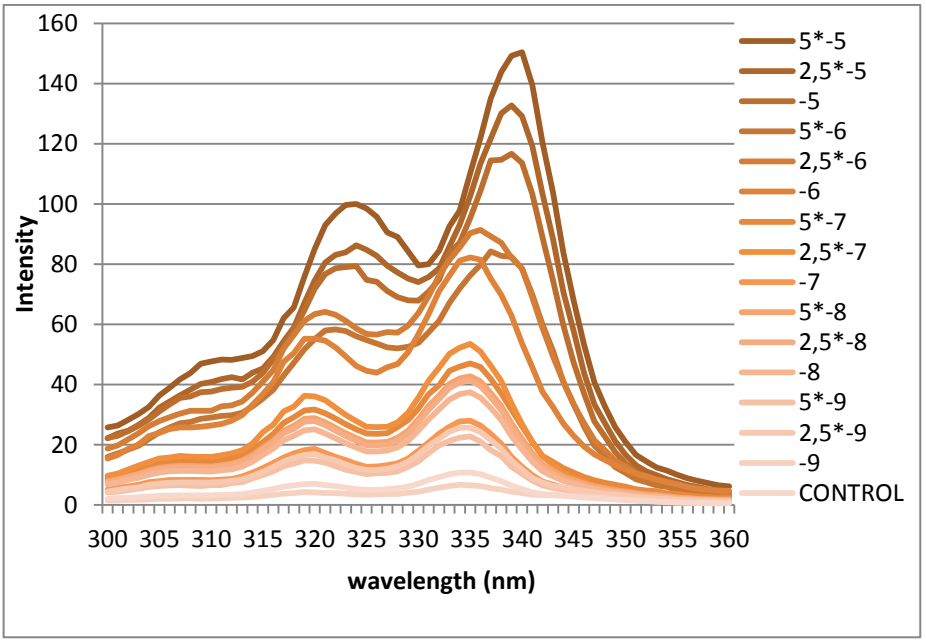
Intensity
wavelength (nm)
5*-5
2,5*-5
-5
5*-6
2,5*-6
-6
5*-7
2,5*-7
-7
5*-8
2,5*-8
-8
5*-9
2,5*-9
-9
CONTROL

c

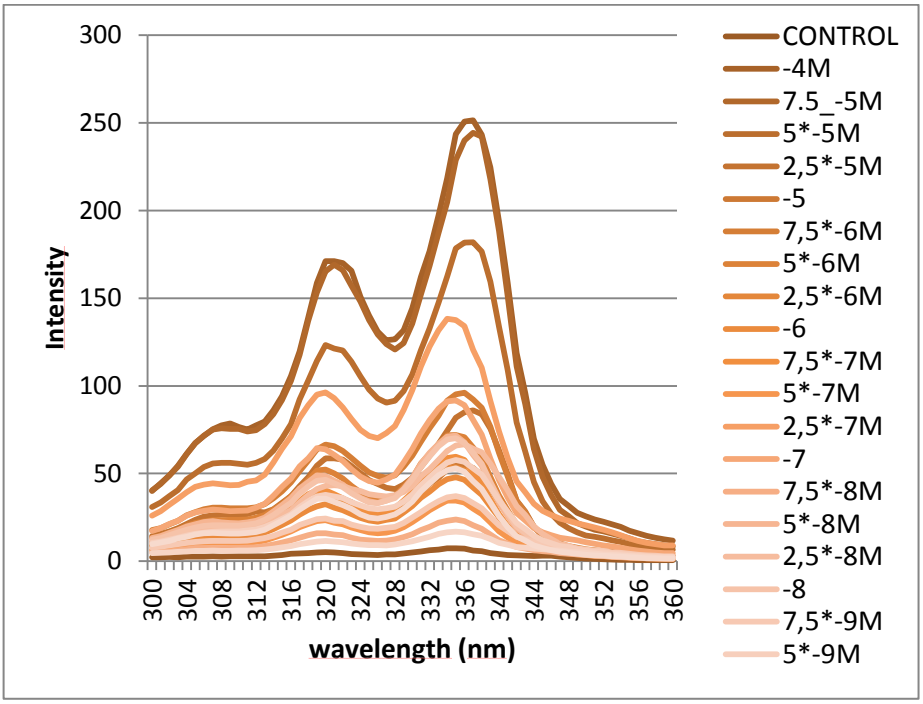

Figure 3.28. Excitation spectra of pyrene loaded (a) [G3]-PEG6K-[G3], (b) [G3]-[Bn]-[PEG6K]-[G3]-[Bn] and (c)[G4]-PEG6K-[G4] micelles.

3.2.2. Calculating the Critical Micelle Concentration and Effects on Micellar Stability

The critical micelle concentration (CMC) indicates the minimum concentration of dendron-linear polymer-dendron conjugates that tend to form micellar structures. The measurement of CMC is generally performed by using fluorescence techniques and the value of the critical micelle concentration also shows the thermodynamic stability of the micelles. In addition, the lower the critical micelle concentration values indicate the higher stability of micelles in aqueous solution.

Critical micelle concentrations for four different copolymers were determined at neutral pH by using fluorescent probe technique. Pyrene was used as a hydrophobic dye for the micellar encapsulation because its fluorescence is negligible in water. It has characteristic peaks at 334 and 338 nm wavelength and the critical micelle concentrations can be determined from the log (concentarion) vs I_{338}/I_{334} graphs. Figure 3.29 (a,b,c) shows the log (concentarion) vs I_{338}/I_{334} graphs for each type of dendron-linear polymer-dendron

conjugates and the cmc values are summarized in Table 3.2, showing the effect of the length of the hydrophilic polymer, the type of the acetal unit at the periphery of the core-forming dendritic block and the dendrimer generation on the values of critical micelle concentrations.

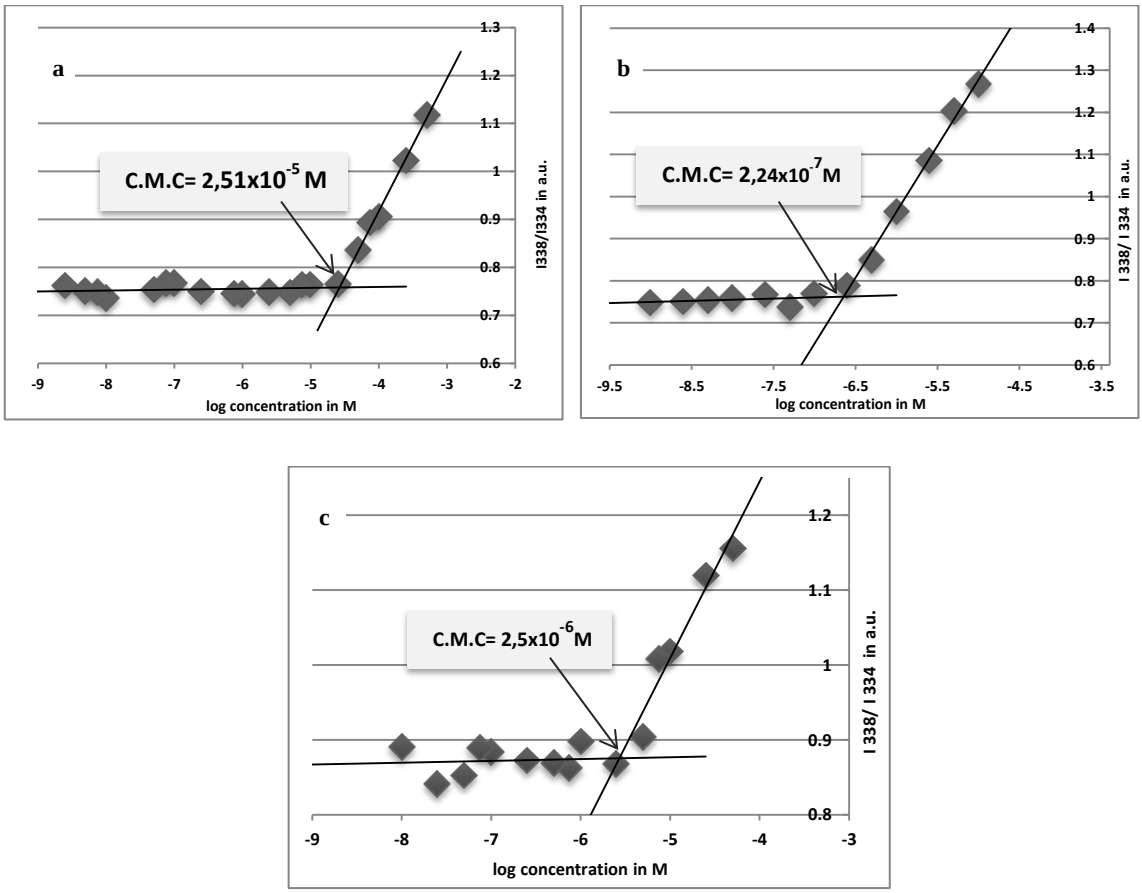

Figure 3.29. Log conc. vs. I_{338}/I_{334} graph of (a) [G3]-PEG6K-[G3], (b) [G3]-[Bn]-[PEG6K]-[G3]-[Bn] and (c) [G4]-PEG6K-[G4] micelles.

Table 3.2. Molecular weight, hydrophobic/hydrophilic ratio and critical micelle concentration of each copolymer conjugate.

PRODUCT	**M_w (g/mole)**	**Hydrophobic/hydrophilic ratio**	**Critical Micelle Concentration(M)**
[G3]-PEG 10K-[G3]	12428	1:5	No formation
[G3]-PEG 6K-[G3]	8467	1:3	$2.5x10^{-5}$
[G3]-[Bn]-[PEG6K]-[G3]-[Bn]	11188	1:1	$2.24x10^{-7}$
[G4]-PEG 6K-[G4]	10311	1:1.5	$2.51x10^{-6}$

As expected, there is no resulting value for the critical micelle concentration of [G3]-PEG 10K-[G3] conjugates due to their high hydrophilic/hydrophobic ratio. However, a decrement in the polymer length shows the tendency to form micellar structures in water by [G3]-PEG6K-[G3] conjugates; therefore, from the crossover point of the log (concentarion) vs I_{338}/I_{334} graph, the CMC value of [G3]-PEG 6K-[G3] micelles calculated as $2.5x10^{-5}$ M (Figure 3.29a). The lower the CMC values indicates the higher the stability of the micelles. Therefore, in order to obtain more stable micelles, the hydrophobic/hydrophilic ratio can be increased by the addition of the hydrophobic moieties to the core-forming block of the dendron. The additional hydrophobicity can be provided by two ways, (1) changing the type of the acetal moiety to more hydrophobic group or (2) addition of the further generation of the dendron. [G3]-[Bn]-[PEG6K]-[G3]-[Bn] micelles indicates a change in the acetal moieties on the periphery of the third generation polyester dendron. The simple benzylidene acetals provide additional hydrophobicity which also affects the critical micelle concentration of the same type of dendron and the same length of polymer conjugates. For these conjugates, the hydrophobic/hydrophilic ratio was higher than the acetal protected core-forming dendritic block which also causes a decrement in the CMC value of the micelles, $2.24x10^{-7}$ M (Figure 3.29b). Because of the large increase in the hydrophobicity which strongly favors the self-assembly in aqueous phase, the stability of the micellar core was also increased by the addition of phenyl ring. The addition of new generation to the periphery of the core-forming dendritic block also increased the hydrophobicity or increased the hydrophobic/hydrophilic ratio, decreased the critical micelle concentration which also affected the micellar stability (Figure 3.29c).

3.2.3. Dynamic Light Scattering Measurements

For targeted drug delivery systems, the sizes of micelles are very significant topic. The ideal micellar size should be less than 100 nm to avoid rapid clearance while facilitating the tumor uptake. The micelle sizes of each copolymer conjugate and the polydispersity of micelles were determined by Dynamic Light Scattering (DLS). After determining the CMC values of each dendron-linear polymer-dendron conjugate, DLS measurements were performed above this concentration. The dispersity of micellar

structures was shown in number vs. diameter graph (Figure 3.30). All the micellar structures are in a unimodular micelle formation and they were in the ideal size range. Table 3.3 shows the comparison of the micelle sizes and the polydisperties obtained by DLS. As expected, as the micellar stability increases, the critical micellar concentrations and the micellar sizes decrease.

Table 3.3. Micellar sizes and polydispersities of each copolymer conjugate.

PRODUCT	**Micelle Size by DLS (nm)**	**PDI**
[G3]-PEG6K-[G3]	83	0.037
[G3]-[Bn]-[PEG6K]-[G3]-[Bn]	52	0.373
[G4]-PEG6K-[G4]	65	0.177

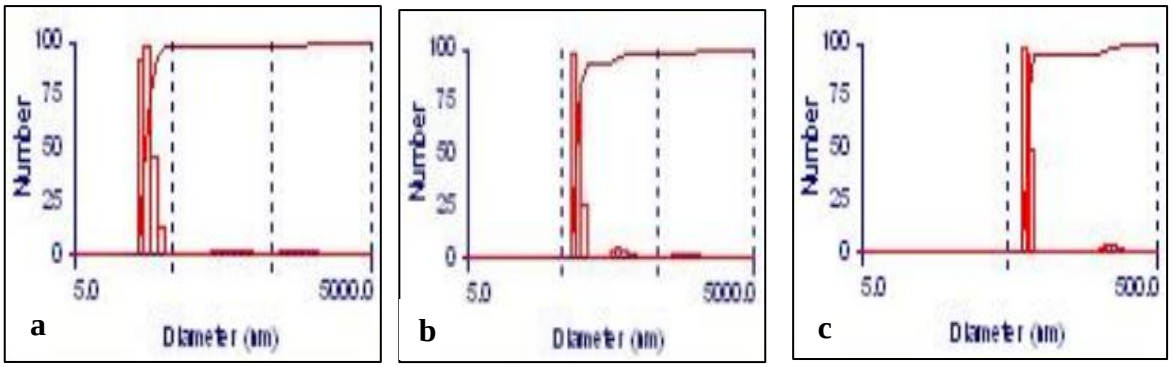

Figure 3.30. The dispersity of micellar structures of (a) [G3]-PEG6K-[G3], (b) [G3]-[Bn]-[PEG6K]-[G3]-[Bn] and (c) [G4]-PEG6K-[G4].

3.2.4. Scanning Transmission Electron Microscopy (STEM) Measurements

The sizes of spherical micelles in diameter were also approved by STEM pictures of pyrene containing micelles in Figure 3.31(a,b,c). After the Fluorescence and DLS measurements, morphological studies of the micellar structures were performed by using Scanning Transmission Electron Microscopy (STEM). As illustrated in Figure 3.31 (a,b,c),

micellar structures of [G3]-PEG6K-[G3], [G3]-[Bn]-[PEG6K]-[G3]-[Bn] and [G4]-PEG6K-[G4] conjugates were in spherical shape and in the expected size range.

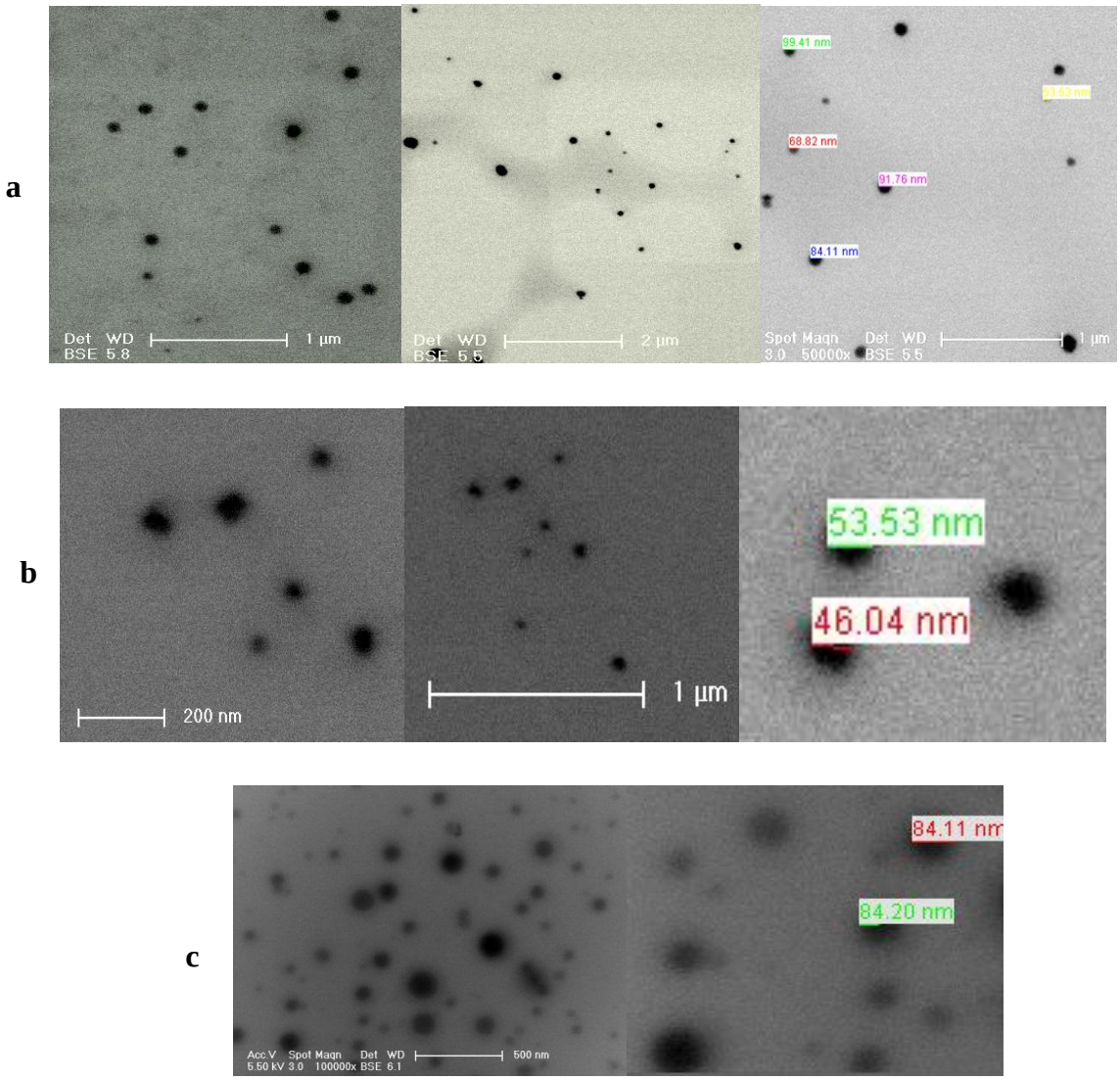

Figure 3.31. STEM images of [G3]-PEG6K-[G3], [G3]-[Bn]-[PEG6K]-[G3]-[Bn] and [G4]-PEG6K-[G4] micelles.

3.3. Hydrolysis of Acetals at the Micellar Core

The micelle stability is very significant point for targeted drug delivery systems. Micellar nanocarriers should carry the whole drug payload at neutral pH like the blood pH and release the drug molecules in a controllable manner inside the tumor tissues while affecting as few healthy cells as possible. The triggered drug release can be achieved by

external or internal stimuli. In this study, in order to test the micellar stability of each conjugate, pyrene release rates of each conjugate were investigated at neutral and acidic pH at body temperature. The acetal moieties were selected as acid degradable linkages for the micelles. The hydrolysis rates of the acetal units located at the micellar core were determined for each conjugate at pH 5.0 acetate buffer and at pH 7.4 phosphate buffer at 37 °C. Figure 3.32 shows the % hydrolysis rate of pyrene from the [G3]-PEG6K-[G3] micelles. In 24 hours, around 80% of pyrene was released from the micelles at acidic pH; however, 60% of pyrene also released at pH 7.4 which indicates the weak stability of micelles at neutral pH. The stability of micelles at neutral pH can be increased by the addition of more hydrophobic acetal moieties to the core-forming block. According to the literature, the cyclic acetals are known to hydrolyze quite slowly than the non-cyclic acetals [46]. As illustrated in Figure 3.33, the pyrene release rates of [G3]-[Bn]-[PEG6K]-[G3]-[Bn] micelles at both pH's are also very similar because these simple benzylidene acetal groups cannot undergo hydrolysis at acidic conditions in contrast to the highly sensitive acetal groups. Keeping these pH insensitive micellar structures as a control, the micellar stability at neutral pH was achieved by the addition of new generation to the core-forming dendritic block. The incorporation of the new generation provided additional hydrophobic acetal moieties at the periphery of the dendron. As illustrated in Figure 3.34, the Fluorescence intensity of pyrene loaded [G4]-PEG6K-[G4] micelles significantly decreased at pH 5.0 while keeping stable at pH 7.4 which shows the stronger dependence of the release rate on pH. Figure 3.35 also shows the greater difference between the release rates of pyrene at neutral and acidic pH. In 30 hours, only 10 % of pyrene was released at neutral pH while releasing 80 % of pyrene from the same micellar nanocarrier. The increment in micellar stability at neutral pH indicates that the drug nanocarrier will not release its drug payload during blood circulation which also provides advantages for targeted drug delivery systems by avoiding the undesirable cell accumulation and toxicity of the therapeutic agent. Therefore, the most stable, [G4]-PEG6K-[G4] micelles were chosen for further drug loading and drug release studies.

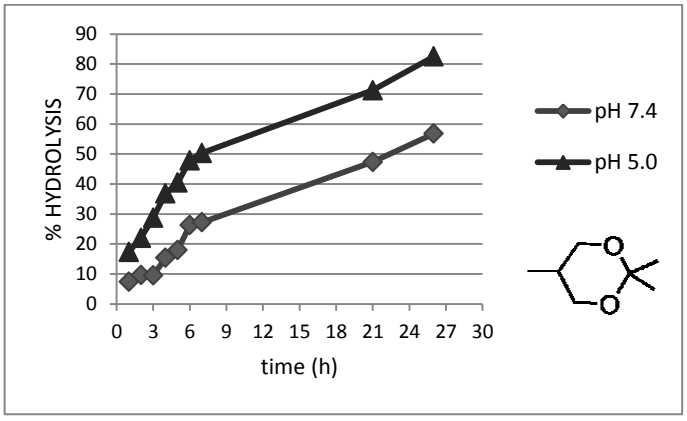

Figure 3.32. Hydrolysis rates of acetals in pyrene loaded [G3]-PEG6K-[G3] micelles at neural and acidic pH.

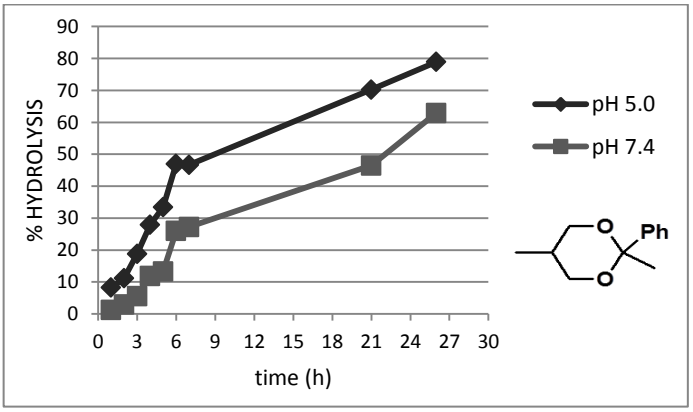

Figure 3.33. Hydrolysis rates of acetals in pyrene loaded [G3]-[Bn]-[PEG6K]-[G3]-[Bn] micelles at neutral and acidic pH

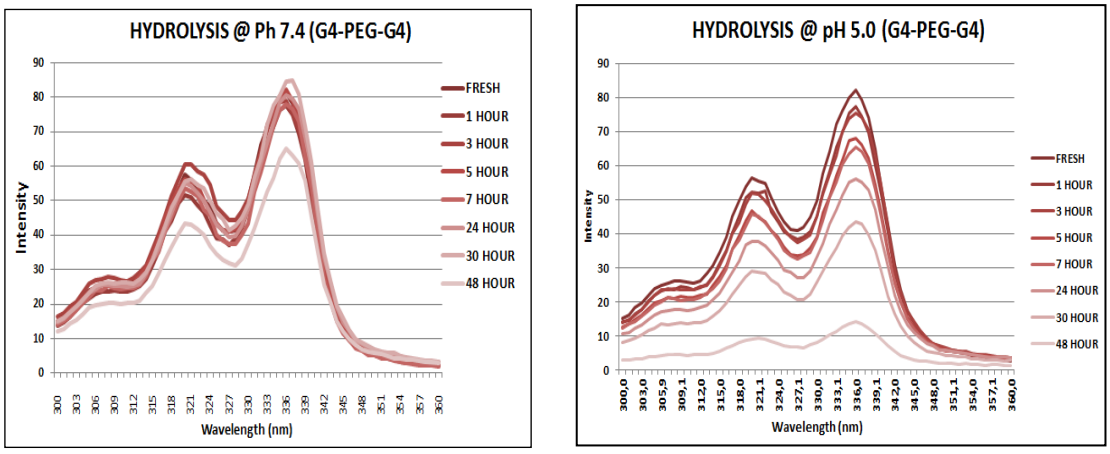

Figure 3.34. Excitation spectra of pyrene loaded [G4]-PEG6K-[G4] micelles at neural and acidic pH.

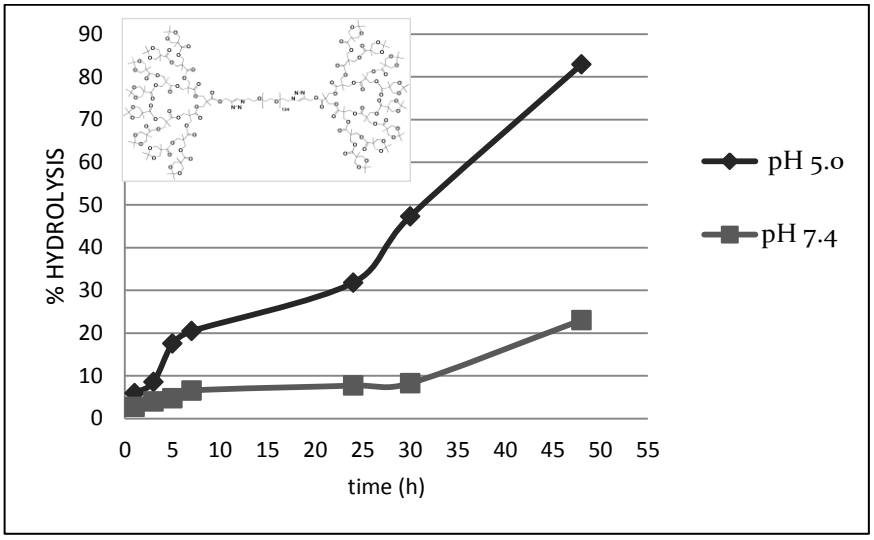

Figure 3.35. Hydrolysis rates of acetals in pyrene loaded [G4]-PEG6K-[G4] micelles at neural and acidic pH.

Table 3.4 compares the stability of pyrene loaded micellar conjugates. [G3]-PEG6K-[G3] and [G3]-[Bn]-[PEG6K]-[G3]-[Bn] micelles show similar stability at pH 5.0 and pH 7.4 by releasing their pyrene payload at both pH conditions; therefore, these micellar carriers are pH insensitive. However, [G4]-PEG6K-[G4] micelles did not released their pyrene payload at neutral pH which also indicates the higher stability of micelles at blood pH; therefore, these dendron- linear polymer-dendron conjugates were chosen for further drug loading studies.

Table 3.4. Comparison of the stability of pyrene loaded [G3]-PEG6K-[G3], [G3]-[Bn]-[PEG6K]-[G3]-[Bn] and [G4]-PEG6K-[G4] micelles.

PRODUCT	**M_W(g/mol)**	**Hydrophobic/ hydrophilic ratio**	**Micelle Size by DLS (nm)**	**C.M.C. (M)**	**STABILITY**	
					@ pH 5.0	**@ pH 7.4**
G3-PEG 10K-G3	12428	1:5	----	----	----	----
G3-PEG 6K-G3	8467	1:3	83	$2.51x10^{-5}$	% 82 of pyrene released in 26h	% 58 of pyrene released in 26h
[G3]-[Bn]-[PEG6K]-[G3]-[Bn]	11188	1:1	72	$2.24x10^{-7}$	% 81 of pyrene released in 26h	%62 of pyrene released in 26h
G4-PEG 6K-G4	10311	1:1.5	65	$2.51x10^{-6}$	% 83 of pyrene released in 48 h	% 21 of pyrene released in 48 h

3.4.Preparation of CA-4-Loaded Micelles

The self-assembly of [G4]-PEG6K-[G4] block copolymers and drug encapsulation in the assembled micelles were achieved by co-solvent evaporation method. The process of encapsulation of hydrophobic drug molecules affects the loading efficiency in micellar structures. Lavasanifar *et al*. have been reported that the co-solvent evaporation method increases the encapsulated levels of hydrophobic therapeutic agents in micelles and they demonstrated that the type of co-solvent, the organic:aqueous phase ratio and the order of the addition of the two phases also affect the loading efficiency [47]. According to this method, the amphiphilic block copolymer, [G4]-PEG6K-[G4], and the hydrophobic drug, CA-4 (10 wt% of drug relative to copolymer), were dissolved in an organic solvent. The co-solvent must be volatile and water-miscible; therefore, acetone was used as the co-solvent at 1:2 organic:aqueous phase ratio. Then, the self-assembly and drug encapsulation were achieved by the drop-wise addition of water to the organic phase followed by sonication and evaporation of the organic co-solvent.

3.4.1. DLS & STEM

After the loading process, dynamic light scattering (DLS) measurement was performed to investigate the change in the micellar size after the encapsulation of the hydrophobic drug. The dispersity of drug loaded micellar structures was shown in number vs. diameter graph (Figure 3.36a). The micellar sizes are in expected size range and spherical in shape. The sizes of drug loaded micelles were also approved by STEM pictures (Figure 3.36b). As expected, encapsulation of the hydrophobic guest molecules increased the hydrophobicity of the core which caused a decrement in the sizes of micellar structures and polydispersity and an increment in the micellar stability.

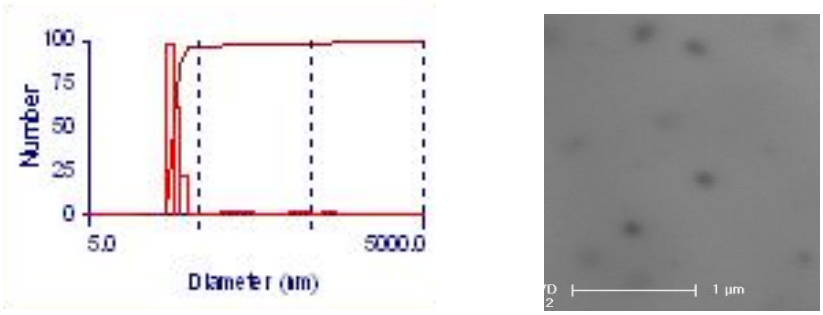

Figure 3.36. (a) DLS measurement and (b) STEM image of CA-4 loaded micelles.

Table 3.5. Comparison of micellar sizes and PDI of pyrene loaded and drug loaded micelles.

PRODUCT	**Micelle Size by DLS (nm)**	**PDI**
[G4]-PEG6K-[G4]	65	0.177
CA-4 loaded [G4]-PEG6K-[G4]	31	0.108

3.4.2. Calculating the Drug Loading Capacity

The drug loading capacity indicates the amount of drug that encapsulated into the micellar core; therefore, to measure the exact amount of drug inside the core, first the non-encapsulated drug molecules should be remove from the micelles. In order to remove these free CA-4 molecules, SEPHADEX G75 chromatography was used. It is a cross-linked dextran gel and mainly used for the separations of low and high molecular weight molecules. This column material provides several advantages over the dialysis method such as considerable time savings, the low dilution factor, and the high activity recoveries even with small amounts of micellar solution. By using SEPHADEX G75, the high molecular weight molecules which are drug encapsulated micelles were collected from the SEPHADEX column before the low molecular weight molecules like free drug. The drug amounts for each collected tube were analyzed by LC/MS technique. Figure 3.37 shows the drug concentration vs. volume of collected sample. According to the drug amounts monitored by LC/MS, it was demonstrated that the free CA-4 was successfully separated

from the drug loaded micelles and the volume 12-15 obviously can be used for the further drug release studies.

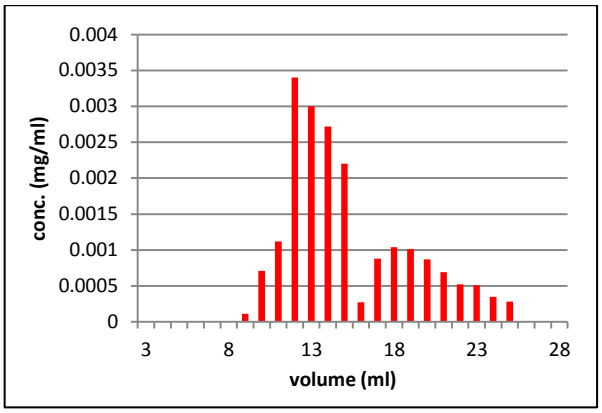

Figure 3.37. Concentration (mg/mL) vs. volume (mL) graph obtained by LC/MS analysis.

Table 3.6. Concentrations of each collected tube after SEPHADEX.

volume (1 mL for each tube)	Conc. (mg/mL)	volume	Conc. (mg/mL)
TUBE 1	----	TUBE 15	0,00372
TUBE 2	----	TUBE 16	0,00027
TUBE 3	----	TUBE 17	0,00088
TUBE 4	----	TUBE 18	0,00104
TUBE 5	----	TUBE 19	0,00101
TUBE 6	----	TUBE 20	0,00087
TUBE 7	----	TUBE 21	0,00069
TUBE 8	----	TUBE 22	0,00052
TUBE 9	0,00011	TUBE 22	0,00051
TUBE 10	0,00112	TUBE 23	0,00035
TUBE 11	0,00071	TUBE 24	0,00028
TUBE 12	0,00340	TUBE 25	----
TUBE 13	0,00300	TUBE 26	----
TUBE 14	0,00220	TUBE 27	----

Drug Loading Capacity= Amount of Loaded Drug/ Total Amount of Drugx100

= 0.00612/0.077x100

Drug Loading Capacity = %79.5

3.5. pH-Dependent Release of CA-4 from the Micelles

The triggered CA-4 release from [G4]-PEG6K-[G4] micelles at acidic and neutral pH was investigated by using dialysis method. A solution of CA-4-loaded micelles in a dialysis bag was dialyzed against pH 7.4 PBS buffer and pH 5.0 acetate buffer at 37 °C. The micellar solution in the dialysis bag was monitored by nano-drop UV-VIS spectroscopy to investigate the decrement in the drug concentration at the desired time points. Also, the buffer solution outside the dialysis bag was monitored by LC/MS to determine the amount of released drug at the desired time points. As illustrated in Figure 3.38, as the pH decreases, the micellar core destabilizes due to the pH-sensitive acetal moieties at the core-forming block of micellar structure; therefore, the hydrophobic core starts to become hydrophilic as the acid sensitive acetal bonds hydrolyzes and triggered drug release profile can be monitored in a controllable manner in acidic environment.

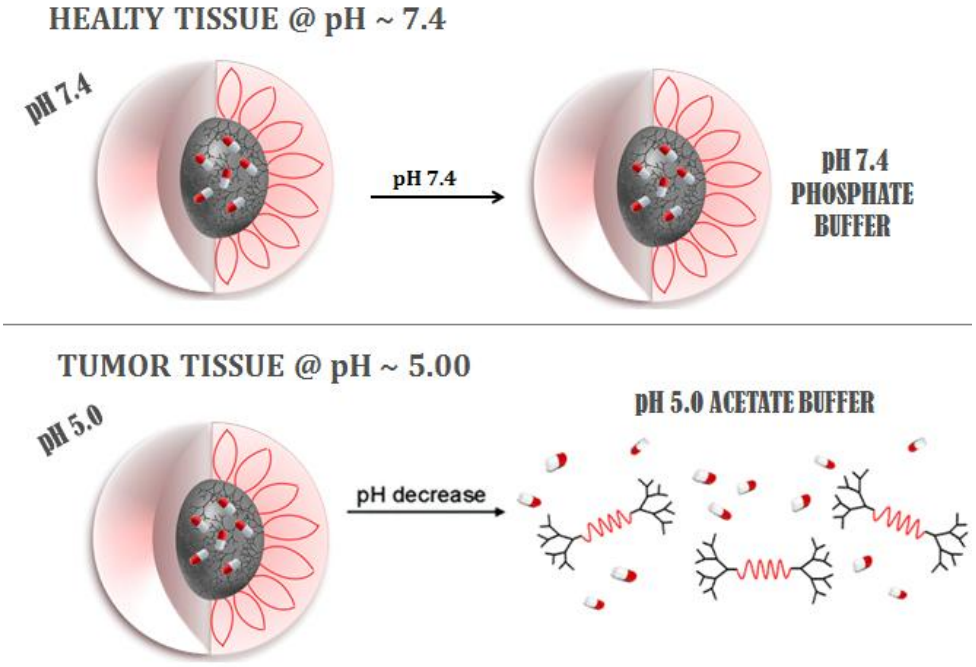

Figure 3.38. Illustration of CA-4 release at pH 5.0.

The ability of releasing the encapsulated drug molecules from the micelles in response to acetal hydrolysis at acidic conditions was investigated by using pH 5.0 acetate buffer. Release of drug molecules from the micellar solution to buffer phase was demonstrated by significant decrement in the intensity absorption by UV-VIS

Spectroscopy. The UV absorption of CA-4 loaded micelles at pH 5.0 significantly decreases due to the CA-4 release, while the UV absorption of the same sample at pH 7.4 remained constant over a time scale; therefore, CA-4 release rate can be calculated from the intensity change at both pHs (Figure 3.39). These results also demonstrate the triggered drug release in a controlled manner by the hydrolysis of acetals bonds at the core-forming block of micelles. After about 8 hours, the absorbance at pH 7.4 does not significantly change, while at pH 5.0, the absorbance change shows that about %70 of CA-4 released from the micellar nanocarrier. This also indicates that these [G4]-PEG 6K-[G4] micelles remains stable at neutral pH while releasing their drug payload at acidic conditions like tumor tissues; therefore, these drug nanocarriers will affect as few healthy cells as possible during the drug transport.

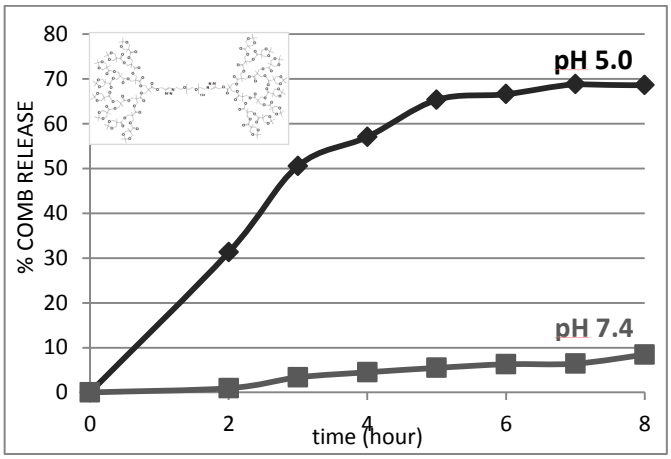

Figure 3.39. CA-4 release rate at pH 5.0 and pH 7.4 from [G4]-PEG6K-[G4] micelles.

3.6. In Vitro Measurements

3.6.1. Cellular Viability and Toxicity Assay

Human umbilical vein endothelial cells (HUVEC) were used to investigate the cytotoxicity of blank micelles after treatment for 72 hours and CA-4 loaded micelles after treatment for 24 hours. The 24 hour treatments were performed as either 2 hours pulse-22 hours chase or 4 hours pulse-20 hours chase. As shown in Figure 3.40, when the concentration of blank micelles was below 100 μg/ mL, the cell viability still retained about 80% which indicates the low cytotoxicity of these dendron-linear polymer-dendron

conjugates. Moreover, the CA-4 loaded micelles were also investigated after cultured for 24 hours. Figure 3.41 shows the percent cell viability of CA-4 loaded micelles after treatment for 24 hours. The dose-dependent cytotoxic effect of CA-4 loaded micelles was observed at the concentration range used for the treatments. At low concentrations of CA-4, 80% viability was observed, while increasing the dose of treatment up to $1.75x10^{-6}$ and $3.5x10^{-6}$ M of CA-4 equivalents resulted in less than 40% of cell viability. This suggests that the dose dependent cytotoxic effect of CA-4 loaded micelles can be observed within micro to nano molar concentration range in 24 hour treatments. No significant difference was observed between treatments for 2 hours and 4 hours (in pulse-chase mode), which indicates that cytotoxic effects due to cellular association of CA-4 loaded micelles was evident at 2 hours, and prolonging the treatment duration did not enhance this effect.

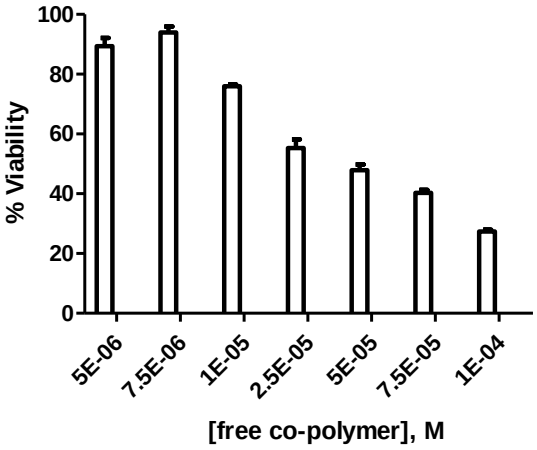

Figure 3.40. % Cell viability of blank micelles after cultured 72 hours.

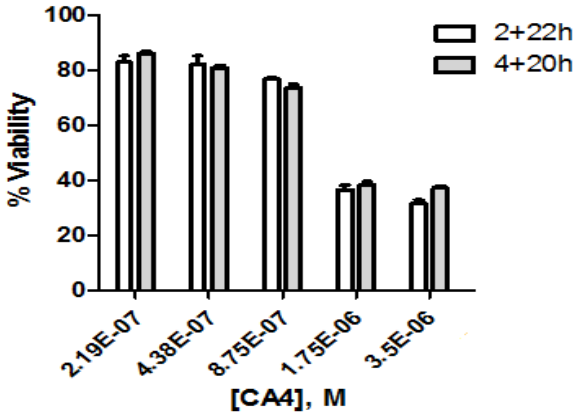

Figure 3.41**.** % Cell viability of CA-4 loaded micelles after cultured 2+22 and 4+20 h.

3.6.2. Cellular Binding and Internalization of Micelles

In order to investigate the cellular binding and internalization of [G4]-[PEG 6K]-[G4] micelles, Nile Red was used as a fluorescent labeled dye. Copolymer conjugate (**16**) (1 mg/mL) and Nile Red (0.001 mg/mL) were added into distilled water and sonicated for an hour to obtain Nile Red loaded micelles. In order to get rid of the free Nile Red into the micellar solution, SEPHADEX G75 column was used and fluorescence intensity of each collected tube was monitored. Figure 3.42 shows the Fluorescence Microscopy images of HUVEC cells incubated with Nile Red loaded micelles for 2 hours and 4 hours. Figure 3.42a. shows the positive controls of HUVEC cells incubated with DAPI and Nile Red. It can be concluded that CA-4 loaded micelles entered into HUVEC cells in a time-dependent manner. HUVEC cells incubated with [G4]-[PEG 6K]-[G4] micelles for 4 hours show stronger red fluorescence in nuclei than the cells incubated for 2 hours. HUVEC cells incubated with [G4]-[PEG 6K]-[G4] micelles for 4 hours show stronger red fluorescence than the cells incubated for 2 hours, indicating that the amount of fluorophore accumulated in the cells is higher. Being a hydrophobic molecule, Nile Red stains the cellular membranes including cytoplasmic membrane and other membranous organelles. In the positive control where Nile Red was dissolved in DMSO, a diffuse staining pattern was obtained since free dye can stain the cytoplasm as well as organelles. However, in the micellar Nile Red treated cells, the signal is observed in a more punctuate pattern.

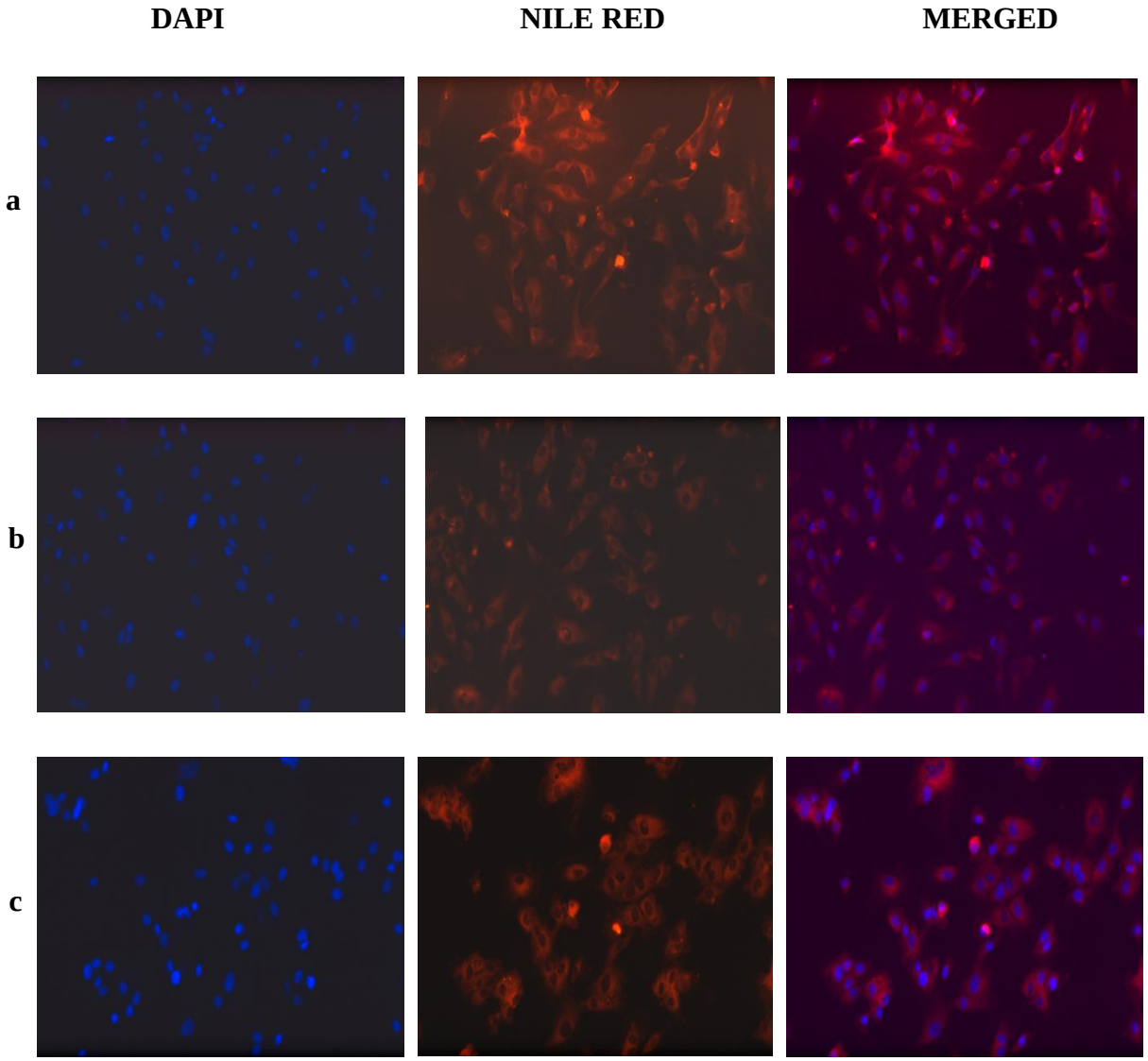

Figure 3.42. Fluorescence microscopy images of HUVEC cells incubated with (a) control and Nile Red loaded micelles for (a) positive control (b) 2 h c) 4 h.

4. EXPERIMENTAL

4.1. General Methods and Materials

2,2-Bis(hydroxymethyl) propionic acid (Bis-MPA), Dowex X50WX2, Propargyl Alcohol were purchased from Alfa Aesar. Polyethylene glycol (PEG) was obtained from Aldrich and DMPA (2,2-Dimethoxy-2-phenylacetophenone) from Acros. All solvents were purchased from Merck and used as obtained without further purification unless noted otherwise. The dendron and copolymer characterizations were done by ^{1}H NMR Spectroscopy (Varian 400 MHz) and Fourier Transform Infrared (ATR-FT-IR) Spectroscopy (Thermo Fisher Scientific Inc. Nicolet 380). Micellar formation was monitored by Fluorescence Spectroscopy (Cary Eclipse), Dynamic Light Scattering (DLS) 90 Plus Particle Size Analyzer instrument (Brookhaven Instruments Cooperation) and the STEM of wet micelles were pictured by ESEM-FEG/EDAX Philips XL-30 (Philips, Eindhoven, The Netherlands) instrument. Molecular weights of the copolymers were estimated by GPC analysis using a Shimadzu GPC furnished with a PSS-SDV (length/ID 8 × 300 mm, 10 mm particle size) mixed-C column calibrated with polystyrene standards (1–150 kDa) using a refractive-index detector. Tetrahydrofuran (THF) was used as eluent at a flow rate of 1 mL/min^{-1} at 30 °C.

4.2. Synthesis of Polyester Dendron

First, second, third and fourth generation polyester dendrons with alkyne units at the core were synthesized according to the literature procedure [45]. The selected synthesis method is based on a biocompatible building block, which is 2,2-bis(hydroxymethyl) propionic acid (Bis-MPA). After the successful access of first generation polyester dendron with alkyne focal unit, removal of the acetonide protecting groups and acylation with the resulting anhydride provide the growth of the dendritic blocks.

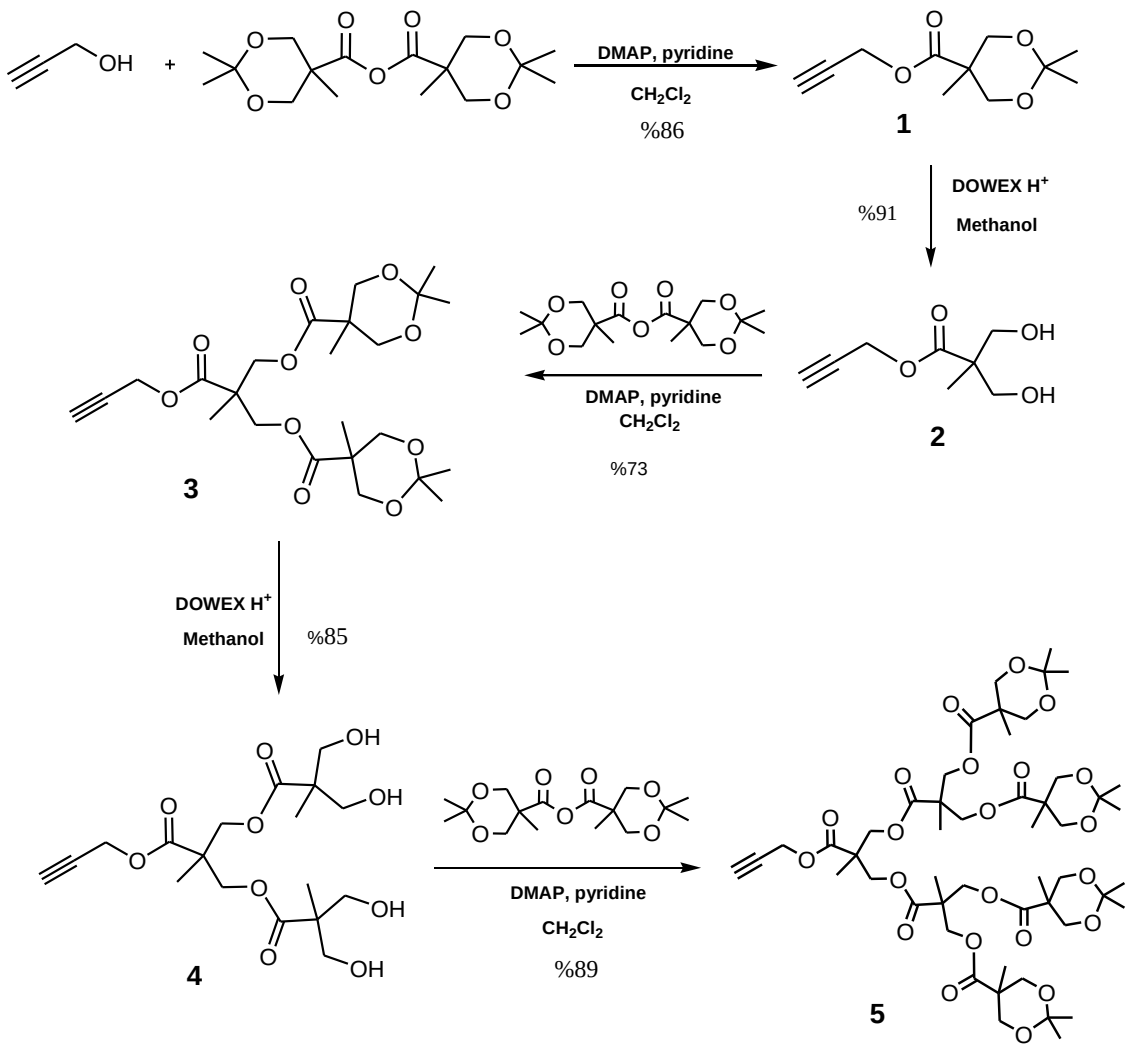

Figure 4.1. General scheme of dendron synthesis.

4.2.1. Synthesis of Third Generation Polyester Dendron

To synthesize third generation polyester Dendron with alkyne focal unit, compound **4** (3.09 g, 7.7 mmol) and DMAP (0.94 g, 7.7 mmol) were dissolved in dry CH_2Cl_2 (50 mL) at room temperature under N_2 atmosphere. The anhydride of isopropylidene-2,2-bis(methoxy)propionic acid (Bis-MPA) (15.19 g, 46.0 mmol) and pyridine (3.72 mL, 46.0 mmol) were added slowly (Figure 4.1.). The reaction mixture was stirred for 24 h, and quenched with distilled water (3.72 mL) after 24 h. The organic phase was diluted with CH_2Cl_2 (50 mL) and extracted with %10 solution of $NaHSO_4$ (3 x 50 mL), % 10 solution of Na_2CO_3 (3 x 50 mL) and brine solution (2 x 50 mL). Finally, organic phase was dried by

Na_2SO4, filtered and concentrated to yield product **5** as a white solid. ^{1}H NMR = ($CDCl_3$, δ ppm) = 4.73 (d, *J* =8 Hz, 2H), 4.31-4.24 (m, 12H), 4.16- 4.13 (d, *J*=12 Hz, 8H), 3.63-3.60 (d, *J*=12 Hz, 8H), 2.54 (t, *J*= 3.2, 1H), 1.41 (s, 12H); 1.35 (s, 12H); 1.30 (s, 3H), 1.28 (s, 6H), 1.14 (s, 12H), FT-IR (cm^{-1}): 3253, 1731.3. (Figure A.1, A.2)

In order to deprotect compound **5**, Dowex X50WX2 (300 mg) and methanol (40 mL) were added into a 100 mL round bottom flask and stirred under N_2 at 40^o C. After 24 hours, DOWEX was filtered and the organic phase concentrated under *vacuo* to obtain **6** as a white solid. ^{1}H NMR ($CDCl_3$, δ ppm) 4.79 (d, *J* = 4 Hz, 2H), 4.35 - 4.24 (m, 12H), 3.69 (d, 8H, *J* = 11.0 Hz), 3.60 (d, 8H, *J* = 10.8 Hz), 2.98 (t, 1H, 2.8 Hz), 1.32 (s, 3H), 1.30 (s, 6H), 1.15 (s, 12H). FT-IR (cm^{-1}): 3286.5, 1726.2. (Figure A.3, A.4)

4.2.2. Synthesis of Fourth Generation Polyester Dendron

Compound **6** (134 mg, 0.154 mmol) and DMAP (18 mg, 0.154 mmol) were dissolved in CH_2Cl_2 (5 mL) at room temperature under N_2 atmosphere. The anhydride of isopropylidene-2,2-bis(methoxy)propionic acid (Bis-MPA) (612 mg, 1.85 mmol) and pyridine (0.15 mL, 1.85 mmol) were added slowly (Figure 4.2). The reaction mixture was stirred for 20 h, and quenched with distilled water (1.25 mL) after 20 hr. The organic phase was diluted with CH_2Cl_2 (10 mL) and extracted with %10 solution of $NaHSO_4$ (3 x 10 mL), % 10 solution of Na_2CO_3 (3 x 10 mL) and brine solution (2 x 10 mL). Finally, organic phase was dried by Na_2SO4, filtered and concentrated to obtain product **7** as a colorless gel. ^{1}H NMR (CD_3OD, δ, ppm) 4.72 (d, *J*=12 Hz, 2H), 4.27 (m, 28H), 4.14 (d, *J*= 17.28 Hz, 16H), 3.61 (d, *J*= 40 Hz, 16H), 2.57 (t, *J*= 3.4, 1H), 1.40 (s, 24H), 1.34 (s, 24H), 1.31 (s, 3H), 1.27 (s, 12H), 1.26 (s, 6H), 1.14 (s, 24H).FT-IR (cm^{-1}): 3260. (Figure A.5, A.6)

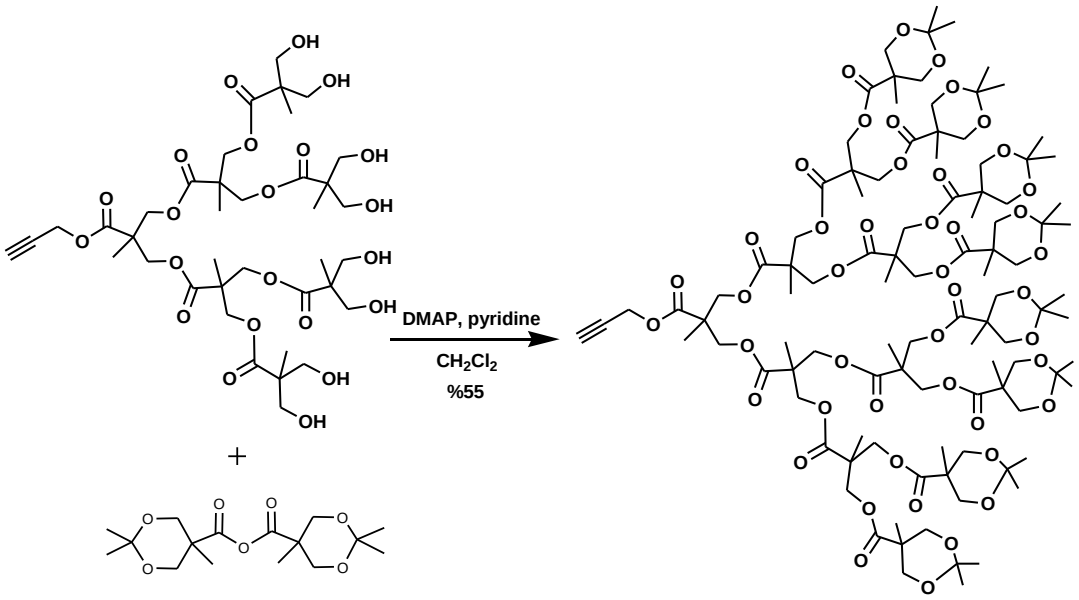

Figure 4.2. Fourth generation polyester dendron synthesis.

4.2.3. Synthesis of Benzylidene-Protected Third Generation Polyester Dendron

To synthesize the benzylidene-protected anhydride derivative of Bis-MPA, first benzaldehyde dimethyl acetal (8.5 g, 5.6 mmol), Bis-MPA (5.00 g, 37.2 mmol) and p-TsOH (0.35 g, 1.86 mmol) were stirred at room temperature for 4 hours under N_2 in Acetone (37.5 mL) to obtain 4.76 g of protected diol group of Bis-MPA. Anhydride **9** is then synthesized by the self-condensation of compound **8** (3.5 g, 15.7 mmol) in CH_2Cl_2 (25 mL) by using DCC (Figure 4.3). The compound **9** was then precipitated in cold Hexane to get rid of the remaining DCU and excess DCC to obtain pure white crystalline product in %68 yield.

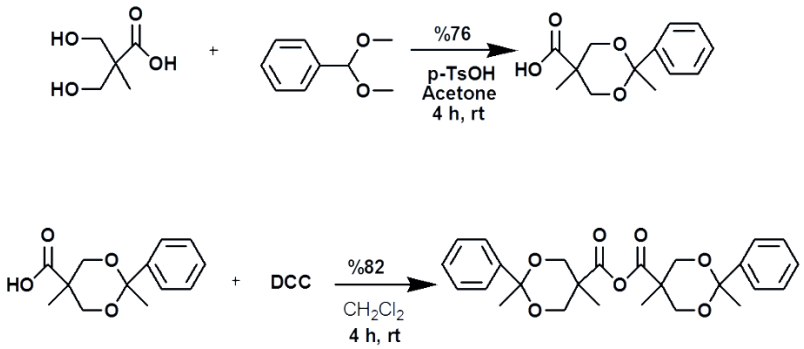

Figure 4.3. Synthesis of benzylidene-protected anhydride.

In order to increase the hydrophobicity of the dendritic block, another type of acetal moieties were attached to the periphery of the dendron. To synthesize the benzylidene protected dendron, compound **6** (0.23 g, 0.26 mmol) and anhydride **9** (1.31g, 3.17 mmol) were stirred with DMAP (0.03 g, 0.026 mmol) and pyridine (0.25 mL, 3.17 mmol) in CH_2Cl_2 (14 mL) under N_2 (Figure 4.4). After 24 hours, the reaction mixture was quenched by distilled water (25 mL) and organic phase was diluted with CH_2Cl_2 (10 mL), followed the extraction with %10 solution of $NaHSO_4$ (3 x 10 mL), % 10 solution of Na_2CO_3 (3 x 10 mL) and brine solution (2 x 10 mL). Finally, organic phase was dried by $NaSO_4$, filtered and concentrated to obtain product **10** in %84 yield.

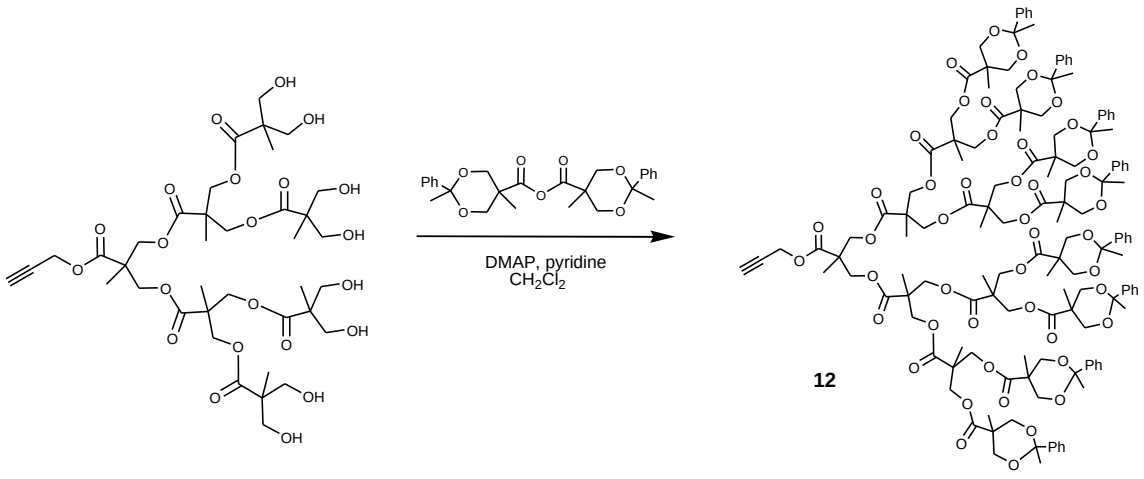

Figure 4.4. Synthesis of dendron 12.

4.3. Synthesis of Diazide Conjugated Poly Ethylene Glycol

4.3.1. Synthesis of Bisazido PEG 10K

First of all 10 K PEG diol was dried with toluene in order to get rid of water, then 4.97 g (0.49 mmol) of OH-PEG10K-OH was stirred with MsCl (0.46 mL (5.97 mmol), and Et_3N (2.50 mL, 17.91 mmol) in CH_2Cl_2 (80 mL) for 20 h at room temperature under N_2 (Figure 4.5). After 20 hours, organic solvent was evaporated and the brownish product was precipitated in cold distilled isopropanol (150 mL). After precipitating for at least 1 hour, it was filtered by a sintered glass with pore size 4. The final solid product was precipitated in

cold ether (150 mL) for 20 h. The precipitated white product was again filtered by sintered glass and finally, 4.5894 g (0.45 mmol) of Ms-PEG10K-Ms in %88 yield. Then, the mesylated PEG 10 K, 4.4460 g (0.44 mmol) reacted with $NaN_3$0.28 g (4.30 mmol) in DMF (17 mL) at 60^oC. After 20 h, DMF was evaporated, the solid product was precipitated in mixture of 12 M HCl (25 mL) and distilled water (25 mL). After diluting the final solution with CH_2Cl_2, extraction was done by distilled water (5x20 mL), the final solution was dried by Na_2SO_4 and filtrated. The final solid product was precipitated in cold ether at least one night at frozen. Finally, the filtrated white product was bisazido PEG 10K (**11**) in %90 yield. ^1H NMR (CD_3OD, δ, ppm) 3.8-3.4 (broad,s, 900 H) 2.15 (s, 4H) FT-IR (cm^{-1}): 2883, 2101. (Figure A.10)

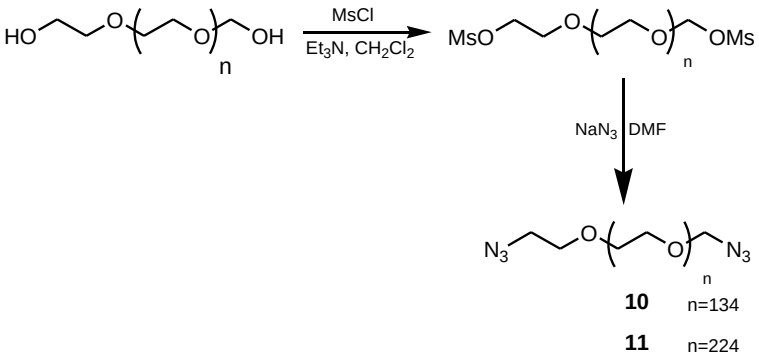

Figure 4.5. Synthesis of bisazido PEG 6K and 10K.

4.3.2. Synthesis of bisazido PEG 6K

In order to synthesize bisazido PEG 6K, same procedure was followed. PEG6K diol (5.91 g , 0.98 mmol) was stirred with MsCl (1.16 mL, 15 mmol) and Et_3N (6.30 mL, 45 mmol)) in CH_2Cl_2 (80 mL) for 20 h at room temperature under N_2 to obtain 4.1 g of Ms-PEG6K-Ms in %68 yield (Figure 4.5). Then, Ms-PEG6K-Ms was reacted with 0.44 g (6.72, mmol) of NaN_3 in 17 mL of DMF to obtain bisazido PEG 6K (**10**) in %63 yield. ^1H NMR (CD_3OD, δ, ppm) 3.8-3.4 (b,s, 756 H) 2.15 (s, 4H) FT-IR (cm^{-1}): 2883, 2100. (Figure A.9, A.11)

4.4. Synthesis of Dendron-Linear Polymer-Dendron Conjugates

4.4.1. Synthesis of [G3]-[PEG 10K]-[G3]

Third generation polyester dendron (**5**) (80 mg, 0.09 mmol) and N_3-PEG 10 K-N_3 (**11**) (300 mg, 0.03 mmol) were dissolved in dry THF (2 mL). In a separate flask, Cu(I)Br (1 mg, 0.003 mmol), PMDETA (10 μL, 0.003 mmol) were dissolved in dry THF (2 mL) and purged with N_2 (Figure 4.6). The mixture was then added into the copolymer solution and stirred at 40 ^oC for 20 h. The solvent was then evaporated and the crude product was dissolved in CH_2Cl_2, which was then extracted by distilled water to remove copper salts. The solvent was concentrated under *vacuo* and the desired product was precipitated 3 times in Et_2O. ^1H NMR (CD_3OD, δ, ppm) 7.86 (s, 2H), 5.23 (d, *J*=8 Hz, 4H), 4.54 (d, J=16 Hz, 4H), 4.28-4.19 (m, 24H), 3.85 (t, *J* = 4.4 Hz, 8H), 3.80-3.40 (b, s, 756 H), 1.41 (s, 24 H); 1.35 (s, 24 H); 1.30 (s, 6 H), 1.28 (s, 12 H), 1.14 (s, 24 H). (Figure A.12, A.13)

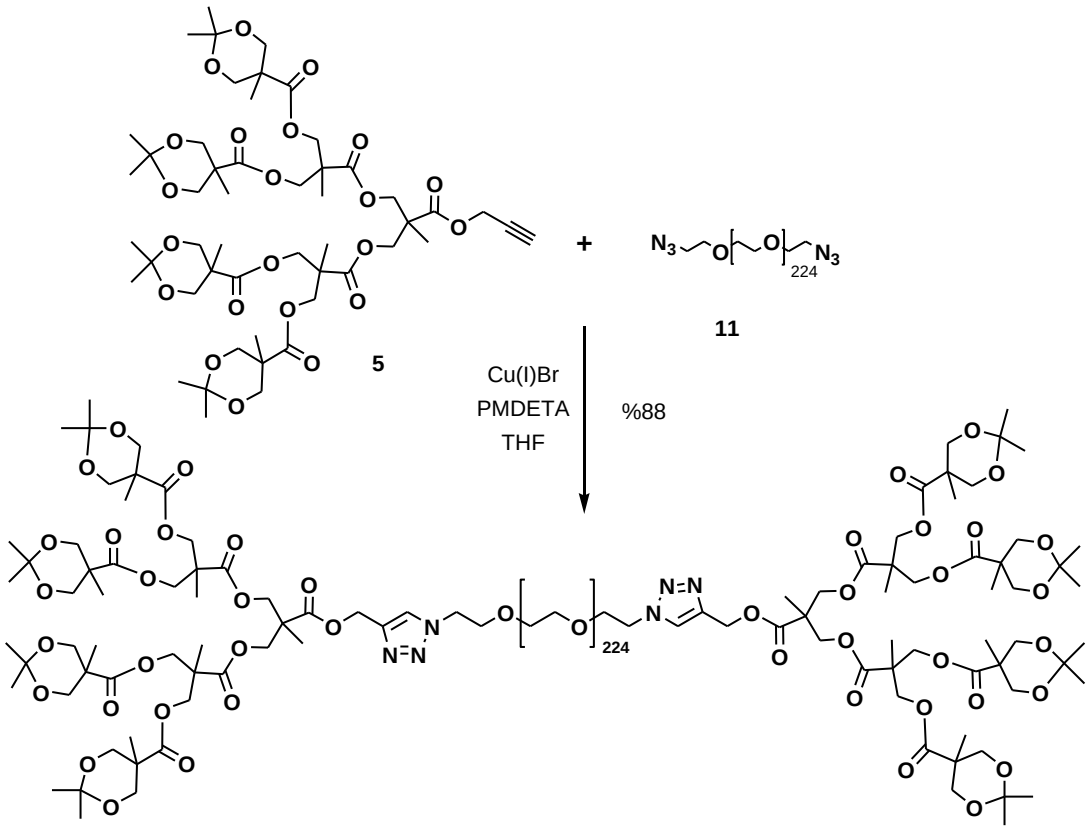

Figure 4.6. Synthesis of [G3]-[PEG 10K]- [G3].

4.4.2. Synthesis of [G3]-[PEG 6K]-[G3]

Third generation polyester dendron (**5**) (132 mg, 0.14 mmol) and N_3-PEG 6 K-N_3 (**10**) (300 mg, 0.04 mmol) were dissolved in dry THF (2 mL). In a separate flask, Cu(I)Br (1 mg, 0.004mmol), PMDETA (10 μL, 0.004 mmol) were dissolved in dry THF (2 mL) and purged with N_2 (Figure 4.7). The mixture was then transferred into copolymer solution and stirred at 40 ^{o}C for 24 h. The solvent was then evaporated and the crude product was dissolved in CH_2Cl_2, which was then extracted by distilled water to remove copper salts. The solvent was concentrated under *vacuo* and the desired product was precipitated 3 times in Et_2O. ^{1}H NMR (CD_3OD, δ, ppm) 7.86 (s, 2H), 5.23 (d, J=12 Hz, 4H), 4.54 (d, J= 8 Hz, 4H), 4.28-4.19 (m, 48H), 3.85 (t, 8H, *J* = 4.4 Hz), 3.80-3.40 (s, 756 H), 1.41 (s, 24H); 1.35 (s, 24H); 1.30 (s, 6H), 1.28 (s, 12H), 1.14 (s, 24H). (Figure A.14, A.15)

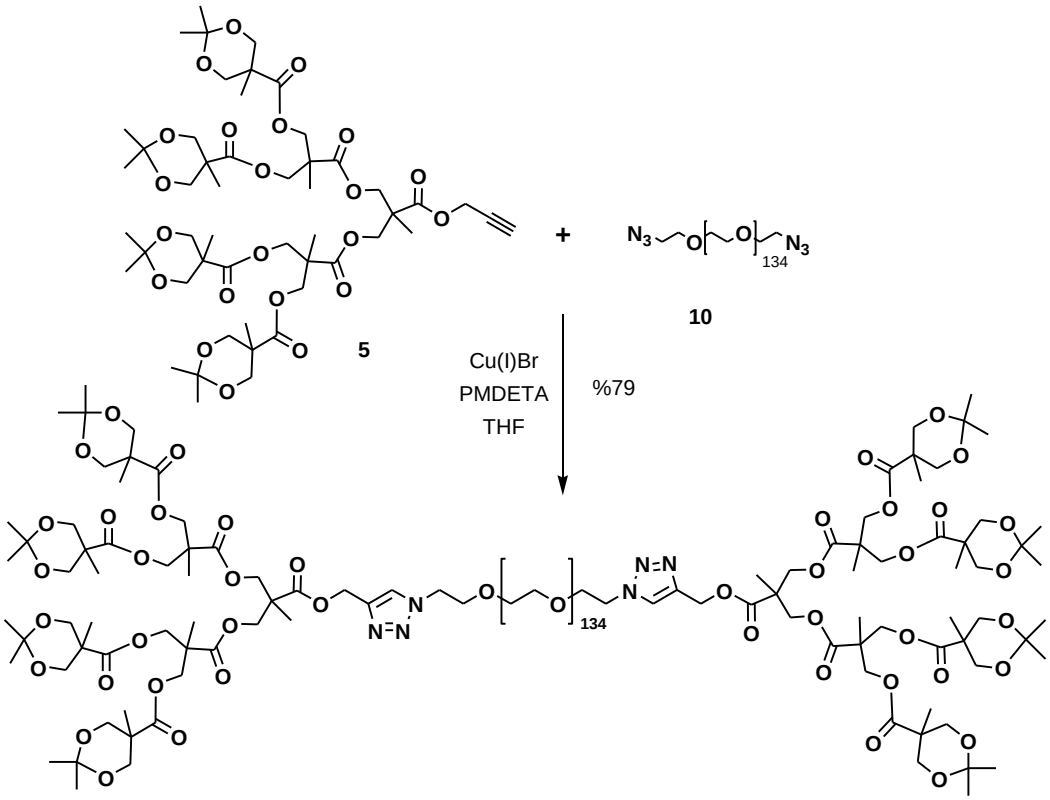

Figure 4.7. Synthesis of [G3]-[PEG 6K]- [G3].

4.4.3. Synthesis of [G3]-[Bn]-[PEG6K]-[G3]-[Bn]

Third generation polyester dendron (**6**) (246 mg, 0.098 mmol) and bisazido PEG 6K (**10**) (mg, 0.033 mmol) were dissolved in dry THF (2 mL). In a separate flask, Cu(I)Br (1 mg, 0.0033 mmol), PMDETA (10 μL, 0.0033 mmol) were dissolved in dry THF (2 mL) and purged with N_2 (Figure 4.8). The mixture was then transferred onto dendron/polymer solution and stirred at 40 ^oC for 24 h. The solvent was then evaporated and the crude product was dissolved in CH_2Cl_2, which was then extracted by distilled water to remove copper salts. The solvent was concentrated under *vacuo* and the desired product was precipitated 3 times in Et_2O.

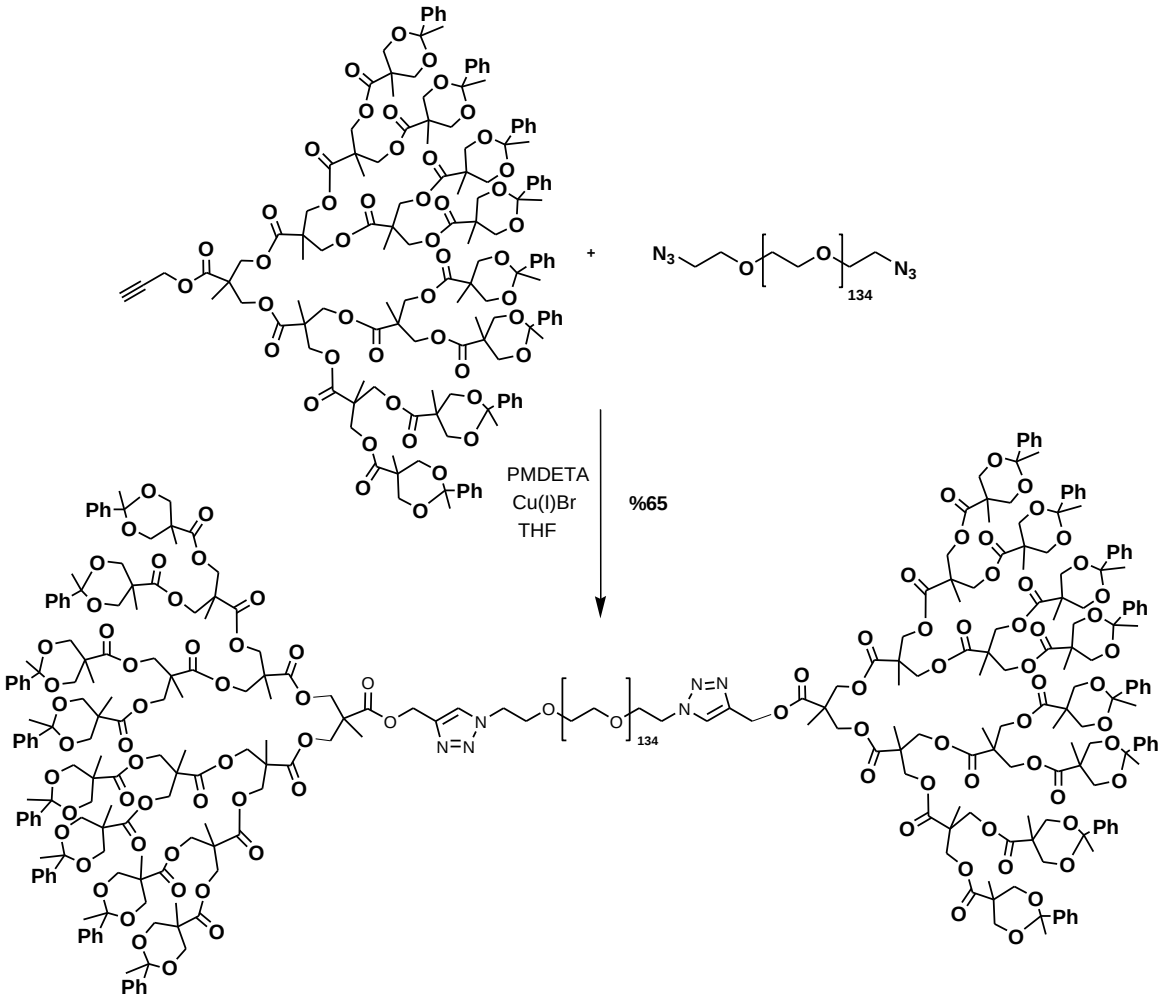

Figure 4.8. Synthesis of [G3]-[Bn]-[PEG6K]-[G3]-[Bn].

4.4.4.Synthesis of [G4]-[PEG6K]-[G4]

Fourth generation polyester dendron (**7**) (53 mg, 0.029 mmol) and N_3-PEG 6 K-N_3 (**10**) (59 mg, 0.0097 mmol) were dissolved in dry THF (2 mL). In a separate flask, Cu(I)Br (1 mg. 0.00097 mmol), PMDETA (10 μL, 0.0097 mmol) were dissolved in dry THF (2 mL) and purged with N_2 (Figure 4.9). The mixture was then transferred onto dendron/polymer solution and stirred at 40 ^oC for 24 h. The solvent was then evaporated and the crude product was dissolved in CH_2Cl_2, which was then extracted by distilled water to remove copper salts. The solvent was concentrated under *vacuo* and the desired product was precipitated 3 times in Et_2O. ^1H NMR (CD_3OD, δ, ppm): 7.86 (s, 2H), 5.23 (d, *J*=7.4 Hz, 4H), 4.54 (t, *J*=10 Hz, 4H), 4.28-4.19 (m, 120 H), 3.80-3.40 (s, 756 H), 1.41 (s, 48H); 1.35 (s, 48H); 1.30 (s, 12H), 1.28 (s, 24H), 1.14 (s, 48H). (Figure A.18, A.19)

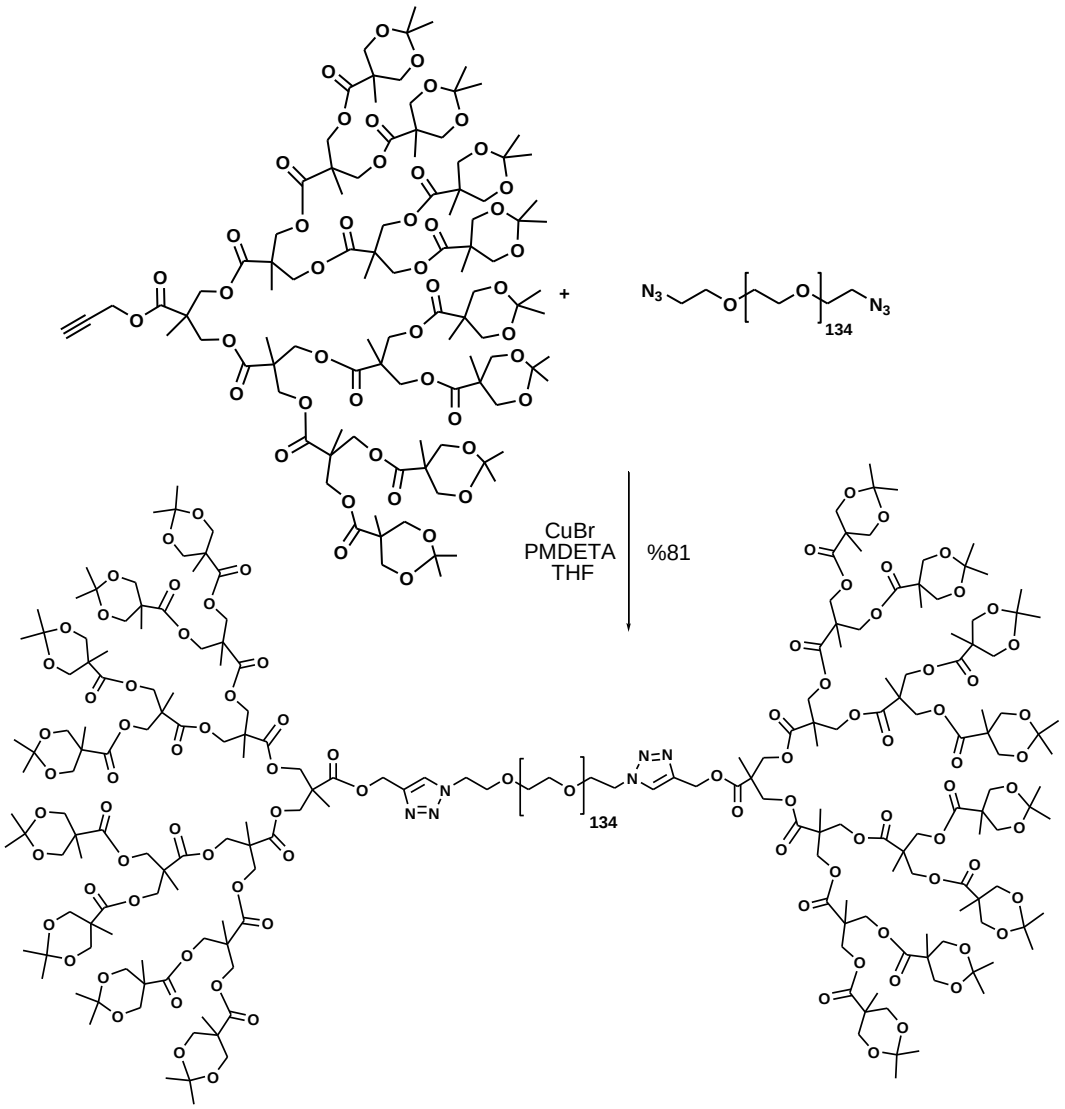

Figure 4.9. Synthesis of [G4]-[PEG 6K]-[G4].

4.5. Micelle Formation from Dendron-Linear Polymer-Dendron Conjugates and Measurements

4.5.1. Fluorescence Measurements

The critical micelle concentrations (CMC) of micelles were calculated from the shift in the excitation peak of pyrene during micellar formation by Fluorescence Sprectroscopy. A hydrophobic dye, pyrene, was used as a Fluorescent probe. Fluorescence spectra were collected at 300-360 nm range using 5 nm width. Pyrene has characteristic peaks at 334 and 338 nm wavelength; therefore, micellar formation can be explained by the shift of the excitation peak of pyrene and the critical micelle concentrations can be determined from the log (concentarion) vs I_{338}/I_{334} graphs. 1.8×10^{-4} M (0.6 mg in 25 mL acetone) of pyrene stock solution was prepared and pyrene-acetone solution (10 µL) was added into vials for each sample. In order to get rid of acetone, all vials waited in decicator in high *vacuo* at least 2 hours. Blank pyrene sample without copolymer for each set of measurements was also prepared as a control and Fluoresence DATA was checked to be sure that all acetone solution was evaporated. Different concentrations of dendron-linear polymer-dendron conjugates (10^{-4} to 10^{-8} M) were prepared in Milli-Q water. After the preparation of each sample, the solutions were sonicated for 1 h at room temperature. The final pyrene concentration was 6×10^{-7} M. After keeping the each sample for 24 h, micelle formations of conjugates were characterized by Fluorescence spectroscopy (Cary Eclipse).

4.5.2. Dynamic Light Scattering (DLS) Measurements

In order to monitor the effective diameter size and the size distribution of pyrene loaded and drug loaded micelles, samples were prepared by using Milli-Q water at desired concentrations and sonicated at room temperature for 1 hour. The micellar sizes were monitored using dynamic light scattering method at 25 ^{o}C and 90^{o} angle. The size distribution were determined using number vs diameter graph which shows the number of micelles at certain diameter. Intensity vs diameter graphs were also checked which shows the intensity at certain diameter of micelles.

4.5.3. Scanning Transmission Electron Microscope (STEM) Images

Pyrene loaded and CA-4 loaded micelles from several dendron-linear polymer-dendron conjugates were prepared in distilled water as described above. The micelle solutions were filtrated through 0.22 μm syringe filter and one drop of micelle solution was put on the copper grid and waited until all water evaporated. In order to image the micellar structures, Scanning Transmission Electron Microscope (STEM) was used with copper grid.

4.6. Hydrolysis Rate of Acetals in Micelles (Measurement of Pyrene Release)

The desired concentrations of copolymers (10 times higher than the critical micelle concentration) and 10 μL of 1.8 x 10^{-4} M pyrene-acetone solution were added into vials for each sample. In order to get rid of acetone, all vials waited in decicator in high *vacuo* at least 2 hours. Blank pyrene sample without copolymer was also prepared as a control and Fluoresence spectrum was checked to be sure that all acetone solution was evaporated. Then, these micelles were prepared in 10 mM pH 7.4 PBS (6mL). After 1 hour sonification, each sample were kept at room temparture in dark for 20 h. The solution was divided into two 3 mL samples and the fluresecence intensity of each sample monitored. One of them adjusted to pH 5.0 to mimic the acidic environment of solid tumors by the addition of 4 M pH 5.0 (100 μL) acetate buffer, while another 4 mL of sample was maintained at neutral pH. However, in order to adjust the salt concentrations of each sample, 4 M (100 μL) pH 7.4 PBS buffer was added. Two of the solutions were stirred in oil bath at 37^0C. The fluorescence spectrum of each solution was monitored at the desired time points to measure the pyrene release rate.

4.7. CA-4 Loading in Micelles

For the self-assembly and drug encapsulation, co-solvent evaporation method was used according to the literature [48]. [G4]-[PEG6K]-[G4] (6 mg) and CA-4 (0.6 mg) were dissolved in acetone (0.5 mL), corresponding to a final 1:6 organic/aqueous phase ratio. This organic solution was then added drop-wise to the aqueous phase (3 mL) and sonicated

for 4 h. at room temperature. Vacuum was applied to get rid of the remaining organic solvent and drug loaded micelle solution was kept at room temperature for 20 h. At the end of encapsulation process, in order to get rid of the free drug in the solution SEPHADEX G75 column was used and the drug amount in each collected 2 mL of tubes were measured by LC/MS.

4.8. Drug Release

After the preparation of 6 mL of micelle solution in 10 mM pH 7.4 PBS without free drug, the solution was divided into two 3 mL of samples and the UV absorption of each sample monitored. These two solutions were put in a dialysis bag. One of them adjusted to pH 5.0 to mimic the acidic environment of solid tumors by the addition of 4 M pH 5.0 acetate buffer (35 mL), while another 3 mL of sample was maintained at neutral pH by the addition of 4 M pH 7.4 PBS buffer (35 mL). Two of the solutions were stirred in oil bath at 37^0C. The UV absorption of each solution in dialysis bag was monitored at the desired time points to measure the drug release rate and also the drug amount out of the dialysis bag was measured by LC/MS at the desired time points.

4.9. Cellular Viability and Toxicity Assay

For the cell culture measurements, Human umbilical vein endothelial cells (HUVEC) were purchased from Lonza Group Ltd. and maintained in EGM-2 complete medium in a humidified atmosphere at 37°C and 5 % CO_2.

In this toxicity assay, the water soluble WST-8 (2-(2-methoxy-4-nitrophenyl)-3-(4-nitrophenyl)-5-(2,4-disulfophenyl)-2H-tetrazolium, monosodium salt) dye is reduced by mitochondrial dehydrogenase enzymes in the viable cells to form water soluble formazan dye.

Cells were cultured as 2000 or 3000 cells/well in 96-well plates and allowed to recover for 24 hours. Cells were treated with the indicated concentrations of micellar CA4 in EGM-2 complete media. After the indicated treatment durations, 10 µL of CCK-8 labeling reagent and 100 µL complete media were added to each well and incubated for 4

hours at 37°C. The absorbance was recorded in a Thermo Scientific Multiskan FC microplate reader at 450 nm and results were analyzed via SkanIt software.

4.10. Cellular Binding and Internalization of Micelles

To investigate the cellular binding and internalization of [G4]-[PEG 6K]-[G4] micelles, Nile Red was used as a fluorescent labeled dye. Copolymer conjugate (**16**) (1 mg/mL), Nile Red (0,001 mg/mL) in acetone were waited in decicator in high *vacuo* at least 2 hours to evaporate the organic solvent. Blank Nile Red sample without copolymer for each set of measurements was also prepared as a control and Fluoresence DATA was checked to be sure that all acetone solution was evaporated. After the addition of water phase and sonication for one hour at room temperature, Nile Red loaded micelles were monitored by Fluorescence Spectroscopy. In order to get rid of the free dye molecules in the micellar solution, SEPHADEX G75 column was used and the dye content in each collected 2 mL of tubes were measured by Fluorescence Spectroscopy.

For fluorescence microscopy experiments, HUVECs were cultured on glass coverslips in 6-well plates and treated with Nile Red loaded micelles as 1:1 or 1:2 dilutions with EGM-2 complete medium containing FBS. After treatment for 2 hours and 4 hours; media containing labeled micelles were removed; cells were washed 3 times with PBS, fixed with 4% formaldehyde solution, and washed 3 additional times with PBS. For nuclear labeling; fixed cells were treated with DAPI (4',6-diamidino-2-phenylindole) at 0.1 µg/mL final concentration for 10 minutes, washed 3 times with PBS followed by mounting on glass slides. Cell culture grade PBS was used as mounting media. Images were obtained using LD-A-Plan 20x/0.30 objective in Zeiss Axio Observer inverted microscope. Untreated cells were used as negative control. Zeiss Filter set 39 (Excitation G 365, Emission BP 445/50) was used for imaging DAPI stained nuclei, while Filter set 43 (Excitation BP 545/25, Emission BP 605/70) was used for imaging Nile Red stained cells. Images were merged using NIH Image J software.

5. CONCLUSION

In this thesis project, various dendron-linear polymer-dendron conjugates were synthesized via Huisgen type ‘click’ reaction using biodegradable polyester dendron and biocompatible PEG. Functionalization of the dendron surface with hydrophobic moieties increased the tendency to form micellar structures in water via self-assembly and also provided pH sensitivity due to acetal units.

To achieve the most stable micellar structure that can encapsulate the effective dose of therapeutic agent at neutral pH, four different amphiphilic copolymers were synthesized. By changing the length of hydrophilic polymer, the type of acetal moiety and the generation of the dendron, the optimum micellar structure that can maximize the therapeutic effect of the drug was achieved with [G4]-[PEG6K]-[G4] micelles. All the micellar structures were in spherical shape and a diameter of 30-80 nm which were characterized by dynamic light scattering (DLS) and scanning transmission electron microscopy (STEM).

The stability of the micelles at neutral pH was demonstrated by the release rate of the hydrophobic dye and the most stable copolymer system, [G4]-[PEG6K]-[G4], was chosen for further drug loading studies. The optimum micellar nanoparticles phsically loaded with anti cancer drug molecules and the drug-release period investigated for the anticancer drug delivery systems.

[G4]-[PEG6K]-[G4] micelles were phsically encapsulated with anti-cancer therapeutic agent (CA-4) by co-solvent evaporation method and the drug release was monitored by UV-VIS spectroscopy and LC/MS. As expected, the drug nanocarrier carried all its payload at neutral pH, while destabilizing the micellar structure and releasing its drug payload under acidic conditions.

In conclusion, pH-sensitive micelles were designed from the self-assembly of novel dendritic hydrophobic block and hydrophilic polymer in aqueous media. These micelles were investigated as promising drug nanocarriers with facile drug loading capacity and high stability at neutral pH.

APPENDIX A: SPECTROSCOPY DATA

^{1}H NMR and FT-IR spectra of the synthesized products are included

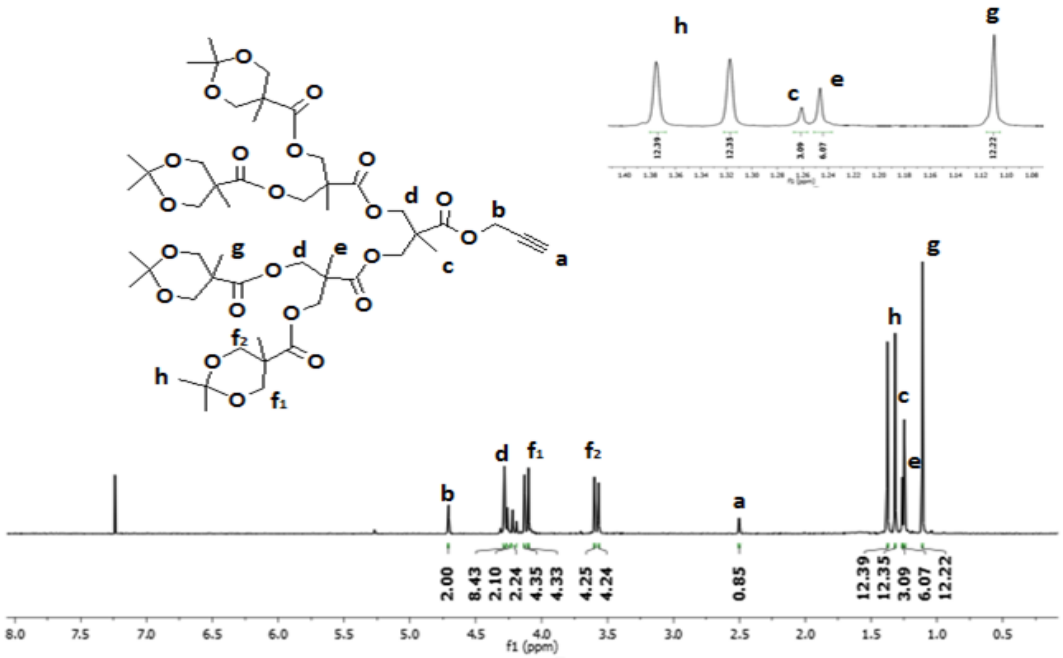

Figure A.1. ^{1}H NMR spectrum of product 5.

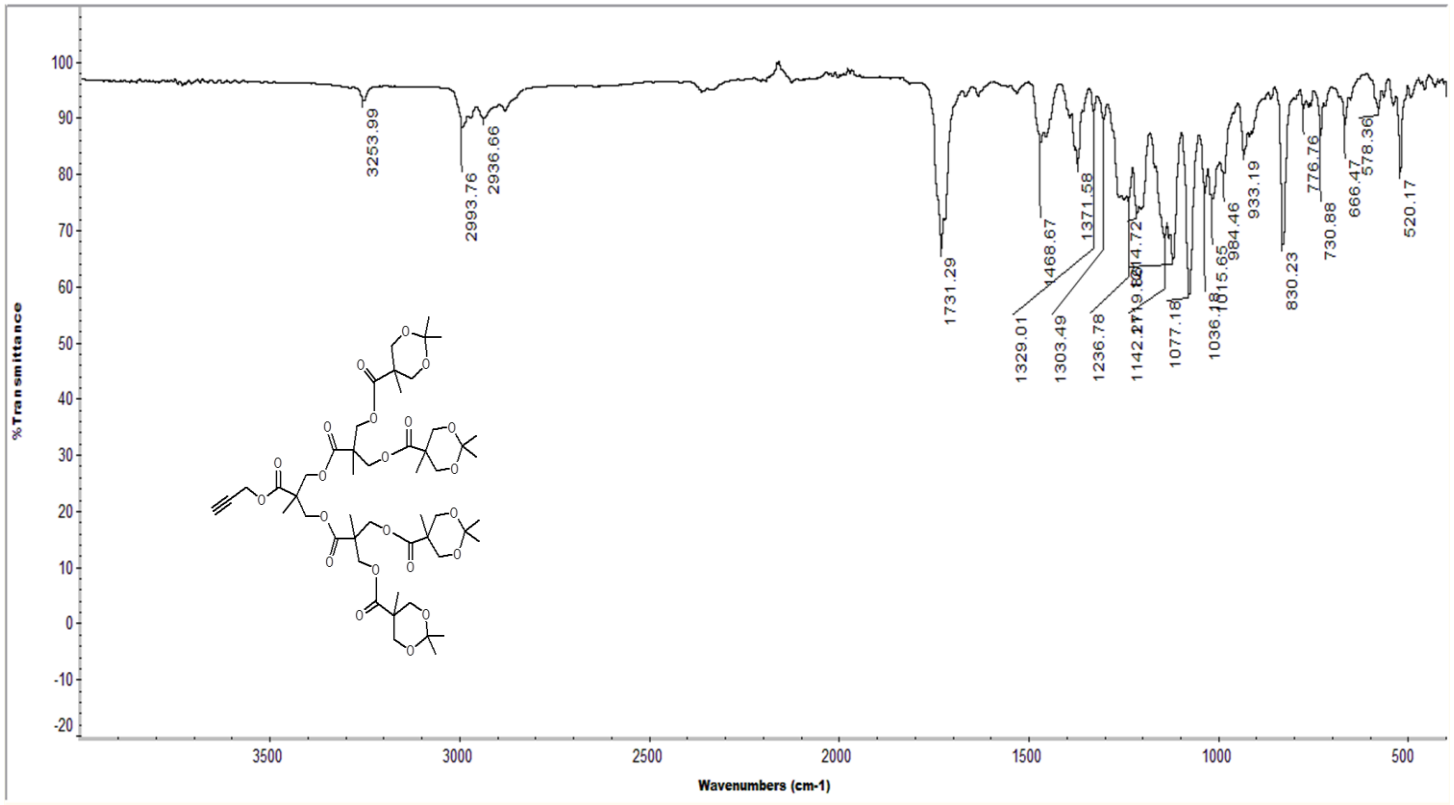

Figure A.2. FT-IR spectrum of product 5.

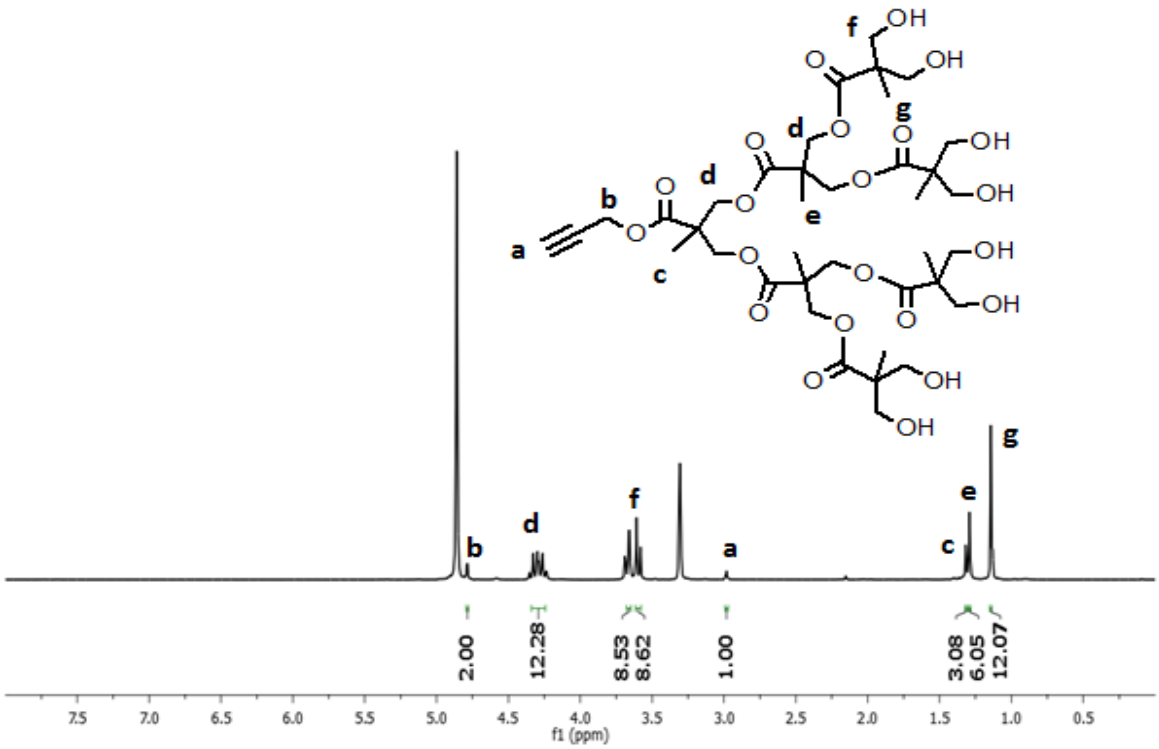

Figure A.3. ^{1}H NMR spectrum of product 6.

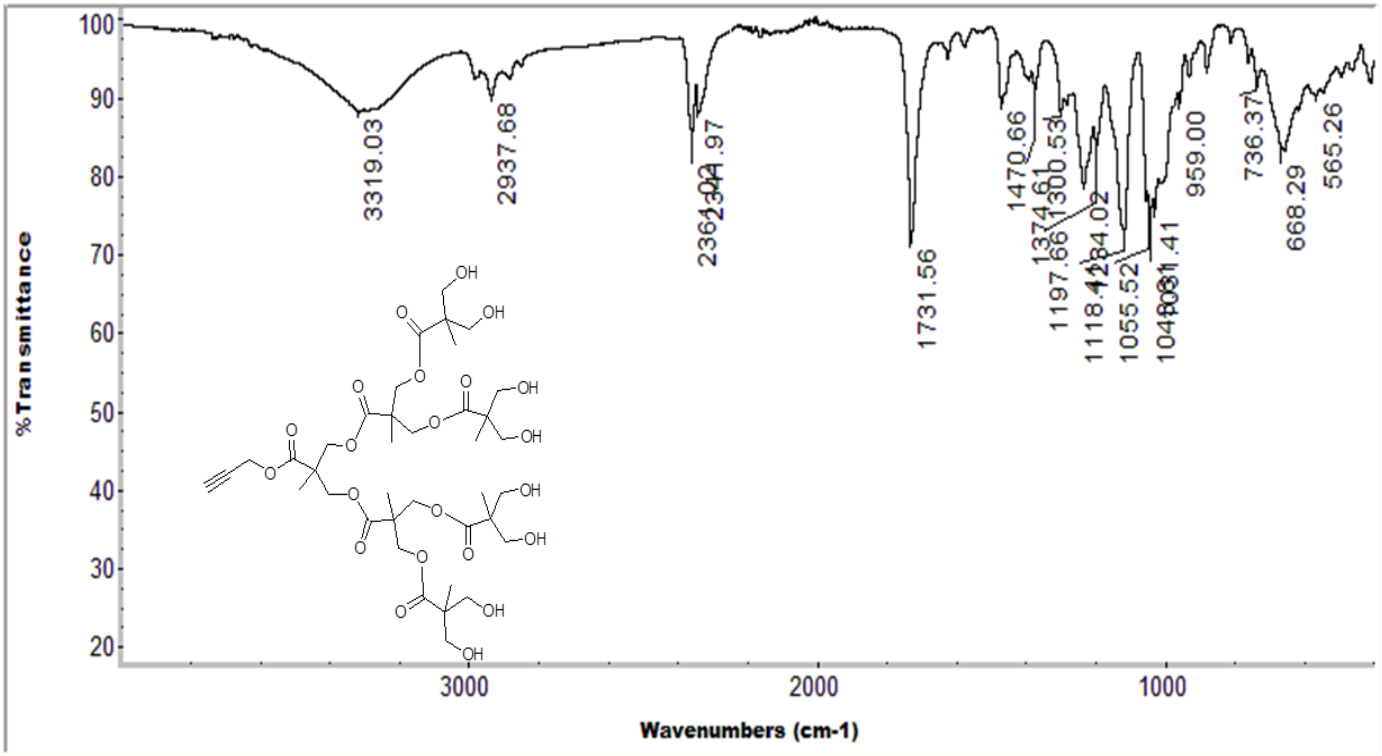

Figure A.4. FT-IR spectrum of product 6.

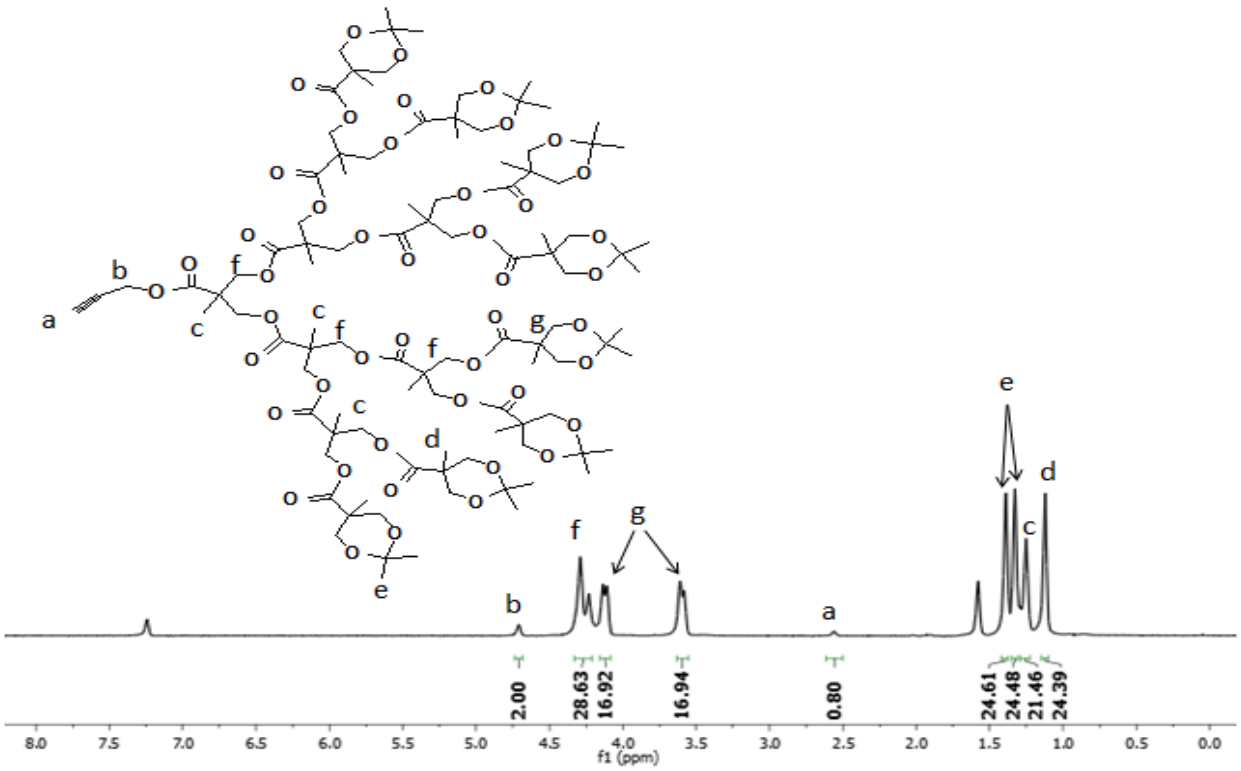

Figure A.5. ^{1}H NMR spectrum of product 7.

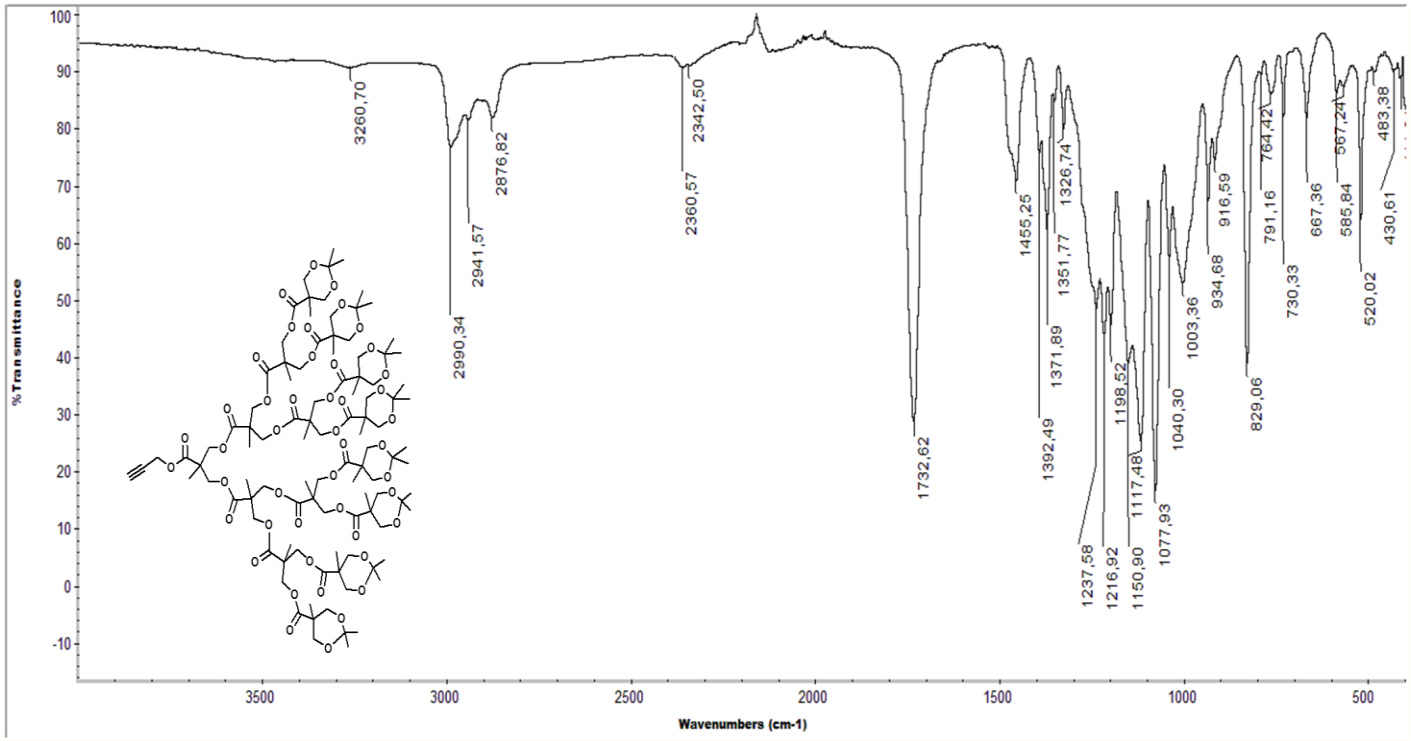

Figure A.6. FT-IR spectrum of product 7

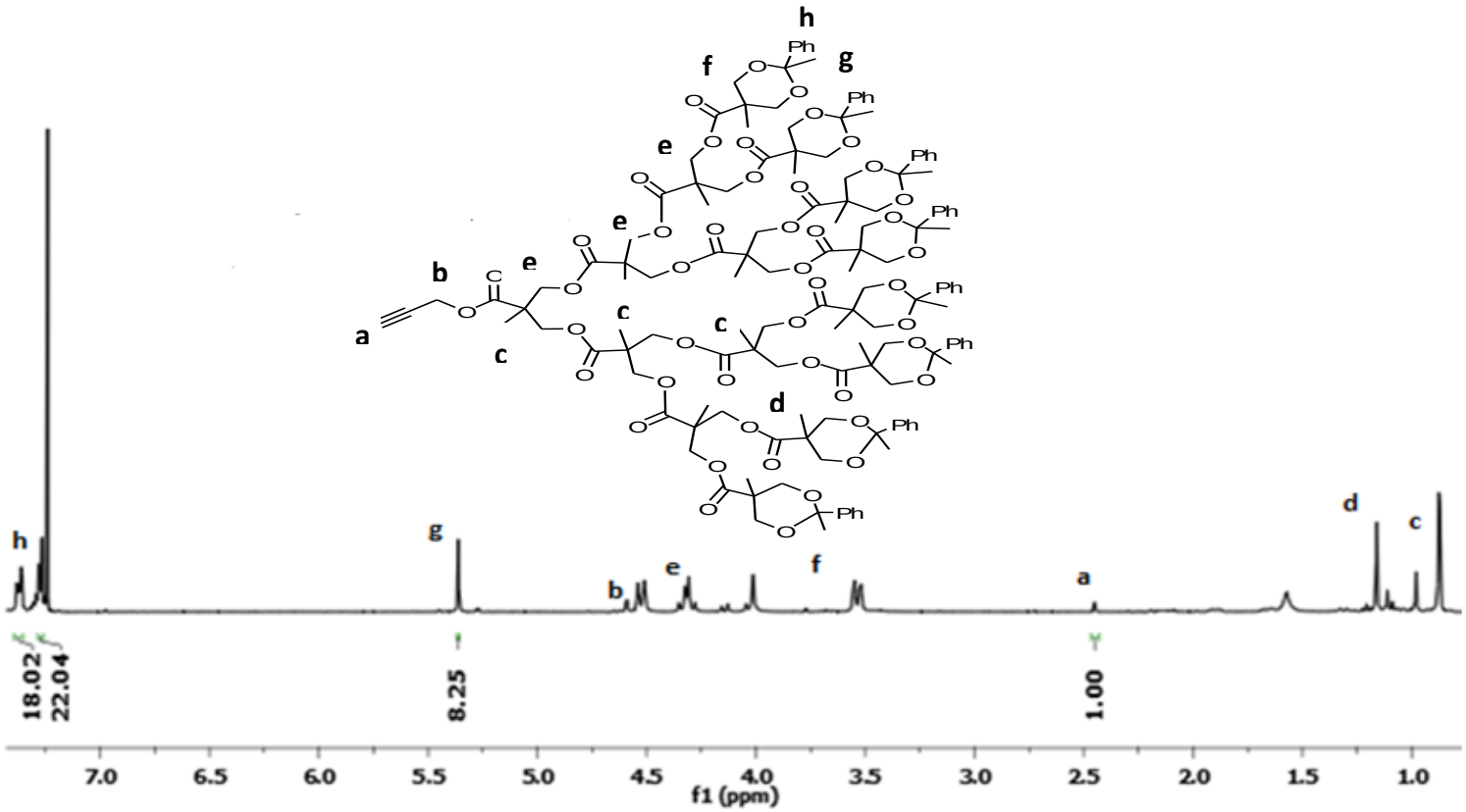

Figure A.7. ^{1}H NMR spectrum of product 12.

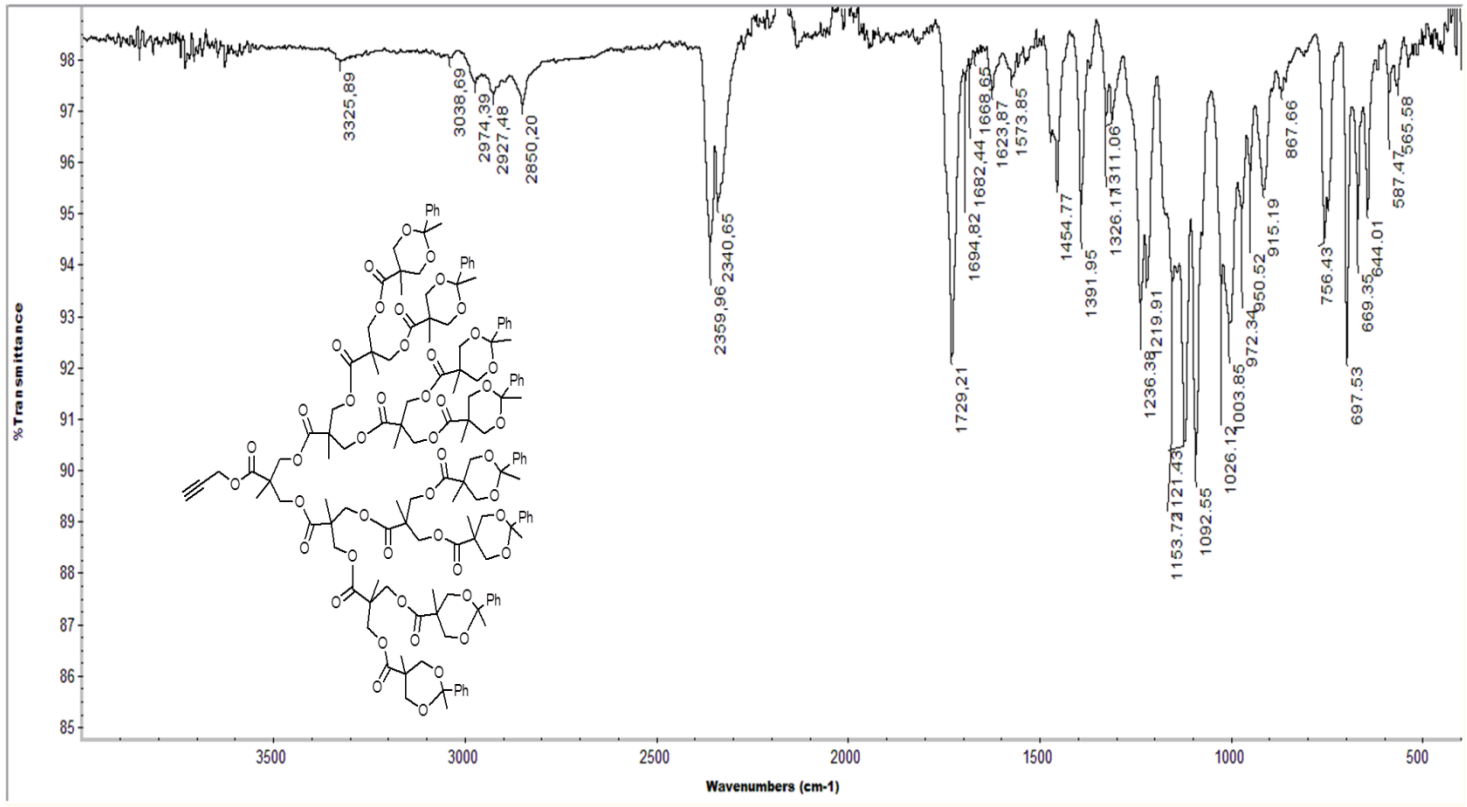

Figure A.8. FT-IR spectrum of product 12.

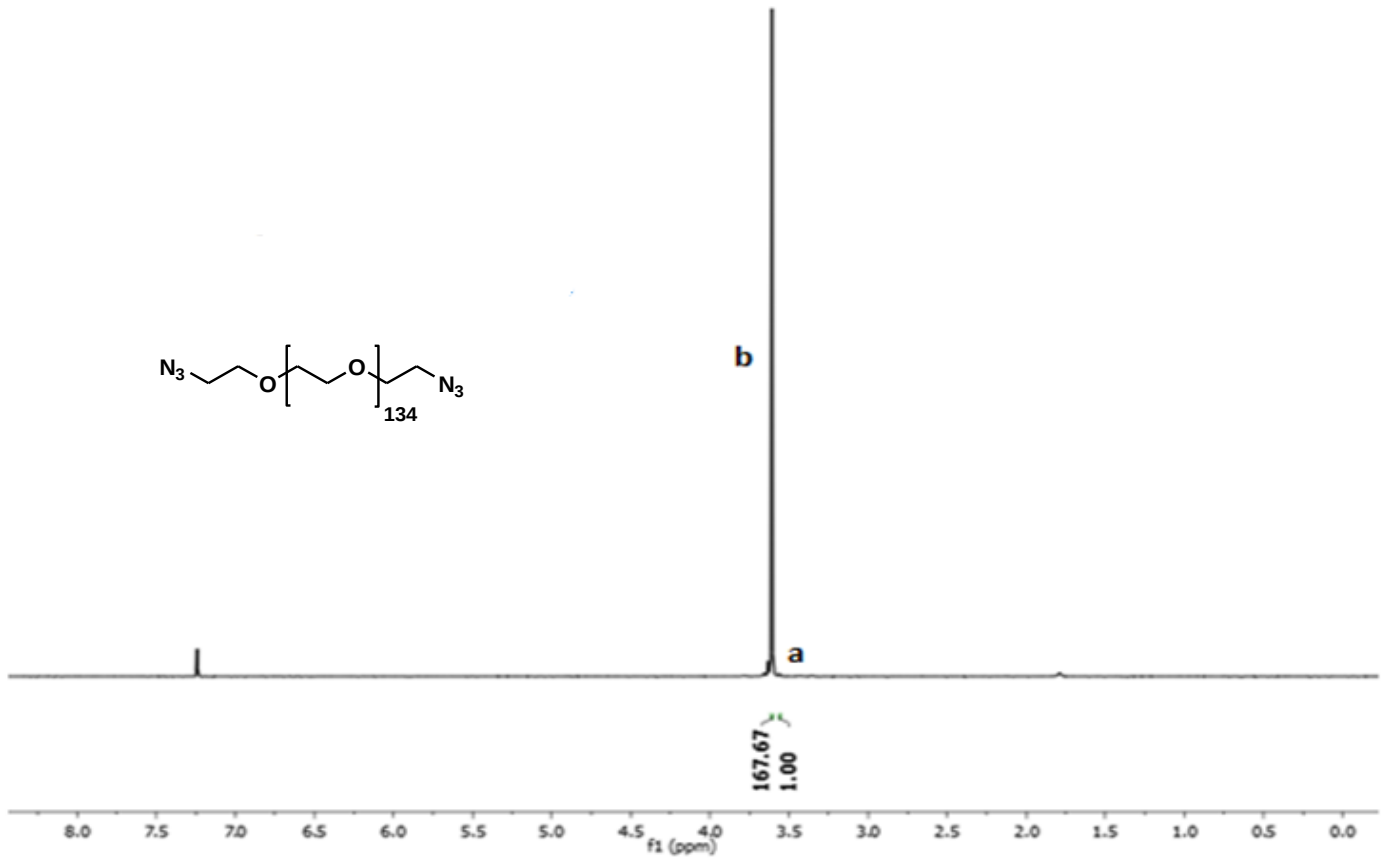

Figure A.9. ^{1}H NMR spectrum of product 10.

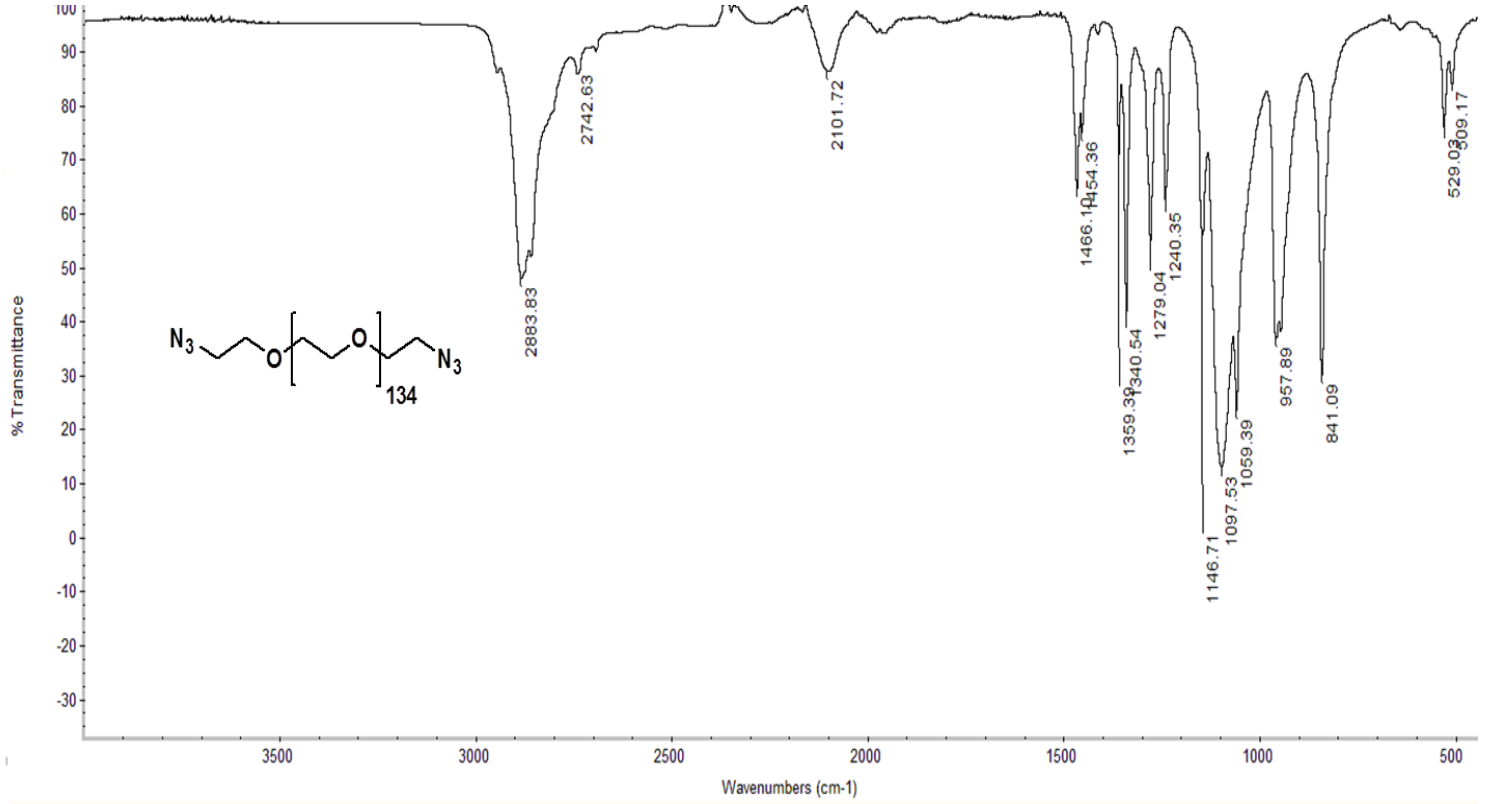

Figure A.10. FT-IR spectrum of product 10.

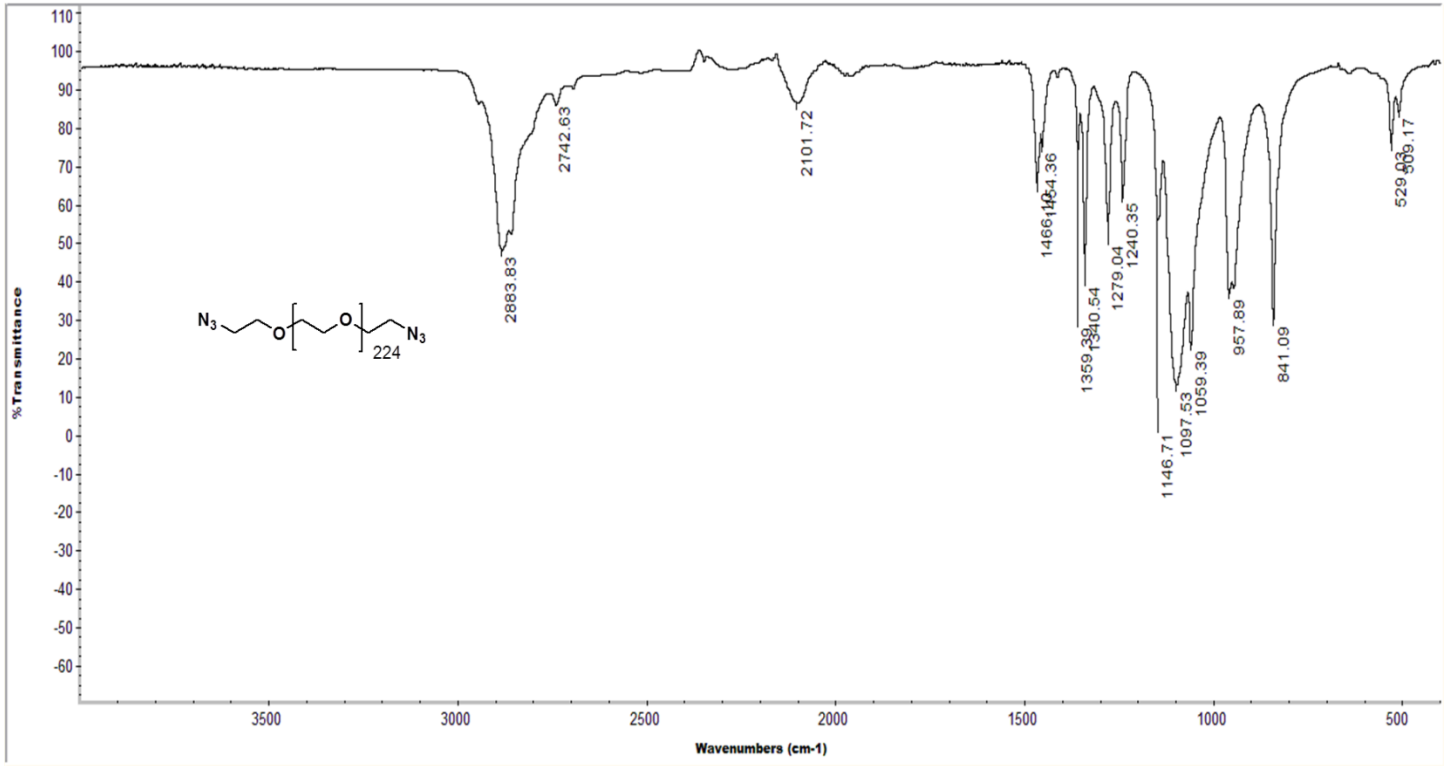

74

Figure A.11. FT-IR spectrum of product 11.

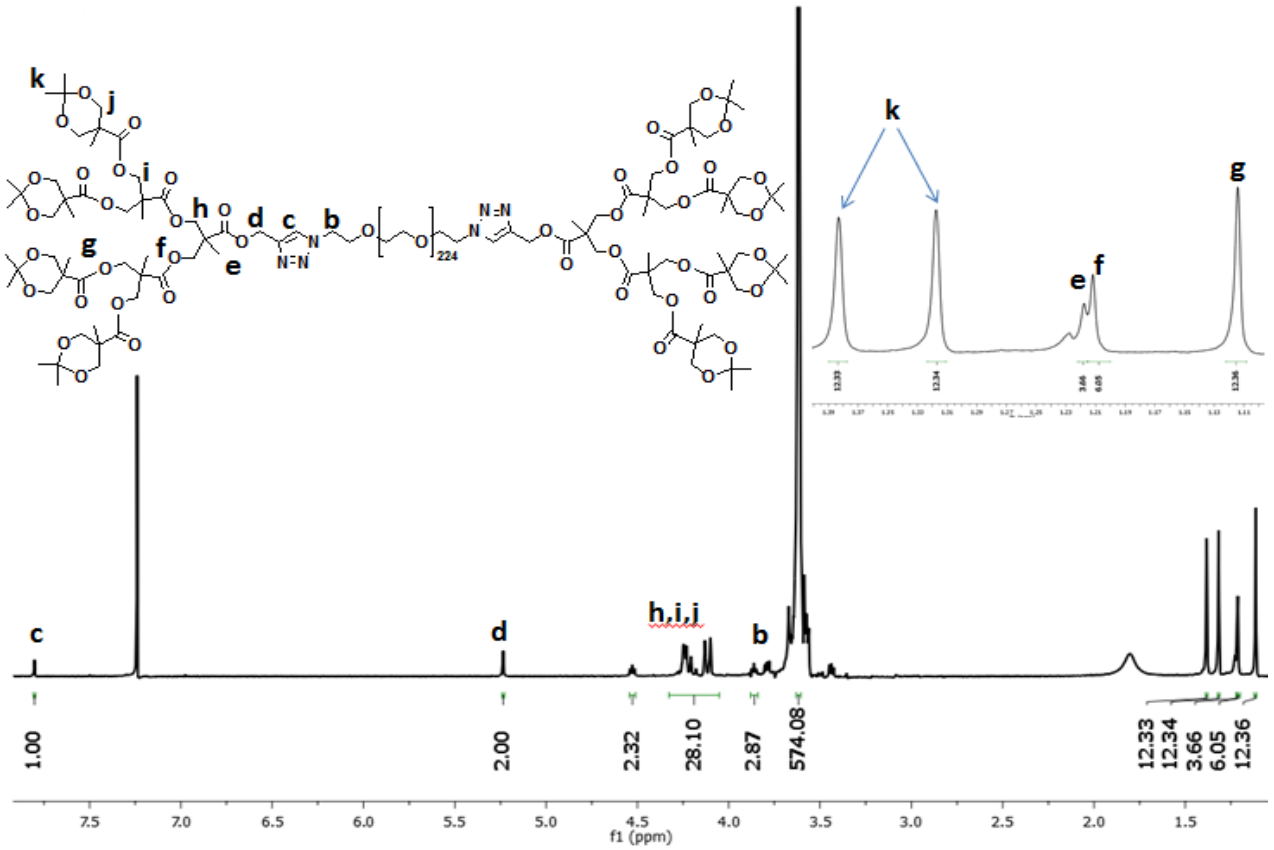

Figure A.12. ^{1}H NMR spectrum of product 13.

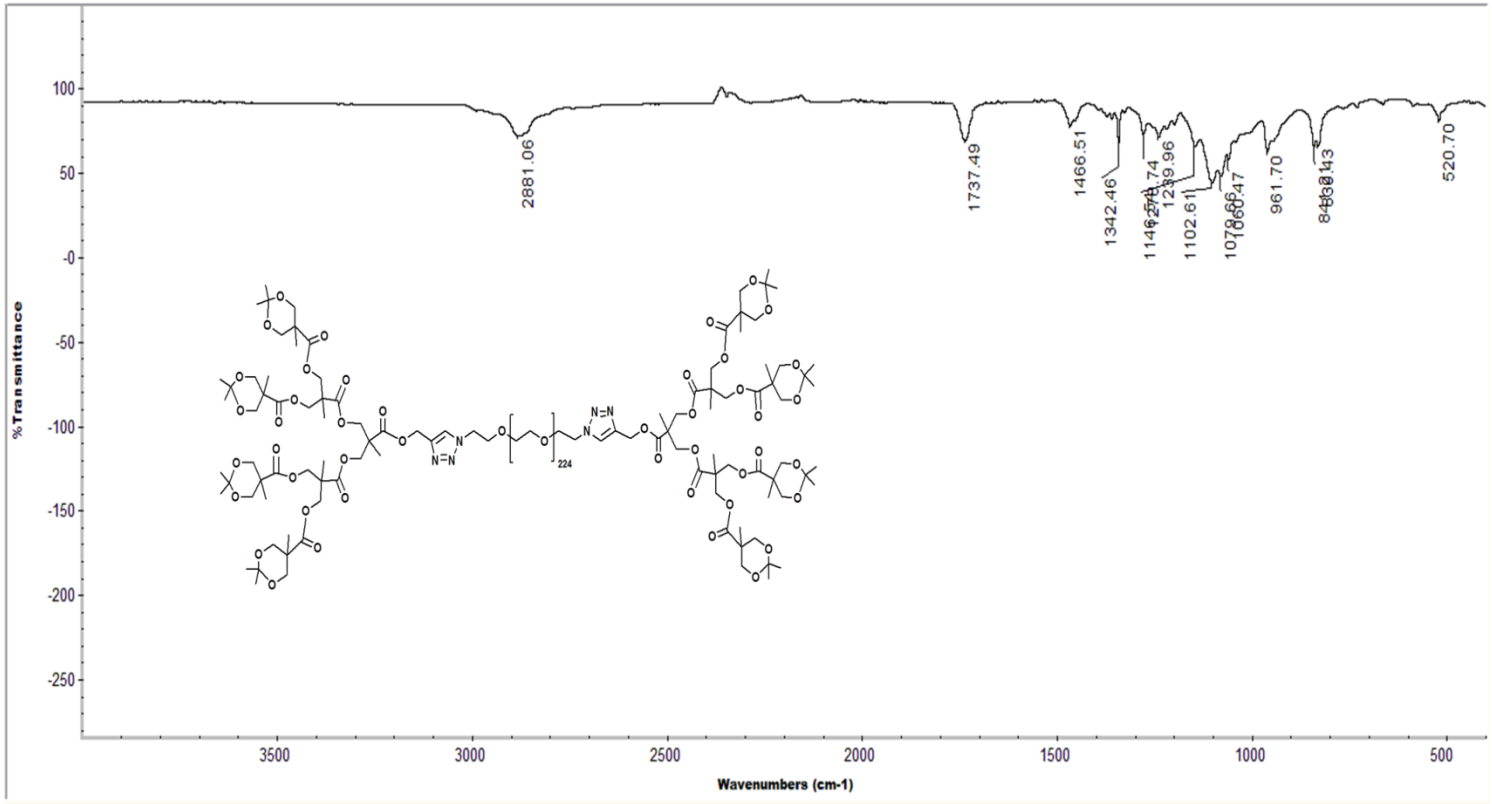

Figure A.13. FT-IR spectrum of product 13.

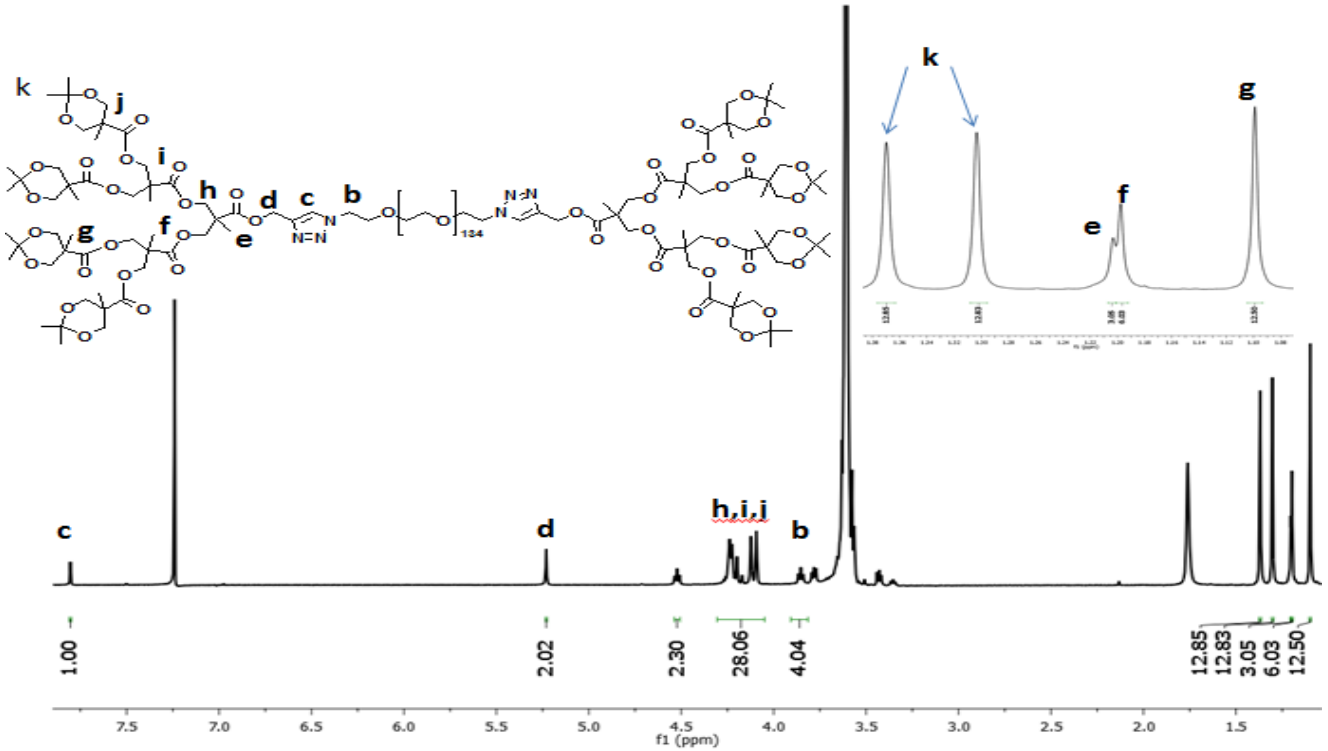

Figure A.14. ^{1}H NMR spectrum of product 14.

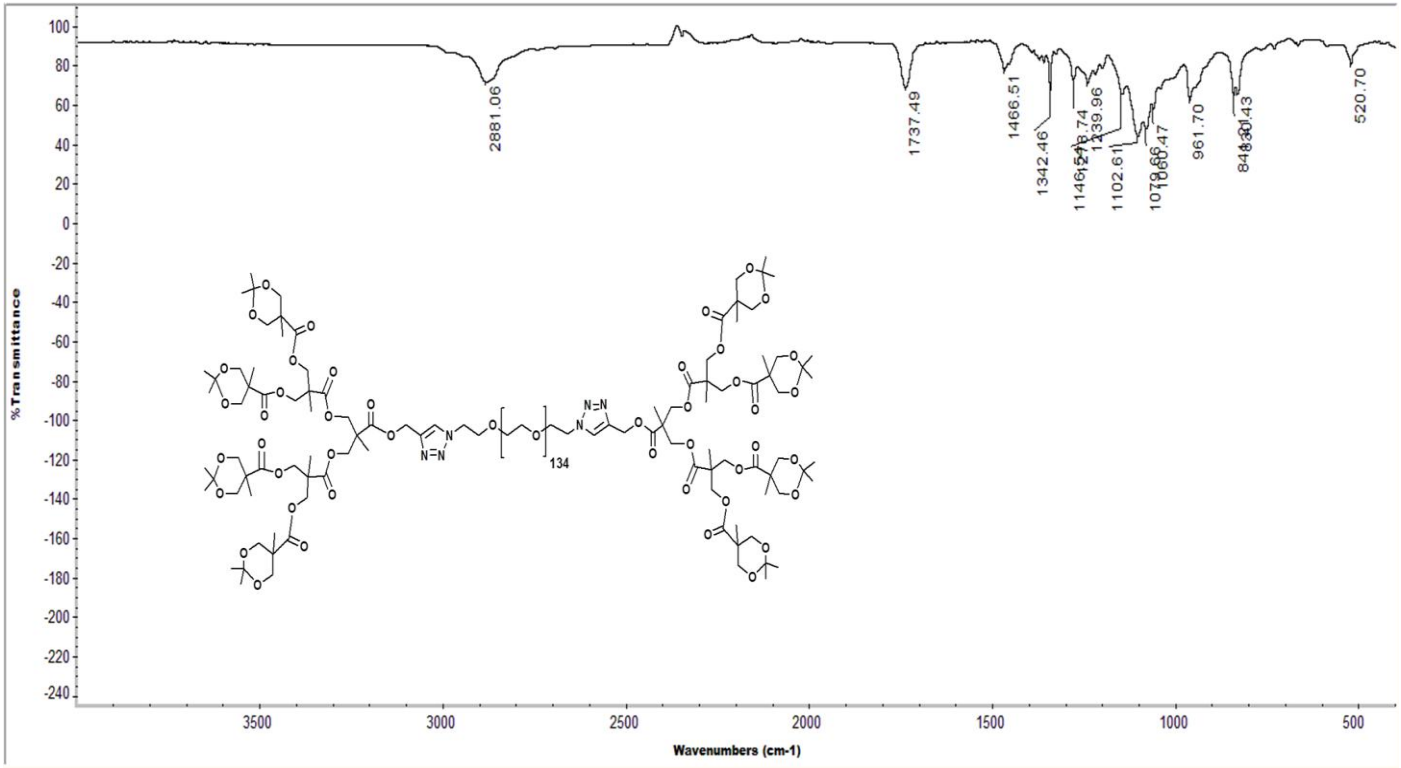

Figure A.15. FT-IR spectrum of product 14.

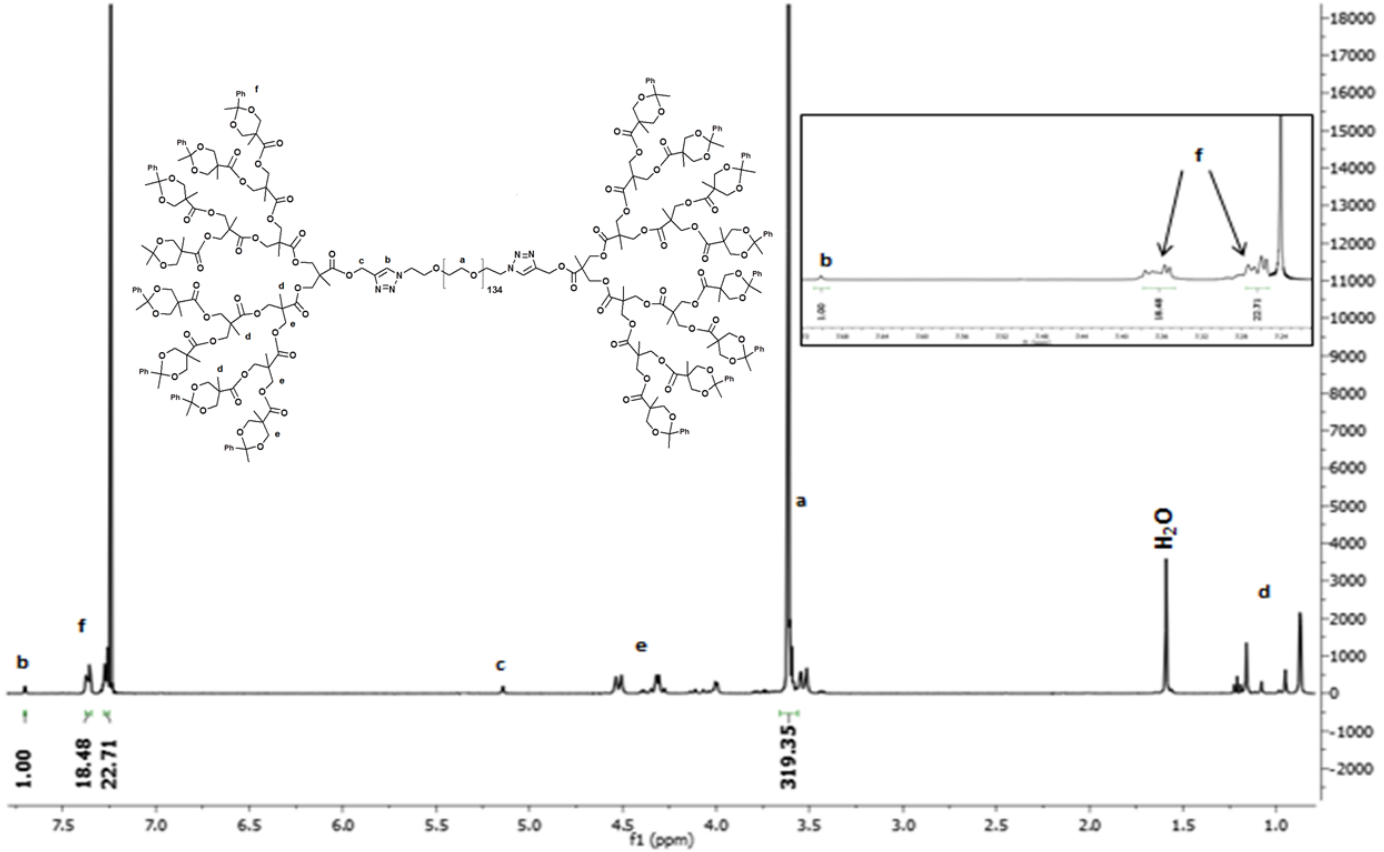

Figure A.16. ^{1}H NMR spectrum of product 15.

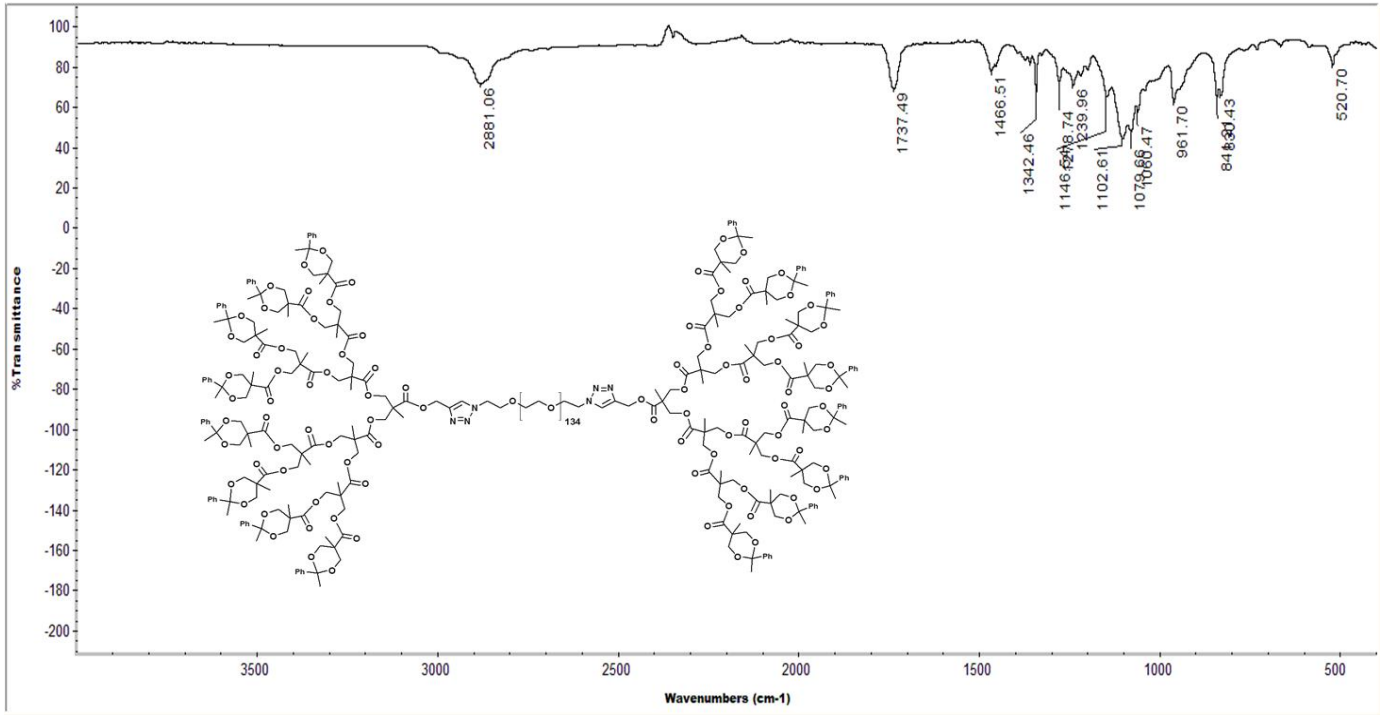

76

Figure A.17. FT-IR spectrum of product 15.

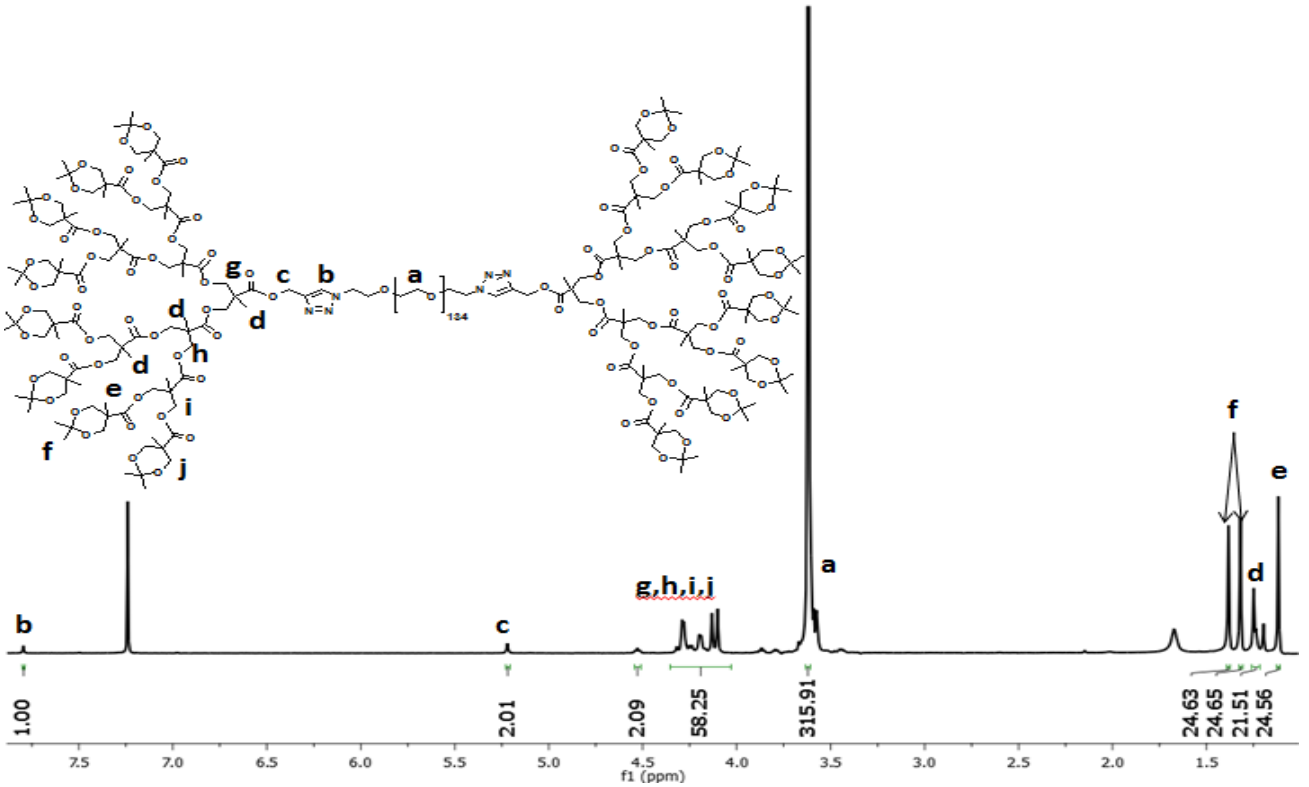

Figure A.18. ^{1}H NMR spectrum of product 16.

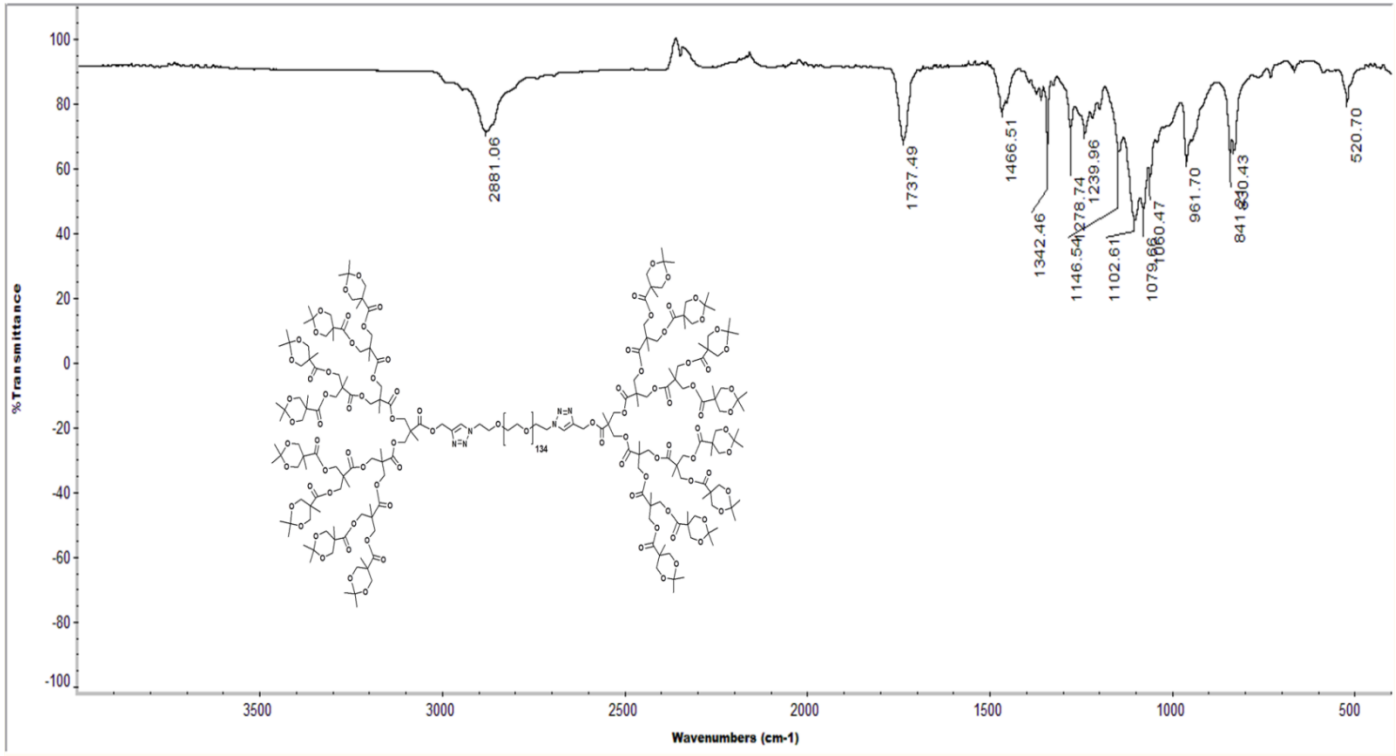

Figure A.19. FT-IR spectrum of product 16.

REFERENCES

1. Jemal, A., R. Siegel, E. Ward, Y. P. Hao, J. Q. Xu, T. Murray, and M. J. Thun, "Cancer Statistics" , *A Cancer Journal for Clinicians*, Vol. 58, pp. 71−96, 2008.

2. Wilson, A., "5-Year Cancer Survival Rates are Increasing", 2011, http://healthhubs.net/cancer/5-year-cancer-survival-rates-are-increasing/, September 2011.

3. Danhier, F., O. Feron, and V. Préat, "To Exploit the Tumor Microenvironment: Passive and Active Tumor Targeting of Nanocarriers for Anti-Cancer Drug Delivery", *Experimental Biology and Medicine*, Vol. 234, pp.123-131, 2008.

4. Kataoka, K., H. Cabral, and N. Nishiyama, "Supramolecular Nanodevices: From Design Validation to Theranostic Nanomedicine", *Accounts of Chemical Research*, Vol. 44, pp. 999–1008, 2011.

5. Matsumura, Y., and H. Maeda, "A New Concept for Macromolecular Therapeutics in Cancer Chemotherapy: Mechanism of Tumoritropic Accumulation of Proteins and the Antitumor Agent Smancs", *Cancer Research*, Vol. 46, pp. 6387–6392, 1986.

6. Lavasanifar, A., X-B. Xiong, Z. Binkhathlan, and O. Molavi, "Amphiphilic block co-polymers: Preparation and application in nanodrug and gene delivery", *Acta Biomaterialia*, Vol. 8, pp. 2017–2033, 2012.

7. Ringsdorf, H., K. Dorn, and G. Hoerpel, "Polymeric Antitumor Agents on a Molecular and Cellular Level", *New York: Plenium Press*, pp. 531–85, 1985.

8. Kataoka, K., M. Yokoyama, S. Inoue, N. Yui, and Y. Sakurai, "Preparation of Adriamycin-Conjugated Poly(ethylene glycol)-Poly(aspartic acid) Block Copolymer", *Macromolecular Rapid Communications*, Vol. 8, pp. 431–5, 1987.

9. Suzuki, M., T. Hamaguchi, Y. Matsumura, K. Shimizu, R. Goda, and I. Nakamura, "NK105, A Paclitaxel-Incorporating Micellar Nanoparticle Formulation, Can Extend in vivo Antitumour Activity and Reduce the Neurotoxicity of Paclitaxel", *British Journal of Cancer*, Vol. 92, pp. 1240–1246, 2005.

10. Suzuki, M., T. Nakanishi, S. Fukushima, K. Okamoto, Y. Matsumura, and M. Yokoyama, "Development of the Polymer Micelle Carrier System for Doxorubicin", *Journal of Controlled Release*, Vol. 74, pp. 295–302, 2001.

11. Kataoka K., N. Nishiyama, M. Yokoyama, T. Aoyagi, T. Okano, and Y. Sakurai, "Polymeric Micelles for Drug Delivery", *Langmuir*, Vol. 15, pp. 377–83, 1998.

12. Zhang, X., H.M. Burt, D. VonHoff, D. Dexter, G. Mangold, and D. Degen, "An Investigation of the Antitumour Activity and Biodistribution of Polymeric Micellar Paclitaxel", *Cancer Chemotherapy and Pharmacology*, Vol. 40, pp. 81–6, 1997.

13. Sutton, D., N. Nasongkla, E. Blanco, and J. Gao, "Functionalized Micellar Systems for Cancer Targeted Drug Delivery", *Pharmaceutical Research*, Vol. 24, No. 6, pp. 1029-1046, 2007.

14. Lavasanifar, A., X-B. Xiong, A. Falamarzian, and S.M. Garg, "Engineering of Amphiphilic Block Copolymers for Polymeric Micellar Drug and Gene Delivery" *Journal of Controlled Release*, Vol. 155, pp. 248–261, 2011.

15. Kim, S., Y. Shi, J. Y. Kim, K. Park, and J. Y. Cheng, "Overcoming the Barriers in Micellar Drug Delivery: Loading Efficiency, in vivo Stability, and Micelle–Cell Interaction", *Expert Opinion on Drug Delivery*, Vol. 7, pp. 49–6, 2010.

16. Kataoka, K., Y. Bae, W. D. Jang, N. Nishiyama, and S. Fukushima, "Multifunctional Polymeric Micelles with Folate-Mediated Cancer Cell Targeting and pH-triggered Drug Releasing Properties for Active Intracellular Drug Delivery*", Molecular BioSystem*, Vol. 1, pp. 242–50, 2005.

17. Gingras, M., J. M. Raimundo, and Y. M. Chabre, "Cleavable Dendrimers", *Angewandthe Chemie International Edition*, Vol. 46, pp. 1010-1017, 2007.

18. Tomalia, D.A., H. Baker, J. R. Dewald, M. Hal, G. Kallos, S. Martin, J. Roeck, J. Ryder, and P. Smith, "A New Class of Polymers:Starburst-Dendritic Macromolecules", *Polymer Journal*, Vol. 17, pp. 117-132, 1985.

19. Newkome, G.R., Z. Yao, G. R. Baker, and V. K. Gupta, "Cascade Molecules: A New Approach to Micelles", *Journal of Organic Chemistry*, Vol.50, pp. 2003-2004, 1985.

20. Hawker, C. J., and J. M. Fréchet, "Preparation of Polymers with Controlled Molecular Architecture: A New Convergent Approach to Dendritic Macromolecules", *Journal of the American Chemical Soiecty*, Vol. 112, pp. 7638-7647, 1990.

21. Meijer, E.W., F. G. A. Johan, and M. M. Ellen, "Encapsulation of Guest Molecules into a Dendritic Box", *Science*, Vol. 266, pp. 1226-1229, 1994.

22. Tomalia D.A., J. Baker, A. Quintana, L. Piehler, M. Banazak-Holl, and E. Raczka, "The Synthesis and Testing of Anti-Cancer Therapeutic Nanodevices", *Biomedical Microdevices,* Vol. 3, pp. 61-69, 2001.

23. Tomalia D. A., J. C. Roberts, Y. E. Adams, J. A. Mercer-Smith, and D. K. Lavallee, "Using Starburst Dendrimers as Linker Molecules to Radiolabel Antibodies*", Bioconjugate Chemistry,* Vol. 1, pp. 305-308, 1990.

24. Moses, J. E., and A. D. Moorhouse, "The Growing Applications of Click Chemistry", *Chemical Society Reviews.,* Vol. 36, pp. 1249–1262, 2007.

25. Yang, Y., C. Hua, and C. M. Dong, "Synthesis, Self-Assembly, and in vitro Doxorubicin Release Behavior of Dendron-Like/Linear/Dendron-Like Poly(epsilon-caprolactone)-b-poly(ethylene glycol)-b-poly(epsilon-caprolactone) Triblock Copolymers", *Biomacromolecules, Vol. 10, pp. 2310-2318,* 2009.

26. Gitsov, I., K. L. Wooley, C. J. Hawker, P. T. Ivanova, and J. M. J. Frechet, "Synthesis and Properties of Novel Linear-Dendritic Block Copolymers. Reactivity of Dendritic Macromolecules Toward Linear Polymers", *Macromolecules,* Vol. 26, pp. 5621-5627, 1993.

27. Fre´chet, J.M.J., and E. R. Gillies, "pH-Responsive Copolymer Assemblies for Controlled Release of Doxorubicin", *Bioconjugate Chemistry,* Vol. 16, pp. 361-368, 2005.

28. Cheng, X., F. Gong, X. Cheng, S. Wang, Y. Wang, Y. Gao, and S. Cheng, "Biodegradable COMB-Dendritic Tri-block Copolymers Consisting of Poly(ethylene glycol) and Poly(l-lactide): Synthesis, Characterizations, and Regulation of Surface Morphology and Cell Responses", *Polymer,* Vol. 50, pp. 2775-2785, 2009.

29. Zhu, L., H. Chen, G. Li, H. Chi, D. Wang, C. Tu, L. Pan, F. Qiu, F. Guo, and X. Zhu, "Alendronate-Conjugated Amphiphilic Hyperbranched Polymer Based on Boltorn H40 and Poly(ethylene glycol) for Bone-Targeted Drug Delivery" *Bioconjugate Chem*istry, Vol. 23, pp. 1915-1924, 2012.

30. Szoka Jr. F. C., and J. Haensler, "Polyamidoamine Cascade Polymers Mediate Efficient Transfection of Cells in Culture", *Bioconjuate. Chemistry,* Vol. 4, pp. 372-379, 1993.

31. Newkome, G.R., C. N. Moorefield, G. R. Baker, M. J. Saunders, and S. H. Grossman, "Unimolecular Micelles", *Angewandthe Chemistry International Edition,* Vol. 30, pp. 1178-1180, 1991.

32. Frechet, J.M., M. Liu, and K. Kono, "Water-Soluble Dendritic Unimolecular Micelles: Their Potential as Drug Delivery Agents", *Journal of Controlled Release*, Vol. 65, pp. 121-131, 2000.

33. Duncan, R., N. Malik, and E. G. Evagorou, "Dendrimer-platinate: A Novel Approach to Cancer Chemotherapy", *Anticancer Drugs,* Vol. 10, pp. 767-776, 1999.

34. Duncan, R., and N. Malik, "Dendrimers: Biocompalibility and Potential for Delivery of Anticancer Agents", *Proceedings International Symposium Control Release Bioactive Mater*ials, Vol. 23, pp. 105-106, 1996.

35. Calderón, M., M. A. Quadir, M. Strumia, and R. Haag, "Functional Dendritic Polymer Architectures as Stimuli-Responsive Nanocarriers", *Biochimie,* Vol. 92, pp. 1242-1251, 2010.

36. Gingras, M., J. M. Raimundo, and Y. M. Chabre, "Cleavable Dendrimers" *Angewandthe Chemie International Edition*, Vol. 46, pp. 1010-1017, 2007.

37. Engin, K., D. B. Leeper, J. R. Cater, A. J. Thistlethwaite, L. Tupchong, and J. D. Mcfarlane, "Extracellular pH Distribution in Human Tumours", *International Journal of Hyperthermia*, Vol. 11, pp. 211-216, 1995.

38. Jin, Y., X. Rena, W. Wangb, L. Kec, E. Ninga, L. Dua, and J. Bradshawc, "A 5-Fluorouracil-Loaded pH-Responsive Dendrimer Nanocarrier for Tumor Targeting", *International Journal of Pharmaceutics*, Vol. 420, pp. 378-384, 2011.

39. Fre´chet, J. M. J., R. G. Elizabeth, and T. B. Jonsson, "Stimuli-Responsive Supramolecular Assemblies of Linear-Dendritic Copolymers", *Journal of American Chemical Society*, Vol. 126, pp. 11936-11943, 2004.

40. Park, C., J. Lim, M. Yun, and C. Kim, "Alendronate-Conjugated Amphiphilic Hyperbranched Polymer Based on Boltorn H40 and Poly(ethylene glycol) for Bone-Targeted Drug Delivery", *Bioconjugate Chemistry*, Vol. 23, pp. 1915-24, 2012.

41. Dong, C-M., L. Sun, X. Ma, B. Zhu, and X. Zhu, "NIR-Responsive and Lectin-Binding Doxorubicin-Loaded Nanomedicine from Janus-Type Dendritic PAMAM Amphiphiles*"*, *Biomacromolecules*, Vol. 13, pp. 3581-91, 2012.

42. Mcelhanon, J.R., and D. R. Wheeler, "Thermally Responsive Dendrons and Dendrimers Based on Reversible Furan-Maleimide Diels-Alder Adducts", *Organic Letters*, Vol. 3, pp. 2681-2683, 2001.

43. Chen, W-C., H. Wei, S-L. Li, J. Feng, J. Nie, X-Z. Zhang, and R-X. Zhuo, "Thermo-Sensitive Polymeric Micelles Based on Poly(N -isopropylacrylamide) as Drug Carriers", *Progress in Polymer Science*, Vol. 30, pp. 893-910, 2009.

44. Calderon, M., R. Graeser, F. Kratz, and R. Haag, "Development of Enzymatically Cleavable Prodrugs Derived from Dendritic Polyglycerol", *Bioorganic&Medicinal Chemistry Letters*, Vol. 19, pp. 3725-3728, 2009.

45. Malkoch, M., W. Peng, J. N. Hunt, R. Vestberg, E. Kaltgrad, M. G. Finn, V.V. Fokin, K. B. Sharpless, and C. J. Hawker, "Multivalent, Bifunctional Dendrimers Prepared by Click Chemistry", *Chemical Communications*, Vol. 46, pp. 5775-5777, 2005.

46. Fife, T., and L. Jao, "Substituent Effects in Acetal Hydrolysis", *Journal of Organic Chemistry*, Vol. 30, pp. 1492-1495, 1965.

47. Lavasanifar, A., J. Samuel, and G. S. Kwon, "Micelles Self-Assembled from Poly(ethylene oxide)-block-poly(*N*-hexyl stearate l-aspartamide) by a Solvent Evaporation Method: Effect on the Solubilization and Hemolytic Activity of Amphotericin", *Journal of Controlled Release*, Vol. 77, pp. 155–160, 2011.

48. Lavasanifar, A., H. M. Aliabadi, A. Mahmud, and A. D. Sharifabadi, "Micelles of Methoxy Poly(ethyleneoxide)-*b*-poly(caprolactone) as Vehicles for the Solubilization and Controlled Delivery of Cyclosporine A", *Journal of Controlled Release*, Vol. 104, pp. 301–311, 2005.